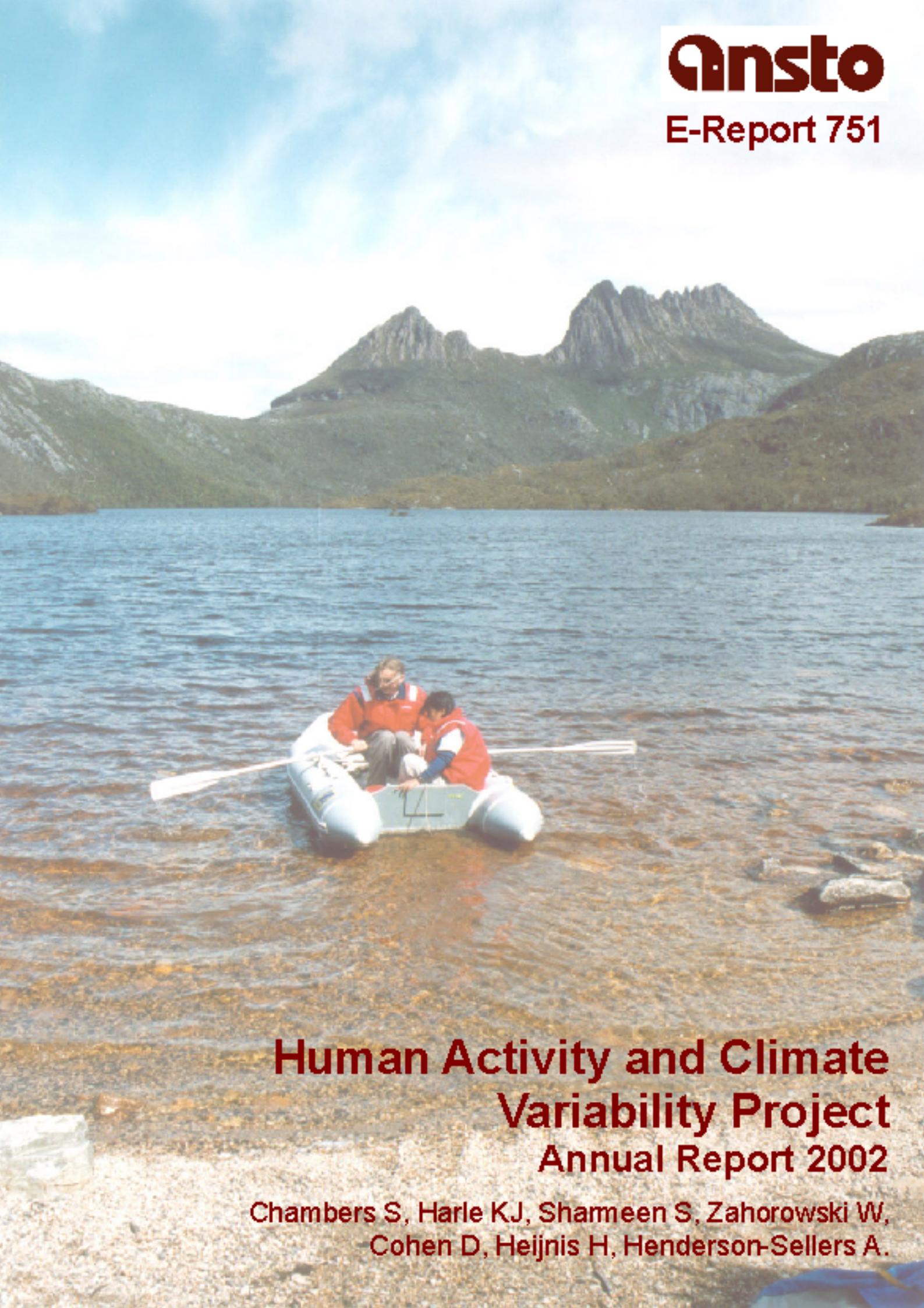

Ansto

E-Report 751

Human Activity and Climate Variability Project

Annual Report 2002

Chambers S, Harle KJ, Shameen S, Zahorowski W,
Cohen D, Heijnis H, Henderson-Sellers A.

E-Report on the Human Activity and Climate Variability Project: Annual Report 2002

By S Chambers, K Harle, S Sharmeen, W Zahorowski, D Cohen, H Heijnis and A Henderson-Sellers.

Published by the Australian Nuclear Science and Technology Organisation (ANSTO), November 2002.

Front Cover	Dr Henk Heijnis and Ms Atun Zawadzki setting out for sediment sampling at Dove Lake, Cradle Mountain National Park, Tasmania.
Photography	Dr Katherine Harle, ANSTO

ANSTO Report No. ANSTO/E-751

ISBN 0 642 59998 X

ANSTO CONTACT DETAILS

Street Address: Australian Nuclear Science and Technology Organisation
New Illawarra Road, Lucas Heights, NSW 2234

Postal Address: ANSTO, Private Mail Bag 1
Menai NSW 2234
Australia

Telephone: + 61 2 9717 3111

Facsimile: + 61 2 9543 5097

E-mail: enquiries@ansto.gov.au

Internet: ANSTO Home Page
http://www.ansto.gov.au

Table of contents

Project OP – 0050: Human Activity and Climate Variability

Project Leader: Dr Henk Heijnis (Henk.Heijnis@ansto.gov.au)

Website: http://home.ansto.gov.au/ansto/environment1/

Table of contents

P1: Project overview

P1.1 Project scope

This project aims to utilise nuclear techniques to investigate evidence of human activity and climate variability in the Asia Australasian regions. It was originally designed to run over three years, commencing July 1999, with three parallel research tasks:

Task 1: Past - Natural archives of human activity and climate variability

Task 2: Present - Characterisation of the global atmosphere using radon and fine particles

Task 3: Future - Climate modelling: evaluation and improvement

P1.2 Main project objectives

- To determine what proportions of changes in natural archives are due to human activity and climate variability.
- To contribute to the understanding of the impact of human induced and natural aerosols in the East Asian region on climate through analysis and sourcing of fine particles and characterisation of air samples using radon concentrations.
- To contribute to the improvement of land surface parameterisation schemes and investigate the potential to use isotopes to improve global climate models and thus improve our understanding of future climate.

P1.3 Significant project outputs

- The Department of Land and Water conservation, National Parks and Wildlife Services, Sydney Water Corporation and the Australian Antarctic Division would use the results of the natural archive studies in their management and policy documents.
- The ACE-Asia project will generate data for the official data archive for this international project. Papers will be prepared for an international journal on air mass characterisation in collaboration with other participants.
- A significant scientific contribution will be made to the understanding and characterisation of regional air masses in Asia/Australia by publishing scientific analysis of measurements, maintaining data quality and guiding the scientific projects at selected observation stations.
- Evaluation of a proposed new technique for determining changes in the surface water budget.
- Analysis of a large number of AGCMs with particular reference to the behaviour of their land-surface schemes.

P1.4 Significant project outcomes

- An improved understanding of natural and anthropogenic factors influencing change in our environment. Results could be used in improving management policies and developing long term management strategies.
- A better understanding of the role of aerosols in climate forcing in the Asian region, leading to improved ability to predict climate change.
- An improved understanding of long term changes in the concentrations of trace species in the atmosphere on a regional and a global basis and their use in model evaluation.
- Improved understanding of the impact of different land-surface schemes on simulations by atmospheric models.

P1.5 Summary of progress (December 2001 - November 2002)

	Task 1	Task 2	Task 3
Milestones set	11	7	10
Milestones achieved	15	6	6
Milestones ongoing	8	7	5
Publications and reports	1 book chapter 11 papers/abstracts 42 reports	8 papers/abstracts 12 reports	23 papers/abstracts 17 reports
Research co-operation	11 universities 1 Government organisation 1 International organisation	2 universities 3 Government organisations ACE-Asia international partners	2 universities 2 Government organisations 27 PILPS international modelling groups 35 AMIP international modelling groups
External usage of facilities	15	0	1
Fieldwork trips (ANSTO)	9	2	NA
Supervision of students	3 PhD 1 Masters 2 Hons	1 PhD	0

NA = Not applicable

P1.6 The next two years of the project

In order to complete our project and increase ANSTO's international profile a two-year extension was requested from the TAC and Senior Management. After a successful presentation to the technical advisory committee, supported by positive recommendations of the external reviewers and CBA-directors, a provisional two-year extension was granted.

Our new and extended projects efforts include:

1) Aligning ourselves with the recently developed mission of the IGBP/PAGES research program "Human Interactions on Terrestrial Ecosystems" and co-ordinating the Australasian research effort. The project leader has been elected to represent the Australasian region and the project team is now actively seeking support from other researchers. An AINSE sponsored workshop was successfully organised to engage the Australian research community (September 2001) and ANSTO's contribution recognised on the HITE-website. A SE-Asian/ Australasian workshop as part of the international INQUA conference will be organised in consultation with the International Project Leader (July 2003).

   Further research will focus on: (1) How widespread and reliable are evidence of major climatic events, such as storms and El Nino/La Nina cycles, in natural archives? This would require more natural archives to be examined from northern Australia and also records to be obtained from southern Australia. (2) The spatial extent of mining related pollutants, in the form of aerosol particles, which is of importance to managing the waste in the future. A combination of aerosol and archival studies will address this issue. The first fieldwork for this was completed in February 2002 and some of the results are already available.

2) The two-year conditional extension to ANSTO's involvement in the ACE-Asia program will be used to achieve our extended scientific objectives. The extension will allow us to collect sufficient data to more accurately quantify seasonal fine particle concentration variations over the region, as well as to fingerprint and quantify source contributions across the study area based on a statistically significant number of pollution events. This will also provide sufficient time to apply Chemical Mass Balance and Positive Matrix Factorisation techniques to integrate aerosol and radon data. Overall, the proposed extension will put us

in a better position to meet the expectations of our international collaborators whose programs rely on our data and require our expertise.

Processed radon and fine particle data for the 2001 Intensive Operation Period (IOP) has been submitted to the ACE-Asia Long-term Data Archive at UCAR/Joint Office for Science Support (JOSS). Over the past year additional extreme pollution episodes of the kind monitored during the 2001 IOP have been characterised, the extension period will further improve this database. Seasonal contrasts in the angular distribution of radon between the east Asian sites has highlighted differences in regional meteorology that will be important for the interpretation of fine particle data. The extension period will enhance the seasonal information presented in this report by enabling an analysis of interannual variability. A first estimate was also made of a regional oceanic radon flux from the Southern Ocean. This analysis will be extended to include a detailed analysis of source areas and the influence of synoptic wind fields.

3) The ANSTO involvement in the international initiatives of AMIP II and GLASS show clearly that June 2002 was a premature closing date for the research in this project. The ANSTO contributions to both research programs are essential to our research partners and therefore a premature end would have caused major disruptions to this international effort.

   To date we have received data from 20 (of 30) AGCMs and are anticipating the release of the remaining 10 AGCMs by June 2003. In the past year we have completed and published the results on the surface energy and water budgets and the lag-correlation analysis of the AMIP II AGCMs. We have also summarised the methodology used in the parameterisation of the AMIP II AGCMs land-surface schemes (LSS) and for the first time our analyses revealed the importance of explicit vegetation in the simulation of land-surface climates. In the coming year we plan to investigate this relationship further using different approaches. Our aim is to determine a meaningful 'complexity index' for each AMIP II LSS based on the important structural representation of the schemes and physical details used to parameterise different processes. We also aim to examine the relationships between model simulation and overall LSS complexity together with the complexity of parameterisation for different processes. In addition, we intend to examine the response of different LSSs to the atmospheric forcing and the possibility of clustering the AGCM simulations with similar LSS complexity by excluding the response of the atmospheric forcing.

   Finally, ANSTO researchers are committed to coordinating the PILPS component of GLASS into early 2004. This is desirable in order to allow us to fulfil our international scientific commitments.

In Summary: To achieve these extended goals we successfully gained another two years of further support for our project. This is a direct result of the project team's successful push to be members of International fora and ANSTO's unique contribution to these international projects. We acknowledge the support of both the external review and CBA-directors.

I would like to thank all involved in securing an extra two years on our project.

Henk Heijnis, Project Leader 11/11/02

P1.7 Project team (December 2001 - November 2002)

ANSTO

Ms Fiona Bertuch
Mr Chris Bowles
Dr Scott Chambers
Mr Robert Chisari
Dr David Cohen
Mr David Garton
Dr Kate Harle
Ms Jennifer Harrison
Dr Henk Heijnis
Professor Ann Henderson-Sellers
Mr Quan Hua
Dr Parviz Irannejad
Dr Geraldine Jacobsen
Mr Andrew Jenkinson
Mr Tom Loosz
Mr Gordon McOrist (to June 2002)
Mr Ot Sisoutham
Ms Lida Mokhber-Shahin
Dr Saniya Sharmeen
Ms Anna Sim
Mr Sylvester Werczynski
Dr Wlodek Zahorowski
Dr Ugo Zoppi
Ms Atun Zawadzki

External collaborators

Dr Richard Arimoto (New Mexico State Uni, USA)
Dr Tim Bates (NOAA/PMEL, USA)
Dr Brendan Brooke (GA)
Mr Paul Fukumura-Sawada (NOAA/CMDL, USA)
Dr Hoshin Gupta (Uni of Arizona, USA)
Dr Simon Haberle (Monash)
Dr Takatoshi Hattori (Central Research Institute of Electric Power Industry, Japan)
Professor Phan Duy Hien (Vietnam Atomic Energy Advisory Board, Vietnam)
Professor Min Hu (Peking Uni, China)
Professor Chang-Hee Kang (Cheju National University)
Professor Peter Kershaw (Monash)
Professor Y.J Kim (Kwangju Institute of Science and Technology, Korea)
Professor Takao Lida (Nagoya Uni, Japan)
Dr John McGregor (CSIRO)
Dr Kendal McGuffie (UTS)
Assoc. Professor Andrew McMinn (IASOS, UTas)
Assoc. Professor David Parry (NTU)
Dr Tom Phillips (LLNL)
Professor Andrew Pitman (Macquarie)
Dr Cath Samson (UTas)
Dr Jie Tang (Chinese Academy of Meteorological Sciences, China)
Mr John Tibby (Monash)
Professor Mitsuo Uematsu (Ocean Research Institute, University of Tokyo)
Professor Tao Wang (Hong Kong Polytechnic University)
Dr Huqiang Zhang (BoM)
Scientists and technical support from CGPAPS, BoM, the Antarctic Division and PCMDI of the Lawrence Livermore National Laboratory.

Students

Mr Charles Agnew (UOW-Hons)
Ms Jennifer Brazier (NTU-PhD)
Ms Megan Coles (NTU-PhD)
Ms Fiona Dick (Newcastle-PhD)
Ms Iona Flett (UTS-Hons)
Ms Nicola Franklin (Sydney-PhD)
Ms Janece McDonald (Newcastle-PhD)
Mr Peter Murry (Newcastle-PhD)
Ms Kate Panyatou (UOW-PhD)
Mr Tim Ralph (Macquarie-PhD)
Ms Bec Scouller (Macq.-Mast.)
Mr Craig Sloss (UOW-PhD)

Task 1: Past - Natural archives of human activity and climate variability

T1.1 Research focus, objectives and scope

T1.1.1 Research focus

With the successful bid for a two year extension on the project, Task 1 has focussed its research effort on answering three main questions:

- What is the spatial extent of pollution from the western Tasmanian mining region? Does this have implications for water quality and biodiversity?
- What are the most important potential sources of pollution in the Lake Burragorang catchment?
- How widespread and reliable are evidence of major climatic events, such as storms and El Nino/La Nina cycles, in natural archives?

These questions were posed as part of the rationale for an extension and are based on issues identified from the first three years of the project. They fall within the objectives and scope originally set for Task 1 of the project. Scientific outcomes will be contributed to the International Geosphere-Biosphere Programme (IGBP) sponsored project Human Impact and Terrestrial Ecosystems subproject (HITE).

T1.1.2 Objectives

Task 1 has three main objectives:

- To identify the best indicators of past human activity and climate variability in sediment records (natural archives);
- To determine what proportion changes in the landscape/terrestrial ecosystems are due to human activity or climate variability or an interaction of both;
- To contribute to the IGBP sponsored project investigating Human Impact on Terrestrial Ecosystems (HITE).

T1.1.3 Scope

Task 1 has and will continue to fulfil these objectives through the:

- location of high-resolution natural archives spanning the last 200 years;
- improvement of isotope-dating techniques in order to establish a reliable chronology;
- identification of geochemical and biological indicators of human activity;
- identification of geochemical and biological indicators for natural climate cycles;
- comparison of records derived from natural archives with available historical records;
- linkage of results with aerosol, radon and climate modelling analyses;
- contribution of data to the following HITE key questions:
    - What have been the major human impacts (driving forces) that have influenced the ecosystems that we see at the present day?
    - How have these interacted with natural environmental variability, such as climate?
    - To what extent and in which ways are the changes brought about by the combination of human and natural influences threatening the future functioning of terrestrial ecosystems systems?

- What evidence does the past record provide as a guide to resilience, rates of recovery, irreversibility and future sensitivity?
- How realistic is it to retain any concept of 'natural' ecosystems?
- In the absence of such a concept, how may evidence about past conditions help to develop realistic policy and management targets?

T1.2 Progress

T1.2.1 Summary of progress

The progress of analyses of sediment cores from sites selected in this thus study are outlined in Table 1.1. More detailed reports of the progress made since the last annual review (November 2001) are given in the following sections.

Table 1.1: Summary of progress made on sediment cores from the project sites.

Site area	Site	^{14}C	^{210}Pb	Sediment	Trace elements	Pollen	Algae	Charcoal
Northern Territory	Annaburroo Billabong+	NA					NA	NA
Atherton Tableland (QLD)	Lake Euramoo*							
Lake Burragorang (NSW)	Tonalli River*	NA				NA	NA	NA
	Lacey's Creek*	NA				NA	NA	NA
	Nattai River+	NA				NA	NA	
	Nattai River II	NA				NA	NA	
Myall Lakes (NSW)	Broadwater	NA						
	Wallis Lake							
Victoria	Hogan's Billabong+	NA			NA	NA		
	Lake Cullulleraine+	NA			NA	NA		
	Tower Hill+				NA			
Tasmania	Lake Dora*							
	Midge Lake*							
	Perched Lake+							
	Lake Cygnus+							
	Parting Creek Lake						ns	ns
	Lake Dobson							ns
	Dove Lake	ns	ns	ns		ns	ns	ns

NA = not applied, ns = not started, completed, in progress
*progress reported in 2000 Annual Report
+progress reported in 2001 Annual Report
New sites and study regions are in blue

T1.2.2 The Great Lakes region, NSW

The Great Lakes of the mid north coast of New South Wales (Figure 1.1) is a system of coastal lagoons formed between 6 and 9 ka as rising post-glacial sea levels flooded coastal river valleys and were then blocked by the formation of coastal sand bars (Harris, 2001). Most of the lakes are naturally fresh to brackish, with flushing from sea water during high tides. Connection to the sea in these lakes naturally occurs during periods of high rainfall. However, the entrances of several of the lakes have been widened and are dredged, creating artificial permanent openings to the sea. The ecologies of these lakes have subsequently shifted from fresh-brackish to more marine. The region is dominated by high summer rainfall and high climate variability.

The Great Lakes region is important for tourism, commercial and recreational fisheries and conservation. A significant proportion of the seagrass population on the NSW coast occur in the lakes and they are home to several rare and endangered species. In recent years there have been increasing pressures on the lakes, with urban, rural, fishery and recreational development.

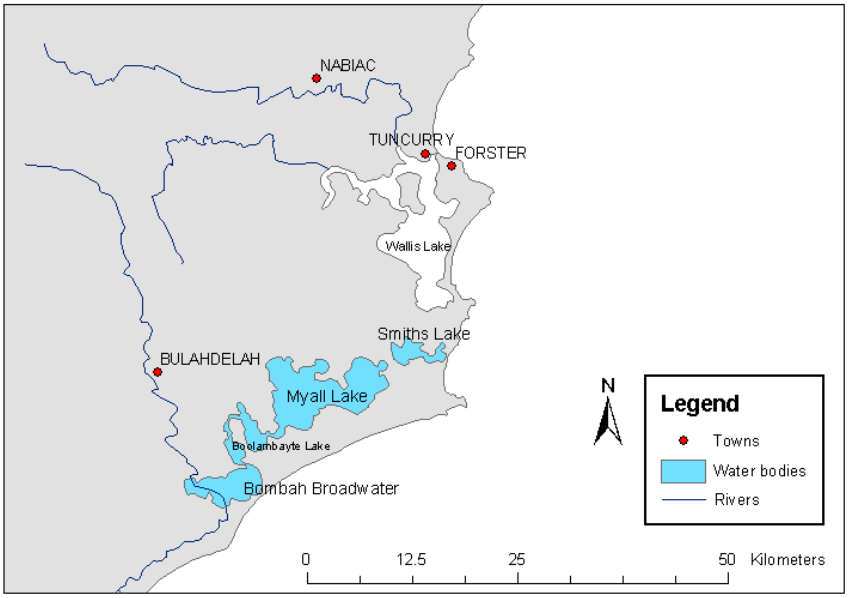

Figure 1.1: Map of the Great Lakes region in NSW

The Myall Lakes

Collaborative researchers: Ms Iona Flett (part-time Honours student UTS), Assoc. Prof. Greg Skilbeck (UTS)

Site description and selection rationale

The Myall Lakes is a coastal lake system of four lakes situated North of Newcastle and Port Stephens, between the inland town of Bulahdelah and Seal Rocks. The lakes drain into Port Stephens via the lower Myall River. They are one of only six RAMSAR[1] listed wetlands of international importance in NSW, due to their huge floristic diversity, complex and unusual aquatic habitats and their habitation of large numbers of migratory birds.

The lakes are generally two to four metres deep, with the deepest being Myall Lake. Anecdotal evidence suggest lake levels fluctuate by up to 3 metres in response to periods of high rainfall. Water circulation in the system is very slow, resulting in a predominantly freshwater ecology.

[1] UNESCO Convention on Wetlands (Ramsar, Iran, 1971)

However, the slow circulation also makes them vulnerable to pollution. Indeed, the lakes have experienced periodic blooms of blue-green algae, often including toxic species.

The catchment of the three main rivers flowing into the Myall Lakes covers 780 square km. An estimated 75% of this catchment has relatively undisturbed vegetation, consisting predominantly of eucalypt woodland and forest. *Melaleuca* wetland and dry sclerophyll forest grows around the perimeter of the lake system, with mangroves and other aquatic communities growing on the margins of the lakes. Most of the catchment is national park and state reserve, with remaining land used for forestry or being privately owned. The lakes themselves have been protected since 1972 as part of the Myall Lakes National Park (Pamplin, 2001).

The lakes have been chosen for the HACV project for a number of reasons. They are of recognised national and international significance, indicated by their RAMSAR listing. They are subject to increasing urban run off (including sewage), with expanding development around the lakes and in the catchment. They are also subject to pollution form recreational and rural activities in the catchment. In the past, natural climate variability may also have influenced the lake system. The lakes are an important resource for recreational and commercial fishing, (including oyster farms) as well as other tourism activities.

Progress

From the first set of cores collected in March, analyses has been performed on the Broadwater-1 core (BW-1), which is 31.8 cm long. The other cores collected were found to be unsuitable for analysis. Lead-210 results have been obtained for ten samples from the top 23 cm of this core (Figure 1.2). Analysis has commenced on a further ten samples to fill in gaps and extend the depth of the chronology. The initial results indicate a fairly rapid sedimentation, with a rate of 0.66 cm/yr and an age of 34 years BP at 22 cm. An age depth plot for the core based on the 210Pb data is presented in Figure 1.3.

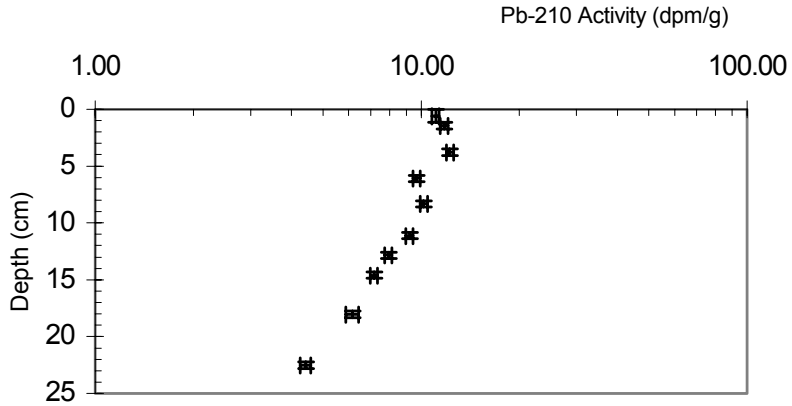

Figure 1.2: Plot of excess ^{210}Pb activity vs depth for Broadwater core BW-1.

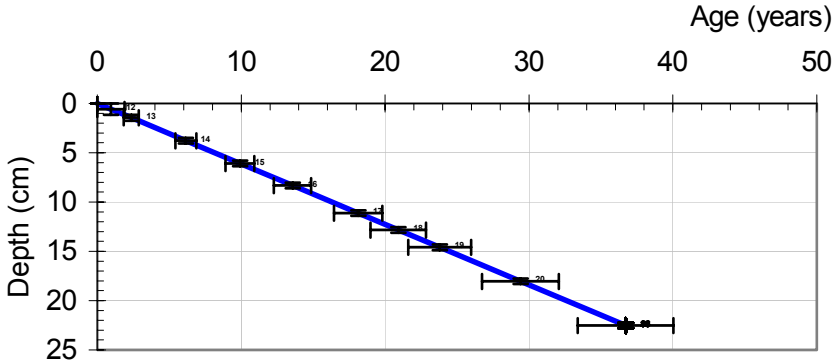

Figure 1.3: Age-depth plot for core BW-1 based on ^{210}Pb data.

Preliminary trace element results (AES) have been obtained for 29 samples from the top 28 cm of core BW-1. Results from the MS analysis are expected by December. The preliminary results (Figure 1.4) demonstrate very little change throughout the sequence for all of the reported elements except aluminium (Al). There are peaks in Al concentrations between 8.5 cm and 15.5 cm and 18 and 20.5 cm. There also appears to be a general decline in Al concentrations from 8 cm to the top. Interpretations will be made once the final data set has been obtained.

Pollen analysis is being carried out on samples from the entire length of core BW-1 at 0.5 cm intervals. Chemical preparation has been completed and counting has commenced, with samples up to 20 cm completed. It has been noted that highly aberrant Casuarinaceae pollen is present in the top samples but not in samples from lower in the core. There is a possibility that this aberrance may be the result of pollution. Further investigations of this are now being undertaken. Akinetes of blue-green algae have been identified, although species have yet to be ascertained. Expert advice has been sought (Bas van Geel, University of Amsterdam).

Grain size analysis has been completed on samples from core BW-1, although there is some concern about the accuracy of the results given that the samples were crushed. Reanalysis of key samples is being carried out to test this. Moisture content and loss-on-ignition analyses have also been completed, with samples combusted at 450 °C to measure the organic content and 1000 °C to measure the carbonate content (Figure 1.5). The moisture content appears to have remained between 70 and 75% for most of the core, except above 10 cm where it steadily increases to around 90%. The inorganic content has remained high throughout the core, with values between 60 and 80%, increasing at the top to over 90%. There appear to be two distinct phases of carbonate deposition - from 14 cm to the base and from the top to just above 5 cm. Organic content remains steady around 20%, except at the top where it declines to under 10%.

A second set of cores have been collected, with magnetic susceptibility, grainsize and density analyses to be carried out using the core logger at UTS. A longer core (ML5-86 cm) has been collected and is currently being sub-sampled for microfossil analysis (pollen and akinetes) and ^{210}Pb dating. It is anticipated that this work will be completed in June 2003.

Wallis Lake

Collaborative researchers: Dr Brendan Brooke (Geoscience Australia)

Site description and selection rationale

Wallis lake (32.174 S 152.51 E) is a wave dominated estuary located on the mid north coast of NSW coast (Figure 1.1). It has an area of 93.82 km^2 and a water depth of between 3 and 4 m. It has a permanent opening formed by breakwaters and dredging of the inlet. Prior to these works the outlet was far more restricted. The lake catchment is around 1440 km^2 and includes the Wallamba River, the Wang Wauk River, the Coolongoolok River and the Wallingat River. Much of the catchment has been cleared for agriculture, mostly in the northwest. However, large areas remain forested and human population density is overall low (Wallis Lake Catchment Management Plan, 2002). Urban development is expanding around the lake itself.

Although land clearance and urban development in the catchment has affected water quality, Wallis Lake is considered to be in reasonable condition compared to other coastal lakes in NSW. It has large areas of seagrasses, overall nitrogen to phosphorous ratios are low and algal blooms are rare except in close proximity to urban development (Wallis Lake Catchment Management Plan, 2002). There is mounting pressure on the lake, however, through increased recreational activity and urban development.

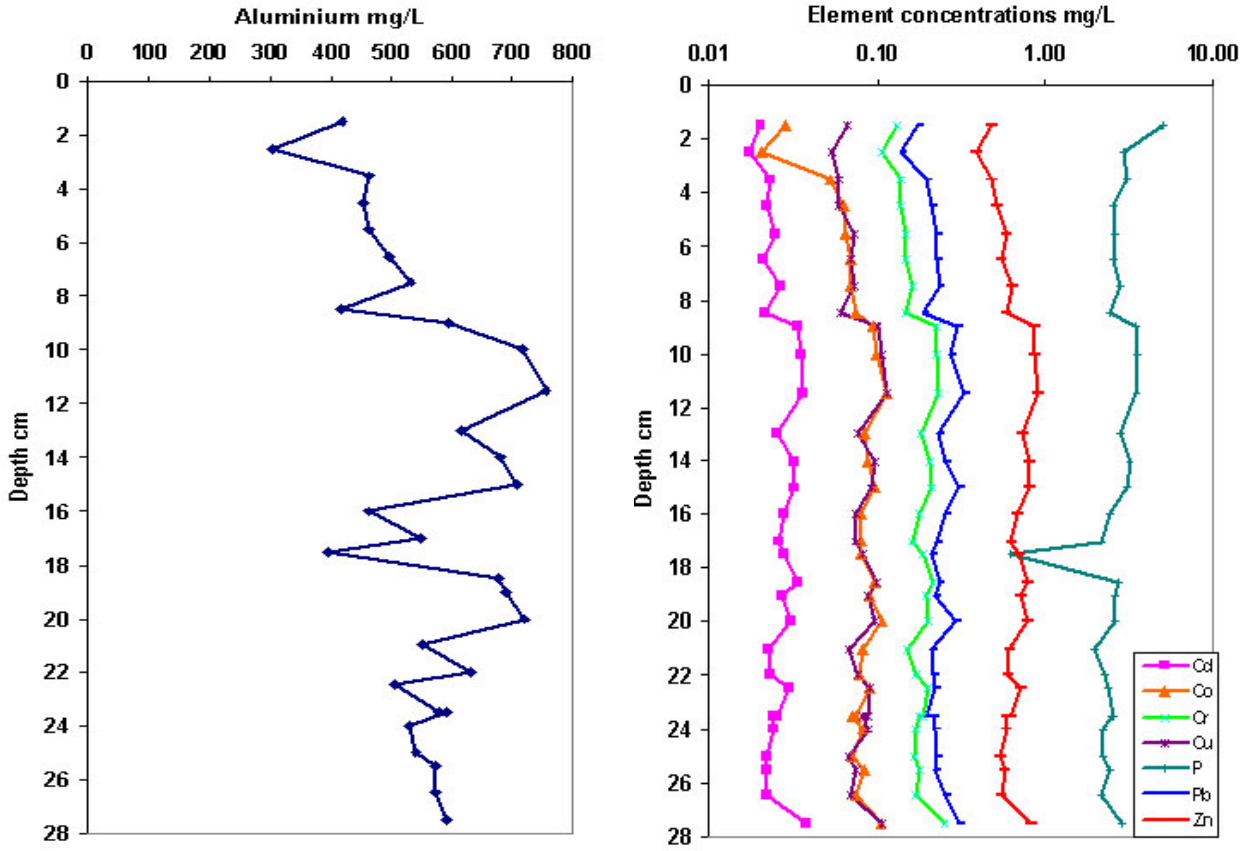

Figure 1.4: Trace element concentrations for core BW-1.

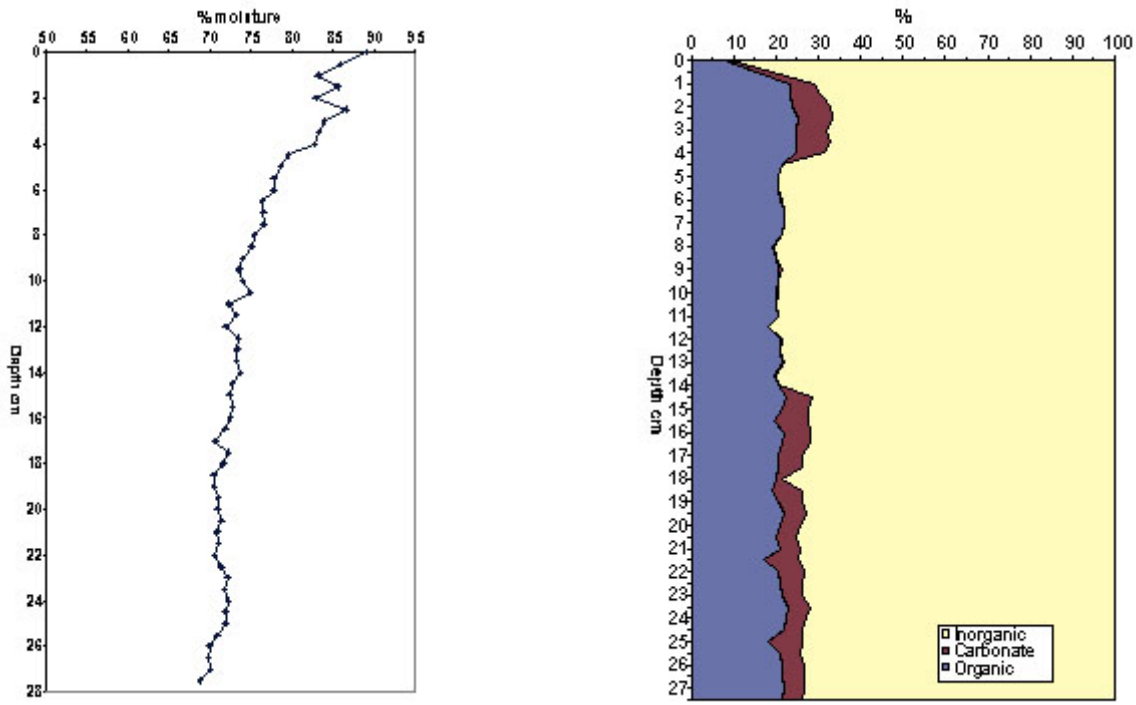

Figure 1.5: % Moisture, organic, inorganic and carbonate concentrations for core BW-1.

Progress

A 31.5 cm core (WL1) was extracted from the deepest part of Wallis Lake (ca 4 m water depth in the central west area). Samples were extracted for ^{210}Pb, trace element, pollen, grainsize and stable isotope analyses, with the latter two being carried out by Geoscience Australia. At this point, results have been obtained for the ^{210}Pb and grainsize analyses (Figure 1.6; Figure 1.7). The ^{210}Pb profile appears to match the <63 μ grainsize profile extremely well. From 4 cm to the top both the <63 μ fraction and the ^{210}Pb activity decrease, then slightly increase in the top sample. An outlying sample at 22 cm in the ^{210}Pb profile matches with a peak in the <63 μ fraction between 20 and 25 cm. Two more ^{210}Pb analysis will be carried out around between 20 and 25 cm to determine if the latter correlation is real. However, overall there appears to be a good correlation between the two profiles suggesting variation in sediment type is having some influence on the ^{210}Pb activity. A chronology was determined for the core using the trend in ^{210}Pb activity from 4 cm down to the base, excluding the 22 cm sample (Figure 1.8).

Samples for trace element, pollen and stable isotope analyses are in the process of being analysed.

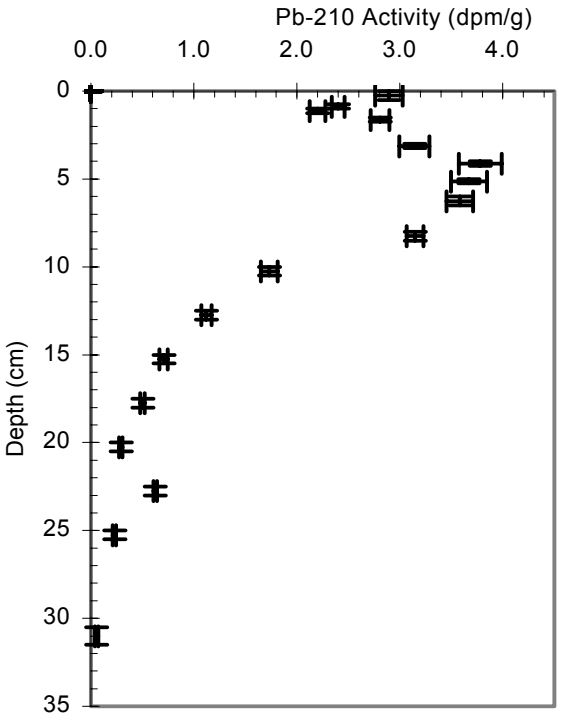

Figure 1.6: Plot of excess ^{210}Pb activity vs depth for Wallis Lake core WL-1.

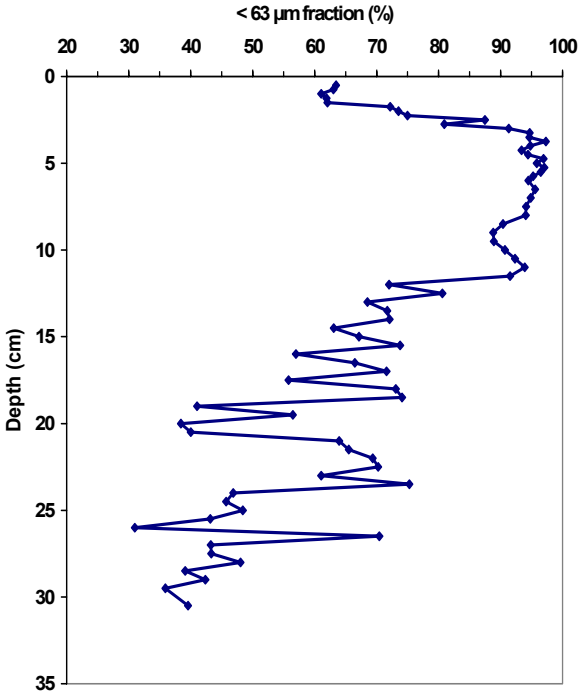

Figure 1.7: Plot of <63 μ grainsize fraction vs depth for Wallis Lake core WL-1.

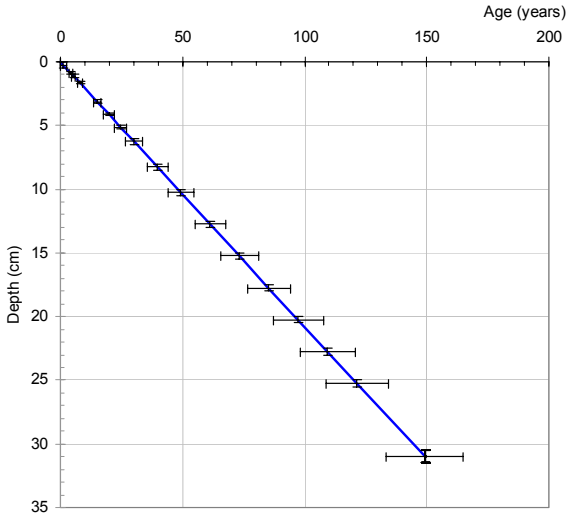

Figure 1.8: Age-depth plot for core WL-1 based on ^{210}Pb data.

T1.2.3 Blue Mountains, NSW

Nattai River

Collaborative researchers: Mr Charles Agnew (Honours student UOW), Dr Brian Jones (UOW), Sydney Catchment Authority

Site description and selection rationale

The Nattai River is one of the source streams for Lake Burragorang, Sydney's largest water reservoir. It lies in the southeast sector of the Burragorang catchment (Figure 1.9; Figure 1.10), extending over 60 km northward from Mittagong to the eastern shore of the lake. The Nattai catchment falls within the Nattai Reserves System, which has recently been awarded World Heritage status. It is dominated by dry sclerophyll communities, with pockets of warm temperate rainforest along the eastern escarpment. Much of the catchment was recently burnt (December 2001).

Figure 1.9: Disused rail bridge on the Nattai River remnant from when mines operated in the region.

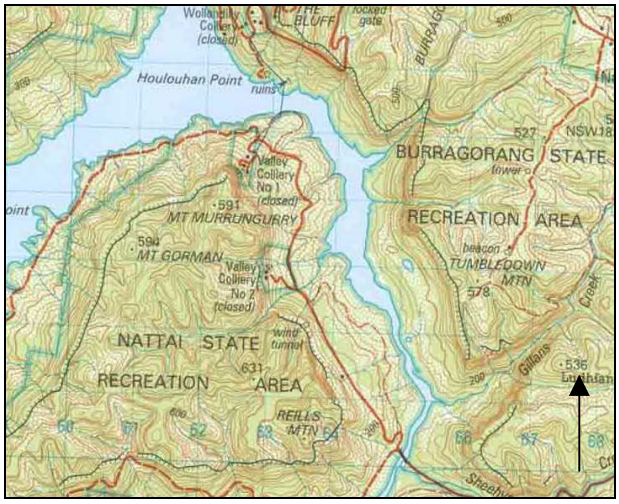

Figure 1.10: Map of the lower reaches of the Nattai River as it enters Lake Burragorang.

Previous research using ^{210}Pb, trace metal and charcoal analyses of sediment cores and surface samples from the Nattai River (reported in HACV, 2001) identified the source and nature of human impact on the Nattai catchment. This study aims to follow up the previous research in the wake of the significant fires in the catchment. Issues under investigation include any affects on sediment movement into the river associated with the fires as well as potential increases in pollution. More emphasis has been placed on charcoal records than in the previous study, with the purpose of identifying the extent of representation of fire events in the fossil record.

Progress

The 2002 Nattai research focussed on the collection and analysis of water samples, sediment cores and sediment surface samples over a 7 month period from March 2002 to September 2002. The results are currently being interpreted and written up by Charles Agnew for his Honours degree (Environmental Science, Wollongong University). Preliminary results are presented below.

Lead-210 analysis of a sediment core extracted from near the mouth of the Nattai River in March 2002 (NM02-1) suggests that the top 4.5 cm of the core has either been mixed or deposited in at the same time, with similar activities in the three samples analysed (Figure 1.11). Further samples will need to be analysed to obtain a more accurate picture. Although there are some coinciding peaks in grainsize (<63 μ) (Figure 1.12) and the macro charcoal concentration

(Figure 1.13), the overall correspondence is low, particularly near the top of the NM02-1 core. This suggests that in general, charcoal content and grainsize are independent. Grainsize (<63 μμ) fluctuates for most of the core between 90 and 98%. Macro charcoal fluctuates throughout the core, with highest values between 1.25 and 4 cm. The variation in charcoal concentration appears to contradict the ^{210}Pb evidence for the top 4.5 cm being mixed. Further analysis, perhaps of microfossils, will be necessary to determine the status of these sediments, ie. mixed or merely open to chemical transport. Results from the trace metal analyses of the cores and the surface samples have yet to be finalised. Final interpretations are expected by the end of the year.

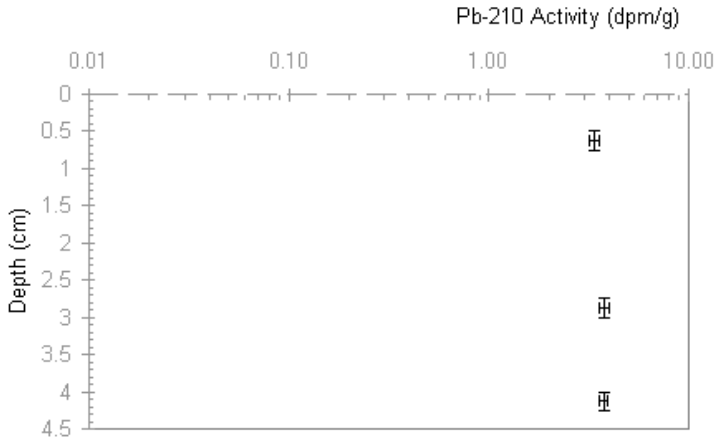

Figure 1.11: Plot of excess ^{210}Pb activity vs depth for Nattai River core NM02-1.

Comparison of the %< 63 μm grainsize 2001 and 2002 results for the surface sample sites in the catchment (Figure 1.14) clearly demonstrate differences. There is a significantly greater percentage of < 63 μm grainsize in 2002, suggesting that there has been a post-fire influx of fine particles in the catchment. Ash and charcoal most likely comprise a significant component of these fine particles, although this has yet to be confirmed through charcoal analysis of the surface samples.

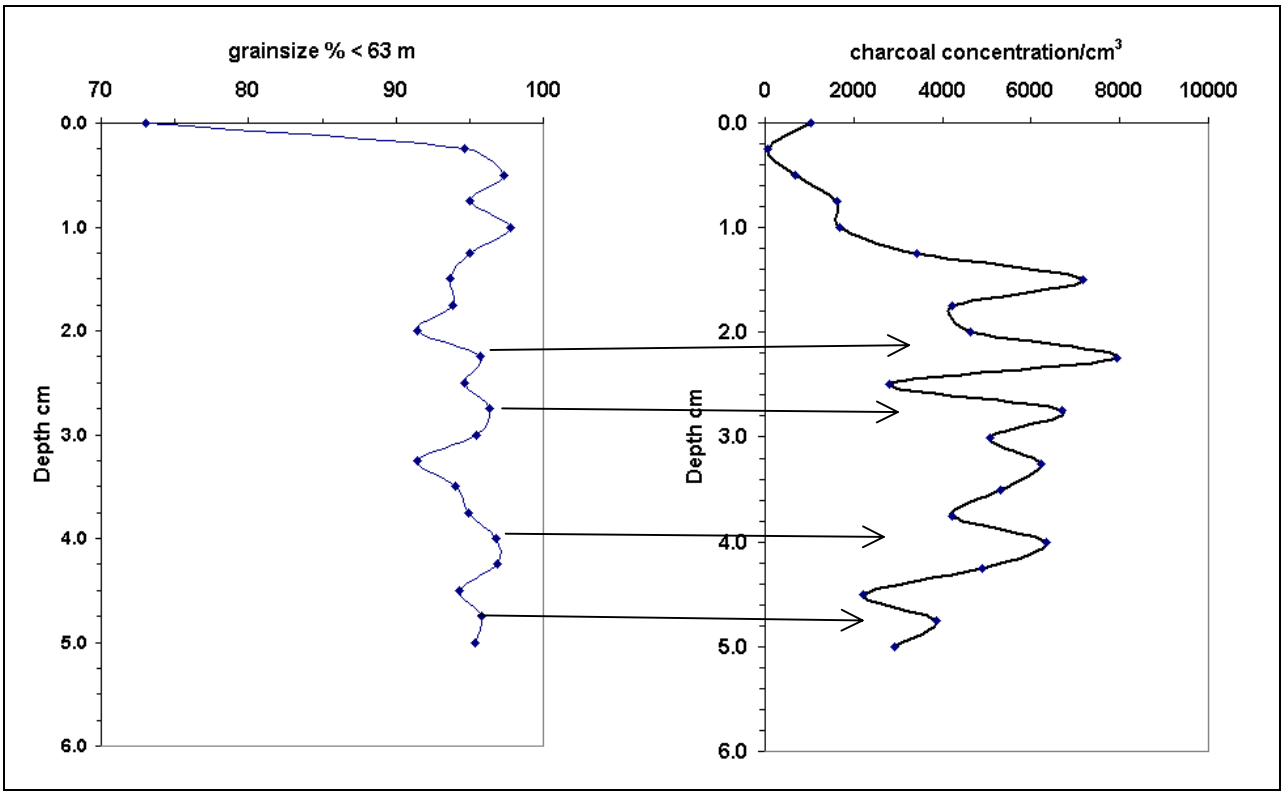

Figure 1.12: Plot of <63 μ grainsize fraction vs depth for Nattai River core NM02-1.

Figure 1.13: Plot of macro charcoal particle vs depth for Nattai River core NM02-1.

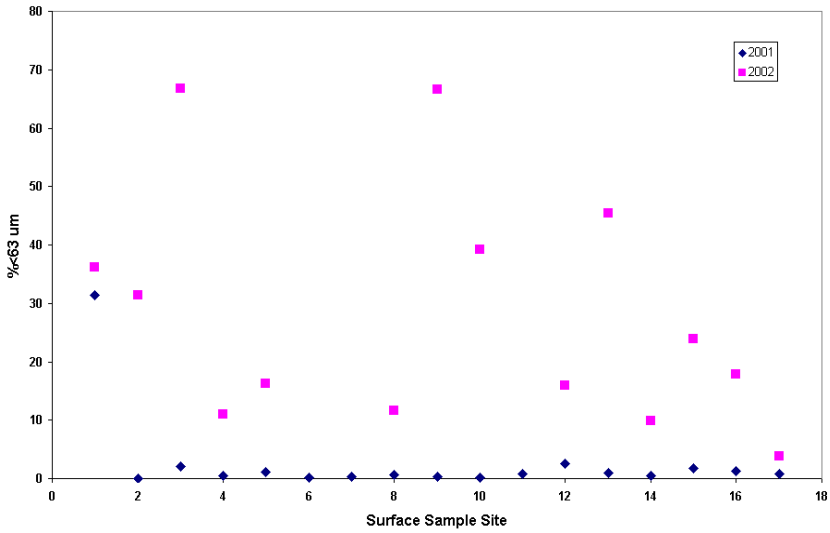

Figure 1.14: Comparison of %<63μm grainsize in surface samples from set sites in the Nattai Catchment for 2001 (J.P. Colliton) and 2002 (C.Agnew).

T1.2.4 Western Tasmania

One of the key issues that has arisen out of the HACV project is the extent to which trace metal pollution has spread across Tasmania. Results from three west Tasmanian sites analysed in stages 1 and 2 of the project (Figure 1.15) indicated that trace metals had been transported into pristine areas in southwestern Tasmania, with concentrations peaking in the 1960s and 70s. This unexpected result raised the question of how extensive was the dispersal of trace elements both in the past and today. It also raised the question of the source of the trace metals.

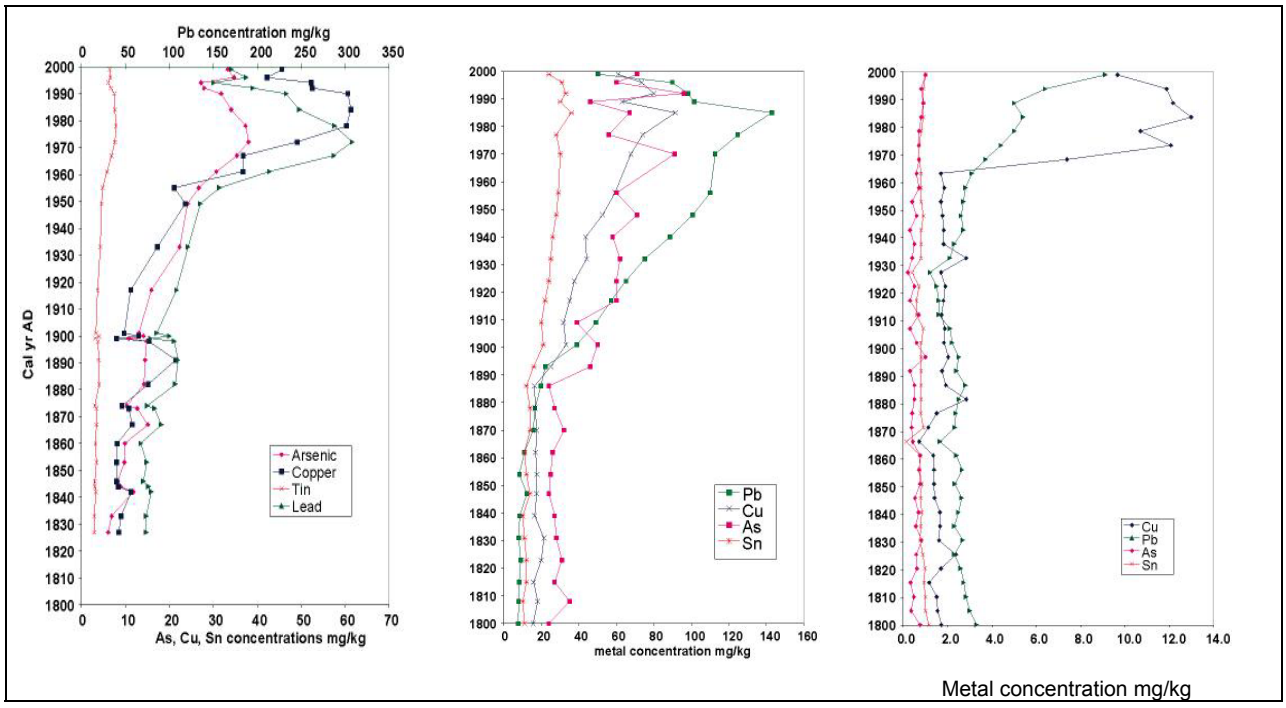

Figure 1.15: Comparison of trace element records from (a) Lake Dora (core LD1), (b) Perched Lake (core PL2) and (c)Lake Cygnus (core LC2).

In order to answer this question the research in Tasmania was extended to include five additional sites at varying distances and trajectories from the Queenstown mining area (Figure 1.16). With the exception of Beehive Marsh, the sites are all small lakes with well defined catchments. Beehive Marsh is a very small marsh/pond located in the low point of a circle of shallow hills. Sediment cores were extracted from each of these sites for trace metal and ^{210}Pb

analyses with the aim in reconstructing the dispersal through both space and time of trace metals from the central western Tasmanian mining area. Microfossil analysis will also be carried out on selected sites to identify any possible impacts on water quality as well reconstructing other possible human impacts on the landscape.

Progress on two of these sites (Parting Creek Lake and Lake Dobson) as well as further progress on a site from the first stage of the project (Perched Lake) is reported below.

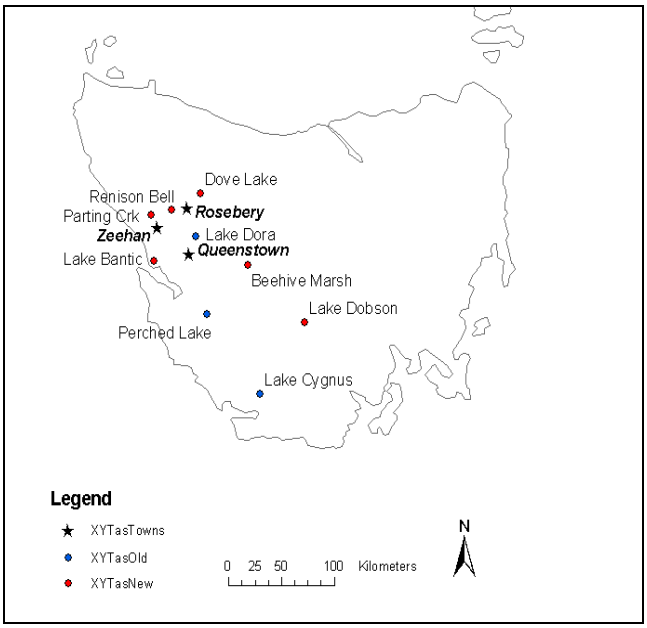

Figure 1.16: Sites selected in Tasmania for the HACV project. Sites analysed in the first three years of the project are in blue. Those selected for the extension of the project are in red.

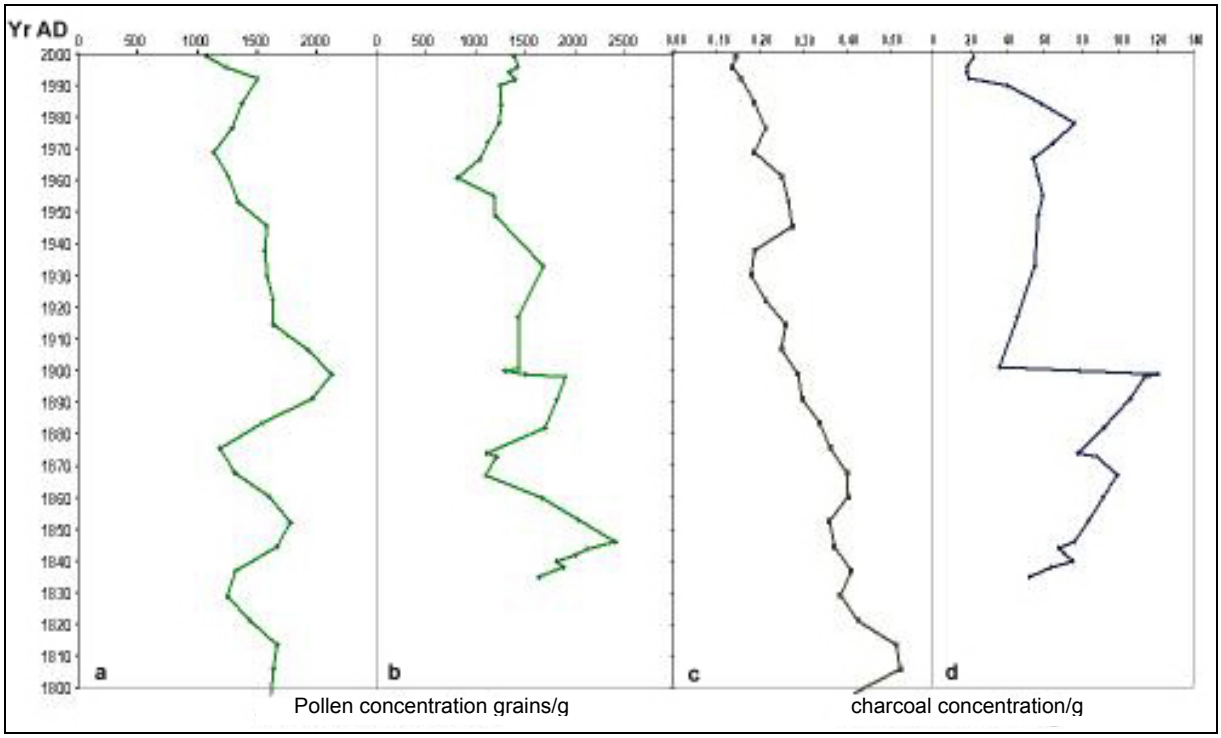

Figure 1.17: Comparison of microscopic charcoal and rainforest pollen counts from Lake Dora (core LD1) and Perched Lake (Core PL2). (a) rainforest tree pollen abundance from Perched Lake, (b) rainforest tree pollen abundance from Lake Dora, (c) charcoal abundance from Perched Lake, (d) charcoal abundance from Lake Dora.

Perched Lake

Collaborative researchers: Mr Ente Rood (University of Amsterdam)

Progress

The work on Perched Lake[2] continued with the completion of a charcoal count of core PL2. This is compared with the total rainforest tree pollen count from the same core as well as the Lake Dora charcoal and total rainforest pollen counts in Figure 1.17. It is clear from this comparison that there is reasonable correlation between the rainforest tree pollen curves from the two sites. This in turn suggests that changes in the rainforest trees recorded at each of the site reflects an overall regional trend. It is equally apparent that there is little correlation between the charcoal records from the two sites. This in turn implies that the charcoal signals reflect local rather than regional trends.

Parting Creek Lake

Site description

Parting Creek Lake (41° 51' 85" S 145° 35' 41"E) is a water reservoir for the township of Zeehan on the west coast of Tasmania. It is situated at 195 m above sea level and has been formed by the damming the two branches of a creek (Parting Creek) in the south (Figure 1.18; Figure 1.19). It has a water depth of around 2.5 m at the deepest part. The lake is surrounded by sandy soils with vegetation dominated by wet heath, button grass moorland and low eucalypt dominated scrub and woodland. *Nothofagus cunninghamii* rainforest also occurs in the region.

The water chemistry of the lake was measured as: pH 4.65, conductivity 8.2 m S/m, turbidity 6-13, dissolved oxygen 12.05 g/L, total dissolved solids 0.05 g/L, oxidation reduction potential 295 mV and temperature 16.85 °C.

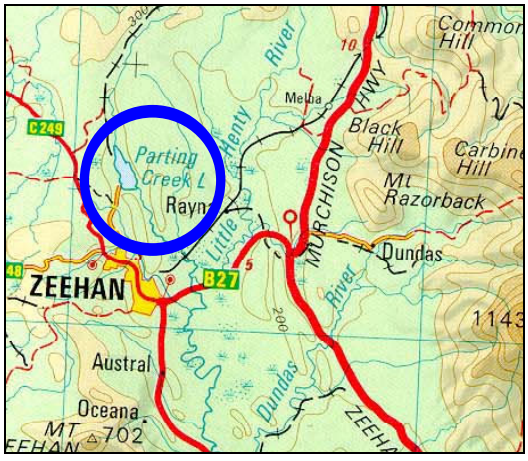

Figure 1.18: Map showing location of Parting Creek Lake

Figure 1.19: View to the southeast of one of the two dams which form Parting Creek Lake.

Progress

Two cores (PCL-1 and PCL-2) were extracted from Parting Creek Lake using a 50 mm diameter and 0.5 m long gravity corer. The 7.0 cm long core PCL-1 was extracted from a water depth of 2.5 m. It was sub-sampled at 0.25 cm intervals for ^{210}Pb, grainsize, trace element and

[2] A description of the site and rationale for its selection is given in HACV (2000) (pp 11-12).

microfossil analyses. A second core (PCL-2), 4.5 cm in length, was collected from a water depth of 1.3 m and was sub-sampled at 0.25 cm intervals.

Lead-210 analysis was carried out on six samples from the top 5 cm of core PCL-1. The results (Figure 1.20) show high ^{210}Pb activity in the top sample (14.34 ± 0.45 dpm/g). The remaining samples have much lower and fairly constant ^{210}Pb activity, with values fluctuating between 0.77 ± 0.05 and 1.32 ± 0.10 dpm/g. This profile suggests sediments between 1 cm and 5.25 cm have either been mixed or were deposited at a similar time, possibly shortly after Parting Creek was dammed. They therefore either represent a post-damming influx and/or sudden accumulation of sediments or alternately bioturbation when the water levels were extremely low. The significantly higher ^{210}Pb in the top sample indicates that mixing has not occurred between the surface sediments and those below. This may be because only sediments in the top 1 cm represent post-dam accumulation or because the water depth in the reservoir has increased thus reducing bioturbation.

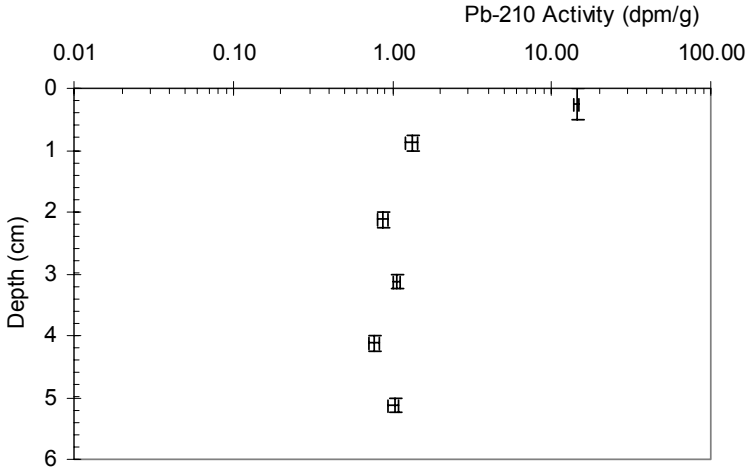

Figure 1.20: ^{210}Pb profile from Parting Creek Lake core PCL-1.

Lake Dobson

Site description and selection rationale

Lake Dobson (42 ° 41' 13" S 146 ° 35' 41" E) is a subalpine tarn located at 1020 m asl in the Mt Field National Park in south-central Tasmania (Figure 1.22; Figure 1.21). The lake is surrounded by *Eucalyptus coccifera /Eucalyptus subcrenulata* woodland grading to *Athrotaxis cupressoides* closed-forest with emergent *Eucalyptus subcrenulata*. Alpine heath, scrub and herbfield communities occur in the wider area. The soil type is a deep uniform yellowish brown stony clay loam occurring on dolerite. The lake is between 5 and 6 m deep.

The water chemistry of the lake was measured as: pH 7, conductivity 5 m S/m, turbidity -10, dissolved oxygen 7.6 g/L, total dissolved solids 0.03 g/L, oxidation reduction potential 250 mV and temperature 16.2 °C.

Progress

Two cores were collected from Lake Dobson at water depths of 5.2 m (LDB-1) and 4.7 m (LDB-2). Core LDB-1 was 22 cm in length and was sampled at 0.5 cm intervals. It was felt that the top sediments may have been lost due to slight over-coring. The second core, LDB-2, was 13.25 cm in length and was sampled at 0.25 cm intervals. Sub-samples from core LDB-2 have been extracted for ^{210}Pb, grainsize, trace element and microfossil analyses.

Figure 1.21: View from the southern shore of Lake Dobson.

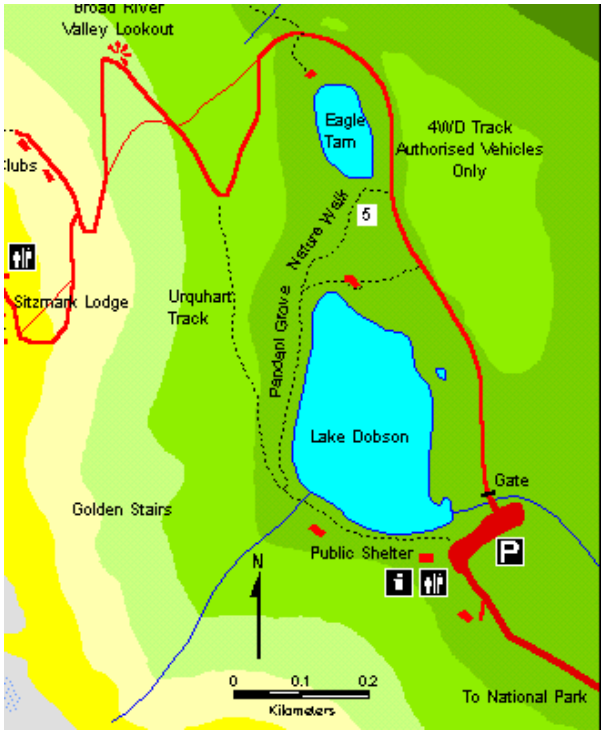

Figure 1.22: Map showing location of Lake Dobson

Preliminary ^{210}Pb results have been obtained for six samples from the top 3.5 cm of core LDB-2 (Figure 1.23). The top sample exhibits higher ^{210}Pb activity than the samples below. The remaining five samples all have similar ^{210}Pb activities suggesting either they have been mixed or were deposited at a similar time. Further analyses will be required using deeper samples in the core before any conclusions can be drawn.

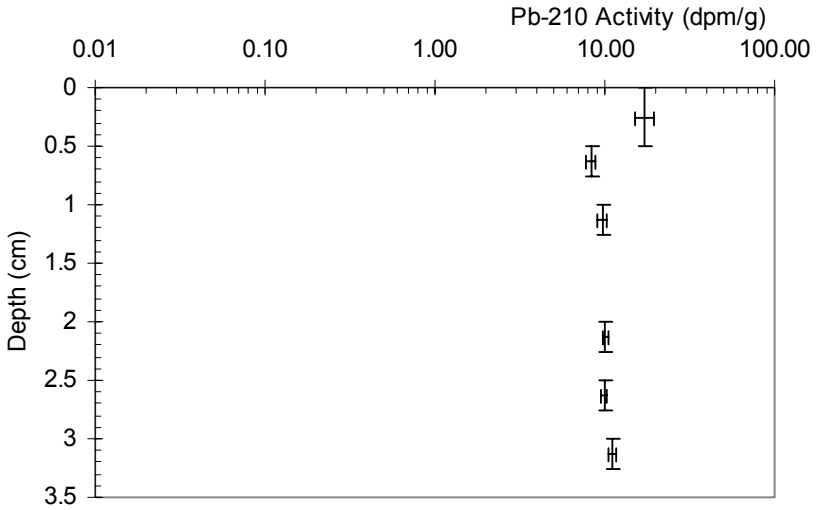

Figure 1.23: ^{210}Pb profile from Lake Dobson core PCL-1.

T1.3 Task 1 reports and papers (December 2001-November 2002)

T1.3.1 Book chapters

- Gardner, C., Jenkinson, A., Heijnis, H. 2002. Estimating Intermolt Duration in Giant Crabs (Pseudocarcinus gigas) In A.J. Paul, E.G. Dawe, R. Elner, G.S. Jamieson, G.H. Kruse, R.S. Otto, B. Sainte-Marie, T.C. Shirley, and D. Woodby (eds.). *Crabs in Cold Water Regions: Biology, Management, and Economics.* University of Alaska Sea Grant, AK-SG-02-01, Fairbanks.

T1.3.2 Journal articles

- Harrison, J., Heijnis, J., Caprarelli, G. Historical pollution variability from abandoned mine sites, Greater Blue Mountains World Heritage Area, NSW, Australia. *Environmental Geology* In press.

T1.3.3 Journal articles on related topics

- Harle, K.J., Heijnis, H., Chisari, R., Kershaw, A.P., Zoppi, U. and Jacobsen, G. 2002. A chronology for the long pollen record from Lake Wangoom, western Victoria (Australia) as derived from uranium/thorium disequilibrium dating. *Journal of Quaternary Science.* 17(1), 51-67.

T1.3.4 Unrefereed articles

- Heijnis, H. 2002. The principle of ^{210}Pb dating of sediments. In V. Cheevaporn and E.Z. Sombrito (Eds.) *Proceedings of the IAEA/RCA Regional Technical Workshop on Radiometric Dating/Cysts Analysis Techniques and Receptor Binding Assay for Harmful Algal Blooms Management 2002.* (C1-RAS/8/076-9009-01). Thailand, Burapha University Press. ISBN 974-352-055-4. pp. 1-16.
- McMinn, A., Heijnis, H. and Hallegraeff, G. 2002. Ballast water transport of toxic dinoflagellatea; sediment core evidence using Pb-210 profiles in marine sediments. In V. Cheevaporn and E.Z. Sombrito (Eds.) *Proceedings of the IAEA/RCA Regional Technical Workshop on Radiometric Dating/Cysts Analysis Techniques and Receptor Binding Assay for Harmful Algal Blooms Management 2002.* (C1-RAS/8/076-9009-01). Thailand, Burapha University Press. ISBN 974-352-055-4. pp. 17-23.

T1.3.5 Internal reports

- K. Harle. Report on Tasmanian fieldwork, 19th-26th February, 2002.
- K. Harle. Report on Nattai River fieldwork, 18th March, 2002.
- J. Harrison. Report on Wallis Lake fieldwork, June, 2002.
- I. Flett. Report on Myall Lakes fieldwork, March, 2002.
- I. Flett. Report on Myall Lakes fieldwork, May, 2002.
- I. Flett. Report on Myall Lakes fieldwork, September, 2002.

T1.3.6 Conference abstracts

- Crighton, P.J., Gore, D.B. and Heijnis, H. 2002. The use of 210-Pb to construct a history of post-European sedimentation in a ground tank, Wannara Creek catchment, semi-arid Australia. *7th South Pacific Environmental Radioactivity Association Conference.* Lucas Heights Science and Technology Centre. 13-17 May, 2002. Abstracts, p 27.
- Harle, K.J., Heijnis, H., Zawadzki, A. and Rood, E. 2002. Timber, tin and convicts: evidence for 180 years of colonial impact in western Tasmania, Australia, derived from high resolution

microfossil records. *3rd International Congress on Environmental Micropaleontology, Microbiology and Meiobenthology*. Vienna, Austria, 1-6 September 2002. Abstracts, p. 97-98.

- Harrison, J., Heijnis, H., Harle, K.J., Colliton, J.P., Organo, R.J. and Rainbow, C.M. 2002. Urbanisation and mining: the effect on Sydney's drinking water catchment. *7th South Pacific Environmental Radioactivity Association Conference.* Lucas Heights Science and Technology Centre. 13-17 May, 2002. Abstracts, p 25.
- Heijnis, H., McMinn, A. and Hallegraeff, G. 2002. The use of ^{210}Pb, ^{226}Ra and ^{13}Cs profiles in marine sediments to assess the sudden occurrence of a toxic dinoflagellate species in Australian waters. *7th South Pacific Environmental Radioactivity Association Conference.* Lucas Heights Science and Technology Centre. 13-17 May, 2002. Abstracts, p 34.
- Jenkinson, A., Chenhall, B., Chisari, R., Fitzgerald, F., Heijnis, H., Illott, P., Jones, B. and Noakes, A. 2002. Pollution history of some catchments from southeastern New South Wales, Australia. *7th South Pacific Environmental Radioactivity Association Conference.* Lucas Heights Science and Technology Centre. 13-17 May, 2002. Abstracts, p 24.
- McOrist, G.D., Chisari, R. and Jenkinson, A.V. 2002. Gamma-ray spectrometric analysis of environmental samples at ANSTO. *7th South Pacific Environmental Radioactivity Association Conference.* Lucas Heights Science and Technology Centre. 13-17 May, 2002. Poster abstracts, p 92.
- Mokhber-Shahin, L. and Zawadzki, A. 2002. ANSTO environmental Alpha spectrometry facility. *7th South Pacific Environmental Radioactivity Association Conference.* Lucas Heights Science and Technology Centre. 13-17 May, 2002. Poster abstracts, p 93.

T1.3.7 Theses

- C. Agnew. 2002. Recent sediment dynamics and contaminant distribution following bushfire in the Nattai River Catchment, NSW. *Unpublished Honours Thesis.* Environmental Science, Wollongong University.

T1.3.8 International contributions - HITE

The conference abstracts from the Archives of Human Impact of the Last 200 Years Conference held at AINSE and ANSTO in July 2001 were sent to the HITE organisers and are now posted on the HITE web site. A series of photos of key sites and summaries of case studies were also sent. A more comprehensive report will be submitted to AINSE when results are more finalised.

T1.4 Task 1 summary and future directions

- Work is well underway on identifying the spatial and temporal extent, direction and range of trace element transport across Tasmania through analysis of lake sediments;
- A follow up investigation of sedimentation and pollution in the Nattai River catchment following the devastating 2001 bushfires in the region has been completed;
- The project has been extended to include investigations of evidence of human impacts in the highly sensitive and ecologically important Great Lakes of coastal NSW. This has involved the expansion of our collaboration to include Geoscience Australia;
- Contributions have been made to the IGBP HITE project. Further contributions will be made as the evidence gathered is drawn together and interpreted;
- Over the coming year, focus will be placed on completion of the investigation of the extent of aerial transport of trace elements across Tasmania over the last 200 years as well as evidence for human activity and impacts on the Great Lakes region of NSW. Further investigation of potential climate signals from sites in northern Australia will also be made.

Task 1 – Natural Archives

Task 2: Present – Characterisation of the global atmosphere using radon and fine particles

T2.1 Research objectives and outputs

The overall goals that span the life of this project component have been elaborated upon in previous progress reports (HACV, 2001; HACV, 2000; HACV, 1999). The objectives and outputs discussed in this progress report pertain only to the past 12-month reporting period.

T2.1.1 Research objectives

ACE-Asia

- Provide continuous, hourly, high sensitivity atmospheric radon concentration data at three sites in southeast Asia for the duration of the ACE-Asia campaign for (i) the experimental estimation of baseline atmospheric conditions, (ii) regional greenhouse gas inventories, (iii) advanced aerosol sourcing and (iv) the evaluation of regional and global atmospheric models;
- Analyse and interpret the first complete year of data from each of the ACE-Asia sites, identify seasonal trends and contrast them between all sites;
- Quantify atmospheric fine particle concentrations and their major components for at least the first 12-months of measurements at the ACE Asia sampling sites.
- Identify and characterise significant PM2.5 and PM10 pollution and soil events transported from mainland China to ACE Asia sites, particularly during the intensive operation period.

Longer term monitoring

- Provide continuous, hourly, high sensitivity radon concentration time series at several baseline stations suitable for model validation/evaluation studies;
- Perform air mass characterisation at these baseline stations for the identification of minimally perturbed oceanic air masses to compliment concurrent aerosol and trace gas observations (determine thresholds and their seasonal trends);
- Characterise radon concentrations and source terms in the remote marine environment to provide better constraints for atmospheric models;
- Characterise atmospheric fine particle concentrations, understand their regional and seasonal variations and trends and develop source fingerprints so quantitative source apportionment can be achieved.

T2.1.2 Summary of outputs

ACE-Asia

- More than 12 months of continuous, high sensitivity, hourly atmospheric radon concentration data is now available from each of the ACE-Asia sites;
- The first 12 months of radon data from each of the ACE-Asia sites has been analysed. This includes characterisation of diurnal and seasonal cycles; characterisation of the angular distribution of radon; determination of recent continental event radon thresholds and their seasonal variability; determination of some initial radon-based benchmarks for model evaluation; and quality control of time-series data for comparison with model output.
- Portable radon calibration units at Kosan, Hok Tsui and Sado Island have all been upgraded to the current standard design;

- The Hok Tsui and Kosan radon detectors were visited for general maintenance and recalibration (this is in addition to routine monthly maintenance by local staff as required following monthly quality control checks of data);
- Aerosol data at 5 sites, Hong Kong, Cheju Island, Manila, Hanoi and Sado Island, have been analysed for the initial 12 month sampling period. Major components related to industrial pollution and soil sources in China have been identified and quantified. Regional and seasonal variations and trends have been measured and compared across more than 2.8Mk^2 of the sampling area.

Longer term monitoring

- A complete overhaul and recalibration of the Australian National Antarctic Research Expeditions (ANARE) Macquarie Island radon detector was conducted in March 2002. The replacement meteorological crew was trained in operation and maintenance of the detector;
- Processing of the Cape Grim Baseline Atmospheric Pollution Station (CGBAPS) radon data was extended to 2001. A description of the extended dataset and an investigation of radon based benchmarks for atmospheric model evaluation was submitted to the Journal of Environmental Radioactivity;
- Improved characterisation of radon sources in the remote marine environment. A new method to estimate regional oceanic radon fluxes (as well as their seasonal variability associated with changes in wind speed) was derived using the extended CGBAPS radon dataset and applied to the Southern Ocean. These finding are being prepared for submission to the Journal of Geophysical Research;
- Radon and meteorological data from the Mauna Loa Observatory for 2001 have been analysed to supplement data from the newly installed ACE-Asia radon detectors.

T2.2 Background

Radon is a naturally occurring radioactive gas with unique physical characteristics that are frequently exploited for atmospheric research. Radon is chemically inert and not susceptible to wet/dry atmospheric removal processes (Jacob and Prather, 1990; Li and Chang, 1996), so its predominant sink is radioactive decay. The well-defined source and sink pathways of radon make it an ideal tracer of atmospheric dynamics. Terrestrial sources of radon are 2-3 orders of magnitude larger than oceanic sources (Wilkening and Clements, 1975) and are relatively consistent regionally, which enables the clear distinction of air masses of either continental or marine origin. The half-life of radon (3.8 days) is comparable with the lifetimes of short-lived atmospheric pollutants and residence times of water and aerosols. This time scale is also comparable to many important aspects of atmospheric dynamics.

High resolution, high sensitivity ANSTO radon detectors are presently in operation at numerous sites around the world. Some of these detectors are intended for long-term operation (eg. at the Global Atmospheric Watch baseline stations Cape Grim, Tasmania; Mauna Loa, Hawaii; Cape Point, South Africa, and the ANARE baseline stations Macquarie Island, and Mawson Base, Antarctica), whilst others are campaign oriented (eg. the ACE-Asia detectors at Hok Tsui, China; Kosan, South Korea and Sado Island, Japan).

The primary purpose of long-term radon observations at baseline stations is for the identification of baseline atmospheric conditions (air masses representative of a minimally perturbed oceanic fetch). This is necessary for the accurate quantification of seasonal, and interannual trends in global mean atmospheric constituents as well as the enhancement of atmospheric constituents as a result of local/regional sources. Over the past decade, the continuous long-term radon time series at baseline stations have also been used for the evaluation of transport and mixing schemes in regional and global models (e.g. Genthon and Armengaud, 1995; Jacob *et al.,* 1997; Dentener *et al*., 1999).

At present there are several ANSTO radon detectors and PM2.5/PM10 aerosol samplers deployed for shorter-term operation as part of the Aerosol Characterisation Experiment in eastern Asia (ACE-Asia) initiated by the International Global Atmospheric Chemistry Project (IGAC). ACE-Asia is a multinational research effort that aims to reduce the uncertainty in radiative forcing of aerosols on global climate by investigating the source and evolution of aerosols in eastern Asia and the northwest Pacific. In addition to identifying reference (baseline) conditions at each site, and providing a tool with which to evaluate some atmospheric models used in this study, radon measurements will be used for air mass source characterisation and inventory analysis of select greenhouse gases.

Fine particle sampling at our suite of sites across Asia will be used to better understand and quantify movement of aerosols from industry in eastern China and soil from the northern regions near the Mongolian-Chinese border across international borders east into Korea and as far as Japan and south in Vietnam and across to the Philippines. With quantitative concentrations at this broad range of sites, models based on emissions inventories can be compared with seasonal trends and regional differences measured at our ground based sites during the study period.

T2.3 ACE-Asia campaign

In collaboration with the respective international teams (Table 2.1), ANSTO is currently monitoring atmospheric radon concentrations and/or aerosols (particulate matter of diameter 2.5μm and 10μm; PM2.5 and PM10 using ASP and GENT units) at 6 ground stations as part of the ACE-Asia campaign. For further information regarding the background and objectives of ACE-Asia, as well as the choice of measurement locations and commissioning of detectors, please refer to HACV (2001).

Table 2.1: Task 2 related ACE-Asia sites, measurements, collaborators and their affiliation.

Station name/ Location	Collaborator(s) and Affiliation	Comments
Hanoi, Vietnam	Pham Duy Hien (Vietnam Atomic Energy Scientific Board, Ministry of Science, Technology and Environment, Hanoi)	Dedicated ACE-Asia site; 21°01'N, 105°51'E; ASP (ASP65) sampler only;
Hok Tsui/Hong Kong Is., Hong Kong, China	Tao Wang and Steven Poon (Hong Kong Polytechnic University, Hong Kong)	Dedicated ACE-Asia site; 22°12'N, 114°15'E; radon, ASP (ASP60) and GENT (GAS61) observations;
Kosan/Cheju Is., South Korea	Chang-Hee Kang (Cheju National University, Cheju), Jiyoung Kim and Hye-Joung Shin (Meteorological Research Institute, Soul)	Dedicated ACE-Asia site; 33°18'N, 126°09'E; radon, ASP (ASP60) and GENT (GAS61) observations;
Sado Is./Sea of Japan, Japan	Mitsuo Uematsu and Kiyoshi Matsumoto (University of Tokyo)	Dedicated ACE-Asia site; 38°12'N, 138°21'E; radon, ASP (ASP60) and GENT (GAS61) observations;
Manila, The Philippines	Flora Santos (Philippines Nuclear Research Institute)	Dedicated ACE-Asia site; 14°39'N, 121°03'E; ASP (ASP59) and GENT (GAS62) observations;
Mauna Loa Observatory, Hawaii, USA	John E Barnes and Paul Fukumura-Sawada (CMDL/NOAA)	Existing Global Atmospheric Watch Baseline Monitoring site; 19°28'N, 155°36'W; radon observations;
NOAA research vessel R/V Ron Brown, Based in Seattle, Washington, USA	Jim Johnson and Tim Bates (PMEL/NOAA)	Not presently operational; Mobile platform deployed for the ACE-Asia intensive operation period March-May 2001; radon observations;

Task 2 – Characterisation of the global atmosphere

The Task II component of HACV (2001) focussed on preliminary findings from only the two longest running new ACE-Asia sites (Hok Tsui and Kosan). At that time neither station had been operational for a complete year, and only 9 months (Dec-2000 to Aug-2001) of data had been analysed for each site. This report summarises the first complete year of observations at all sites. The specific period of interest is January to December 2001, with the exception of Sado Island for which data is presently only available for the 12-month period September 2001 to August 2002. Detailed analysis cannot be completed to the most recently available radon data (January to September 2002) for Hok Tsui and Kosan since the meteorological data has not yet been made available.

Throughout this chapter when reference is made to seasons, they are defined as follows: Winter (December to February); Spring (March to May); Summer (June to August); Autumn (September to November).

The core research collaborative team formed in 1999/2000 has remained the same throughout 2001/2002, although there have been some additions as a result of staff relocations in the Meteorological Research Institute (Korea) and CMDL/NOAA. A summary of the present list of collaborators and their affiliations is shown in Table 2.1.

T2.4 Progress: ACE-Asia aerosol monitoring

The uncertainty in fine particle aerosol concentrations and chemistry significantly limits our ability to assess the effect of natural and human induced changes on global climate forcing (IPCC, 1995) and human health (Dockery, 1993). Since the beginning of 2001 we have been regularly monitoring both fine (PM2.5) and coarse (2.5µm to 10µm) size fractions in collaboration with researchers from Australia, Hong Kong, Korea, Philippines, Vietnam and Japan as part of a five year Aerosol Characterisation Experiment in Asia called ACE Asia (Arimoto et al., 1999). Accelerator based ion beam analysis (IBA) techniques, described previously, (Cohen *et al*., 1996, 2000; Cohen, 1998; Cohen and Gras, 1998; Cohen, 1999) have been used to quantify and characterise aerosols collected on filters at sites in these five Asian countries during 2001.

T2.4.1 Sampling and sites

Two different types of sampling unit were used in this study, the ASP PM2.5 fine sampler (Cohen *et al*., 1996), based on the US IMPROVE cyclone system (Malm *et al*., 1994) and the GENT stacked filter unit (SFU) with a coarse (2.5µm to 10µm) and a fine (less than 2.5µm) 47 mm Nuclepore filter (Hopke *et al*., 1997; Maenhaut *et al*., 1993). The ASP sampler used a 25 mm stretched Teflon filter and had a flow rate of 22 l/min, the GENT sampler used a flow rate of 16 l/min.

The ASP samplers were used to fully characterise the fine fraction (PM2.5) as collection on Teflon substrate allowed for excellent 'mass closure' (Cohen *et al*., 1996, 2000; Cohen and Gras, 1998). Data from the GENT sampler primarily provided [PM10/PM2.5] ratios for the total masses and elemental and chemical species measured. PM10 concentrations were obtained by the addition of the fine (PM2.5) and the coarse (2.5µm to 10µm) fractions.

The locations and equipment at the sampling sites are summarised in Table 2.1. At the Manila site, samplers are located 13 km NE of central Manila. For this study sampling commenced on 16 January 2001. At Hok Tsui, samplers located on the SE corner of Hong Kong Island at Cape D'Aguilar, 60 m above sea level on a cliff facing the South China Sea. The population density on the Cape is relatively low and the closest industrial town is Chai Wan 10 km to the NW. Prevailing winds for this site are E-SE in the summer (June to August) and N-NE in the winter (December to February) bringing pollution from the Chinese mainland. For this study sampling commenced on 3 January 2001. At Cheju Island, samplers are located on the western coast of the Island, facing the Chinese mainland across the Yellow Sea. The island is approximately

480 km south of Seoul. For this study sampling commenced on 30 March 2001. At Hanoi, the sampler is located outside Hanoi, 100 km west of the South China Sea and NE of central Hanoi in an urban/ industrial area. A GENT sampler data was not reported here as similar data for Vietnam has been reported previously by Hien *et al*., (2002). For this study sampling commenced on 25 April 2001. At Sado Island, samplers are located on the north western coast of the Island off the western coast of central Japan, atop a 90 m cliff facing the Korean mainland across the Sea of Japan. The island is approximately 304 km NW of Tokyo. For this study sampling commenced somewhat later than the other sites on 16 September 2001. These five sites within east and south east Asia cover a triangular area bordered by Hanoi, Sado and Manila of approximately 2.8Mkm^2.

Where possible samples were generally collected over a 24 hour period from midnight to midnight every Wednesday and Sunday throughout the year. For some sites during heavily polluted periods samplers were operated on a two hours on two hours off basis over the 24 hour collection period to avoid reduced flow rate and filter clogging problems.

T2.4.2 Results and discussion

The Teflon and Nuclepore filters collected were posted to Australia for analysis at ANSTO. During the twelve-month sampling period 249, 327, 237, 68 and 91 filters were analysed from the Manila, Hong Kong, Cheju Island, Hanoi and Sado Island sites respectively. Each filter was weighed to ±2µg before and after exposure to determine the total particulate mass deposited. Standard He/Ne laser (wavelength 633nm) absorption techniques were used (Cohen *et al*., 2000) to measure the elemental carbon concentration, assuming a mass absorption coefficient of 7 m^2/g.

IBA techniques (Cohen *et al*.,1996; Cohen,1998) were used to determine H, C, N, O, F, Na, Al, Si, P, Si, Cl, K, Ca, Ti, V, Cr, Mn, Fe, Co, Ni, Cu, Zn, Br and Pb at concentrations with sensitivities close to or below 1ng/m^3. The measurement of so many different elemental species allowed estimates of the significant aerosol components to be made in the standard way (Malm *et al*.,1994). For example, soil was estimated from the five key elements Al, Si, Ca, Ti and Fe assuming they occurred in their oxide states, ammonium sulfate from sulfur assuming the sulfate ion was fully neutralised, sea salt from Na and Cl concentrations and organic matter from the hydrogen, not associated with ammonium sulfate, assuming an average organic matter composition of 9%H, 20%O and 71%C. These five major components generally accounted for 70% to 95% of the fine (PM2.5) gravimetric mass.

PM2.5 data

The 24-hour average daily mass concentrations for each of the five sites during the sampling period are shown in Figure 2.1. Each of the graphs has the same vertical mass scale except for the Sado Island site, which was a more remote site and experienced lower mass concentrations. The US EPA PM2.5 goal is 15 µg/m^3 for the annual average and 65 µg/m^3 for 24 hour maximum. All sites, except the Sado site exceeded both these goals. At each site the daily variations were large and varied by a factor of 5 or more.

Seasonal variations of a factor of 2 to 5 are also obvious, particularly in the longer-term records at the Manila, Hong Kong and Cheju Island sites. Hien *et al*., (2002) report annual PM2.5 values between 33 µg/m^3 and 36 µg/m^3 for the past three years at Hanoi totally consistent with the data of Figure 2.1d.

Table 2.2 shows the annual average concentrations of the major aerosol components for the fine fraction for each site. The sum of all measured components lies between 74% and 96% of the measured gravimetric mass. Demonstrating the good mass closure obtained for this data.

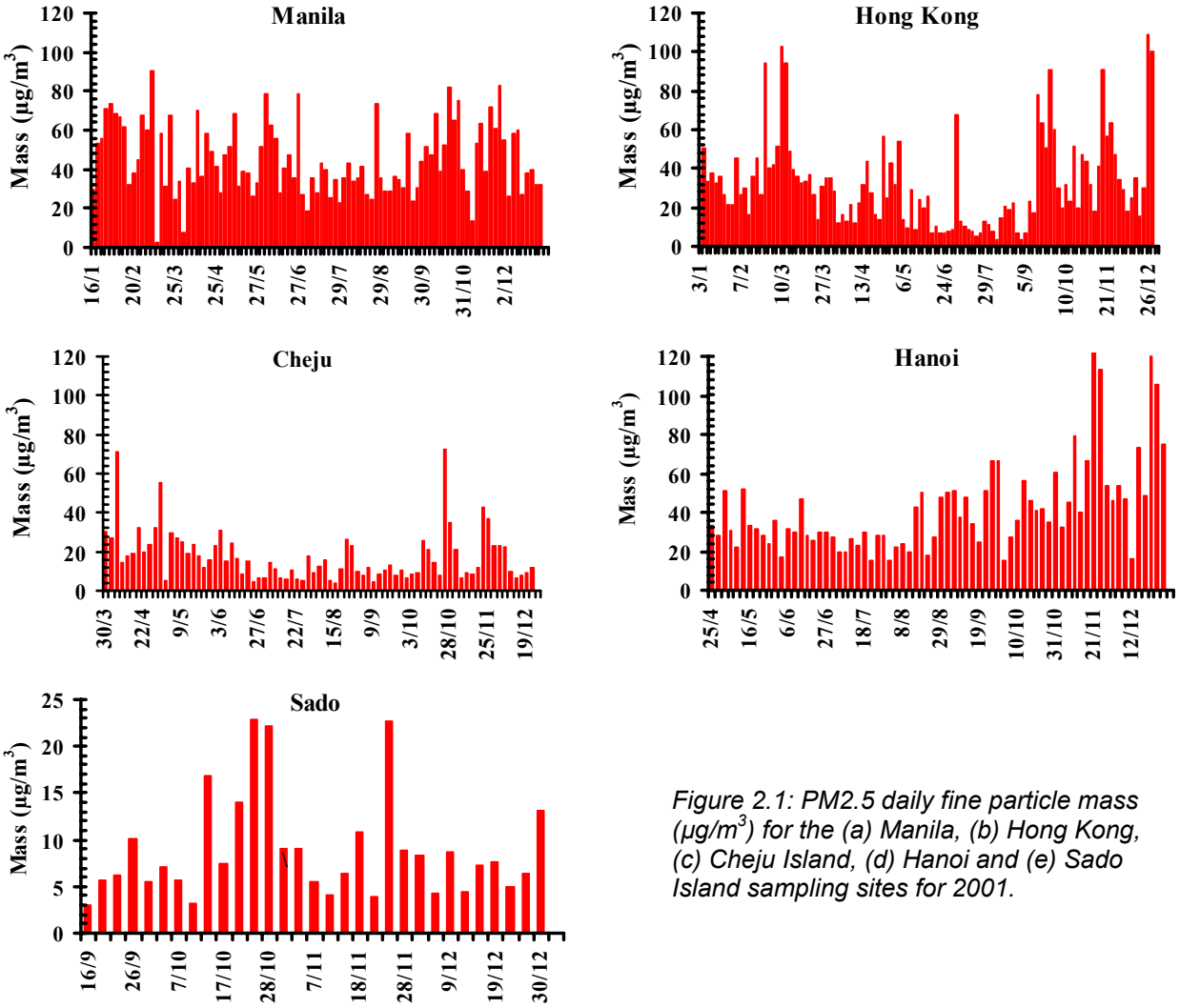

Figure 2.1: PM2.5 daily fine particle mass (µg/m^3) for the (a) Manila, (b) Hong Kong, (c) Cheju Island, (d) Hanoi and (e) Sado Island sampling sites for 2001.

The 4% to 26% missing mass was mainly water vapour and nitrates. The IBA measurements were performed in vacuum, hence all water vapour was lost during analysis and nitrates were not measured and are not well held on Teflon filters. The errors quoted are the standard deviations for the sampling period. These were large because of the large daily variations as demonstrated by the plots of Figure 2.1. Measurement errors were much smaller typically ±5% to ±15%. Trace elements were calculated from the sum of P, V, Cr, Mn, Co, Ni, Cu, Zn, Br and Pb. Non soil K was an estimate of potassium associated with smoke and biomass burning. The urban site of Manila had the highest organic matter and elemental carbon but the lowest smoke (non soil K) probably associated with the combustion of organic material not related to vegetation burning.

The percentage of Cl loss was calculated by subtracting the Cl associated with seasalt from the total measured Cl. Chlorine has several sources besides seasalt (automobiles, industry etc). The fact that the Cl loss, in the fine fraction, was large at all sites can be explained by the relatively high percentage of sulfate present at all sites. Cl loss correlates well with high sulfate concentrations. The 65%-96% Cl loss in the PM2.5 fraction reported here was significantly higher than the 15%-16% reported by Cheng *et al*., (2000) for PM10 at the same site.

Soil is a key component in aerosols in the Asian region (Arimoto *et al*., 1999). In particular fine soils can be transported many hundreds if not thousands of kilometres from their source. Northwestern China and the Gobi Desert region are known sources of 'yellow dust' across our sampling region at particular times of the year. If the soil component measured at each of our

five sites originated from a similar source then we would expect it to have similar elemental characteristics.

Table 2.2: Annual average concentrations of the major aerosol components for the fine fraction for each site.

PMPM2.5	Manila	Hong Kong	Cheju Island	Hanoi	Sado
EltC (%)	28±11	7.0±5	8.3±7	8.1±3	8.8±4
Soil (%)	2.74±2	7.5±9	10.4±18	10.5±9	5.36±5
Amm. Sulfate (%)	16±8	40±26	43±25	25±12	39±28
Organics (%)	45±22	19±24	11±17	25±14	7.9±14
Seaspray (%)	3.39±3	9.5±7	8.3±6	2.44±2	14±10
Trace Elt (%)	0.63±0.3	0.79±0.3	0.46±0.2	1.65±2	0.39±0.1
Non Soil K (%)	0.46±0.4	1.41±1.5	0.86±1.0	1.24±0.6	0.92±0.9
Sum (%)	96±47	85±72	82±77	74±42	77±62
Av. Mass (μg/m^3)	45±18	31±22	18±13	42±26	8.9±6
Max. Mass (μg/m^3)	90	109	73	155	23
Cl loss (%)	83±29	89±19	96±11	83±18	65±36

Figure 2.2 is a correlation plot for the five major soil components used here for all sites during the 2001 sampling period. It shows remarkably consistent correlations for all elements across all five sites. Suggesting a similar and common soil component for the region. Elements associated with Ca have the largest spread suggesting that at least one of the sites has more than one source of Ca (cement production or construction activities maybe).

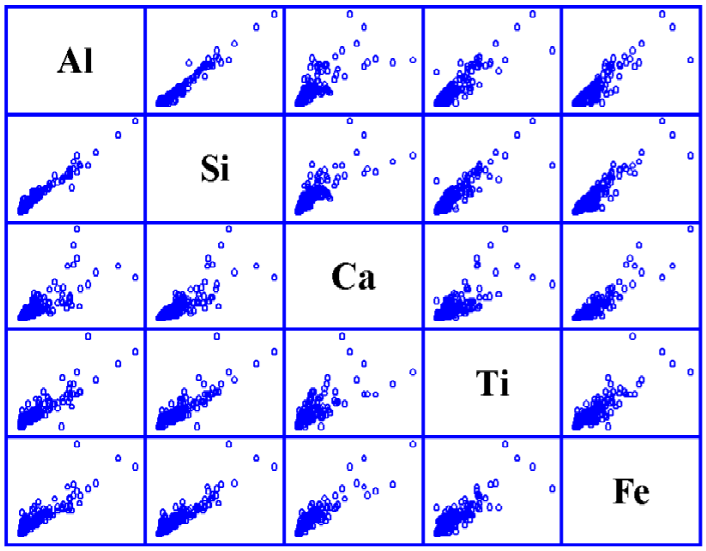

Figure 2.2: Correlation plot for the five major soil components for all sites for PM2.5 data taken during 2001.

Temporal variations of the PM2.5 soil component show similar correlations between sites as demonstrated by the monthly average box and whisker plots of Figure 2.3 for the Hong Kong and Cheju Island sites, for example. The box encloses the middle 50%, the horizontal line in the box represents the median. Each whisker is drawn from the 1st and 3rd quartile to the smallest or largest point 1.5 inter-quartile ranges from the box. Outliers outside the whiskers are plotted separately as filled circles. The + symbol inside the box represents the mean.

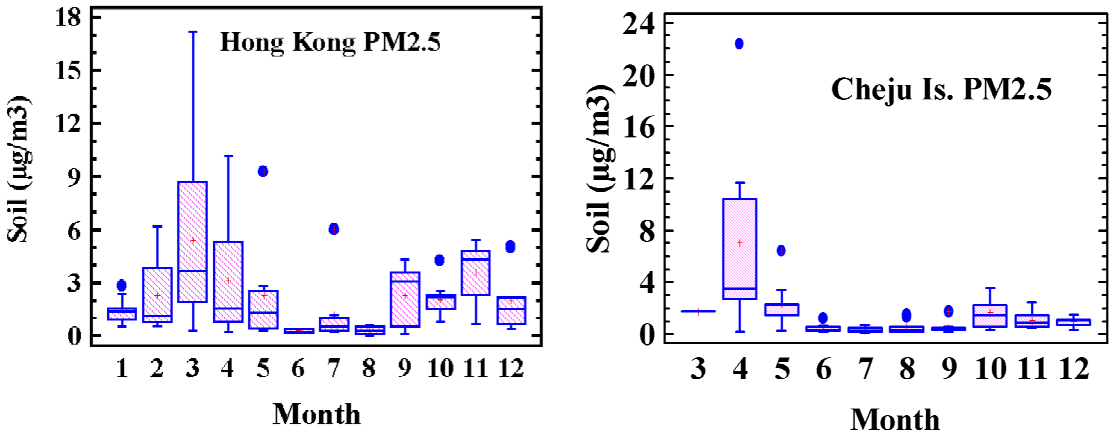

Figure 2.3: Box and whisker plots for monthly average PM2.5 soil at Hong Kong and Cheju Island sites for 2001.

The Hong Kong and Cheju Island sites are some 1,800 km apart, but both showed significant increases in soil in the months of April, September and October. In particular, the 7 to 18 April 2001 was an exceptional period at both these sites. On 13 April the PM2.5 masses were 32µg/m^3 and 71µg/m^3 and the soils were 10.2µg/m^3 and 22.3µg/m^3 at the Hong Kong and Cheju Island sites respectively. That is, the soil fraction of the fine component at both these sites was 32% of the total fine mass on this day, far in excess of the mean values quoted in Table 2.2.

Figure 2.4 is a five day back trajectory plot from the NOAA Air Resources Laboratory for the Hong Kong site for air masses originating at three heights 100m, 200m and 500m above sea level for 12 April 2001 showing clearly that dust from the central and western regions of China would impact on the Hong Kong site after only a couple of days. However, this could only happen with fine particles, large or coarse particles would not be transported over these large distances.

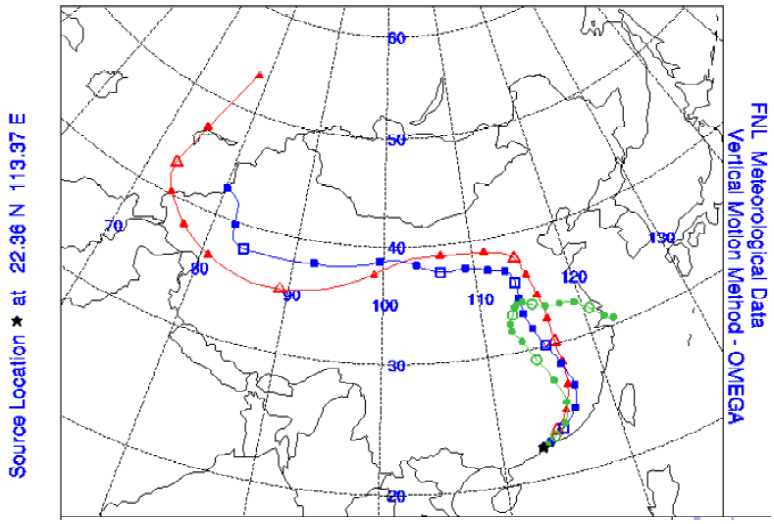

Figure 2.4: NOAA Air Resources 5 day back trajectory plot from Hong Kong for 12 April 2001, triangles 100m, squares 200m and circles 500m above seas level.

Ammonium sulfate was the major component at all of the sites except Manila. In the fine fraction it is typically anthropogenic and has several sources including automobiles, coal and oil combustion and industry. It was estimated from the total sulfur concentration assuming the sulfate ion was fully neutralised. This assumption does not hold at all sites at all times, as suggested by the large chlorine loss which requires significant acidic aerosols as discussed earlier. The Hong site had one of the consistently largest average percentage sulfate concentrations (40±26)% with a PM2.5 total mass of (31±22) µg/m^3. Figure 2.5 is a box and whisker plot for the average monthly ammonium sulfate concentration at Hong Kong during the study period. It shows strong seasonal variations having maximum concentrations with large excursions in the winter periods and minimal concentrations in the summer.

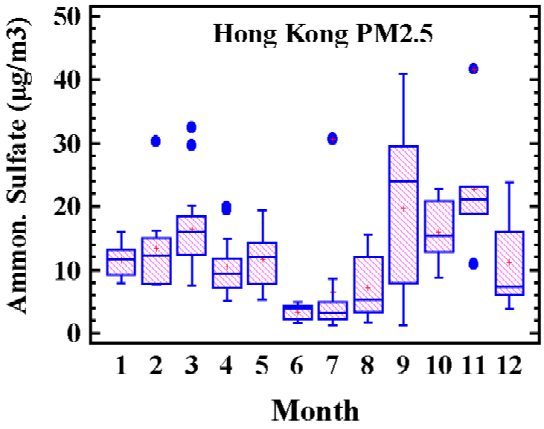

Figure 2.5: Box and whisker plots for monthly average PM2.5 ammonium sulfate at Hong Kong for 2001.

Elemental carbon is a key component of many combustion products such as coal, oil and vegetable matter. For sulfur containing products such as coal or oil we would expect elemental carbon to correlate with sulfur. Figure 2.6 is a plot of elemental carbon against sulfur for all sites during the study period. There are two distinct data groups, those with elemental carbon associated with sulfur and those with excess elemental carbon not associated with sulfur. For the first group the correlation is good with EltC =(0.695±0.024)*S and a correlation coefficient of R^2=0.78. The bulk of the points with large elemental carbon (EltC > 6 µg/m^3) and low sulfur originated from the Manila data, demonstrating that elemental carbon in Manila is not dominated by coal or oil combustion products.

Fine K is a recognised tracer for biomass mass burning (Cohen *et al*., 1996, Malm *et al*., 1994). Figure 2.7 is a plot of fine potassium against elemental carbon for all sites. Again there are two distinct groups of data, namely, elemental carbon associated with vegetation burning with EltC=(887±66)+(2.39±0.11)*K with R^2=0.66 and, excess elemental carbon not associated with fine K.

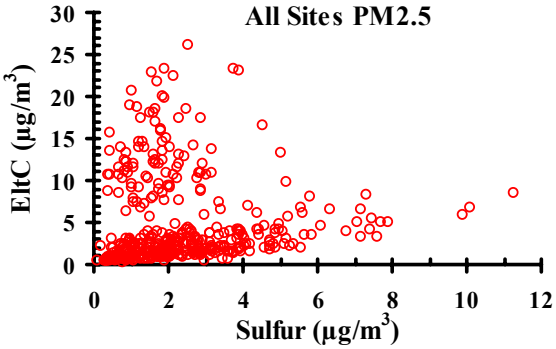

Figure 2.6: A plot of elemental carbon against sulfur for all sites during the study period.

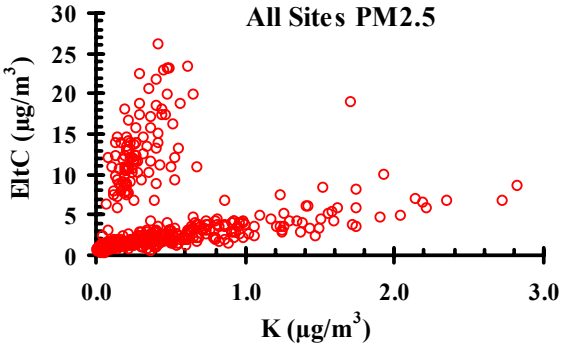

Figure 2.7: A plot of fine potassium against elemental carbon for all sites.

Again the second group with high elemental carbon above 6 µg/m^3 was associated mainly with data from Manila site, demonstrating that the elemental carbon at Manila was not dominated by smoke from vegetation burning.

Figure 2.8 shows a similar plot of elemental carbon against estimated organic matter. Again there are the two distinct groups, high elemental carbon associated with medium to high organic matter and low elemental carbon associated with low to medium organic matter. The first group is again associated with data from the Manila site and, unlike all other sites, elemental carbon and organic matter in this group were strongly correlated. This group represents sources of combustion of C, H, and O containing compounds. For Manila alone EltC=(0.549±0.018)*Org with an R^2=0.92.

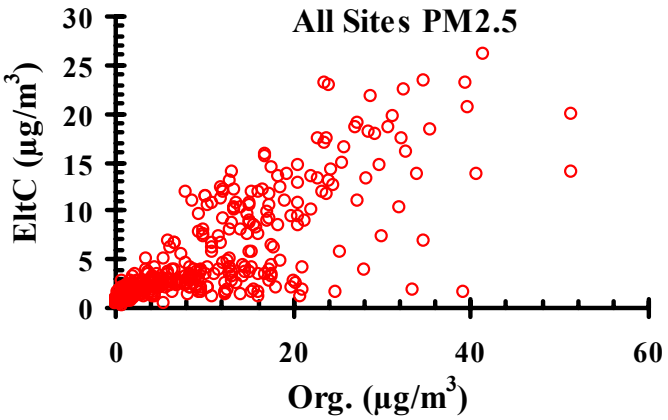

Figure 2.8: A plot of fine organic matter against elemental carbon for all sites.

PM10 Data

Data from the GENT samplers at all sites except Hanoi were used to determine the [PM10/PM2.5] size fraction ratios for the total mass as well as each measured elemental species. The PM10 fraction is obtained by summing the coarse and fine fractions as measured by the GENT samplers. Figure 2.9 is a plot of PM2.5 against PM10 mass fractions for all sites for the study period.

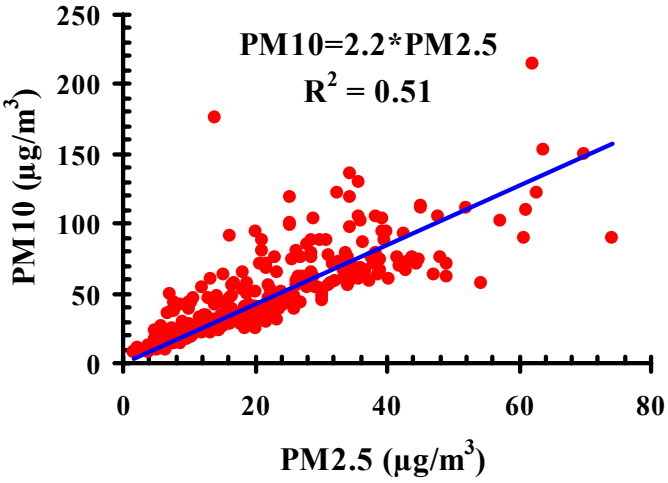

Figure 2.9: GENT sampler PM10 versus PM2.5 data

The correlation is good with the average ratio being [PM10/PM2.5]=(2.2±0.4), demonstrating that on average the fine fraction is about 45% of the PM10 fraction. The high points above the line of best fit with high PM10 values were days associated with the extreme soil events at Hong Kong and Cheju Island in April 2001 previously discussed. As expected these showed a higher coarse fraction.

T2.4.3 Summary

The average PM2.5 aerosol size fractions for five Asian sites have been measured and found at four of the sites to exceed the current US EPA annual and daily goals. Up to 25 different chemical and elemental species have been measured with sensitivities down to 1ng/m^3. Five major components of elemental carbon, ammonium sulfate, soil, organic matter and sea spray were found to account for more than 70% of the total fine particle mass. The [PM10/PM2.5] ratios were very consistent across all sites and seasons being around (2.2±0.4) demonstrating that on average the fine fraction is about 45% of the PM10 fraction.

The data collected to date will put the Project in a strong position to quantitatively determine source fingerprints and relative source contributions to the total PM2.5 and PM10 size fractions across the large Asian regions sampled. One significant Asian dust episode has already been

observed across our sampling region and analysed during February to March 2001. Other dust episodes were observed (but not reported here) in January and February 2002 and are currently being interpreted. This will lead to a better understanding of dust and anthropogenic pollution transported from main land China across Korea and Japan and south into Hong Kong.

T2.5 Progress: ACE-Asia radon monitoring

Firstly, data recovery rates for the year are compared between each site, followed by a brief comparison of site meteorological conditions. Seasonal and diurnal radon trends are then characterised for each site individually. Finally, selected aspects of the results and their implications are discussed in a broader context.

T2.5.1 Data availability

The Mauna Loa Observatory (MLO) is part of the World Meteorological Organisation's (WMO) Global Atmosphere Watch (GAW) station network. Consequently, there is considerable logistical support for the meteorological, radon and other observations being conducted at this site. The mean monthly data recovery rate at MLO for 2001 was 83% (Figure 2.10). This represents the percentage of hourly samples for which there was overlapping meteorological and radon concentration data of acceptable quality.

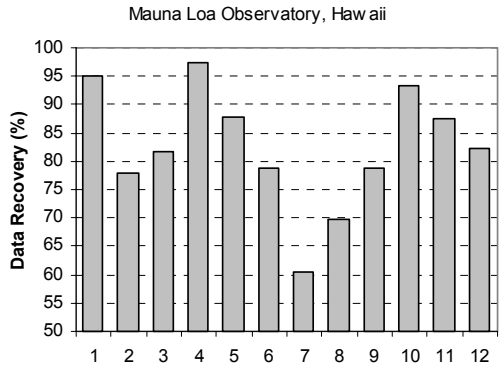

Figure 2.10: Monthly data recovery (%) of overlapping radon and meteorological data at Mauna Loa Observatory, Hawaii.

By comparison, mean monthly data recovery from the east Asian radon monitoring sites that have considerably less logistical support, has been very good (Figure 2.11), 91%, 87% and 98%[1] for Hok Tsui, Kosan and Sado Island, respectively. This is a reflection of both the competency of the local teams, and the reliability of the equipment.

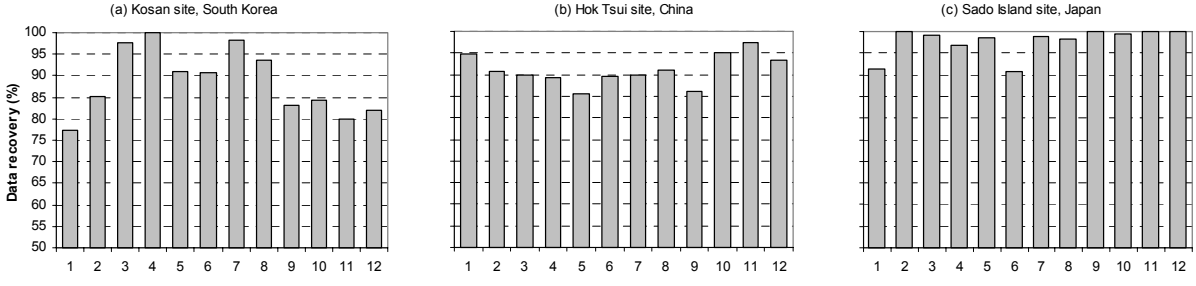

Figure 2.11: Monthly data recovery (%) of overlapping radon and meteorological data at (a) Kosan, South Korea, (b) Hok Tsui, China and (c) Sado Island, Japan.

[1] Radon data only. No overlapping meteorological data has yet been released for this site.

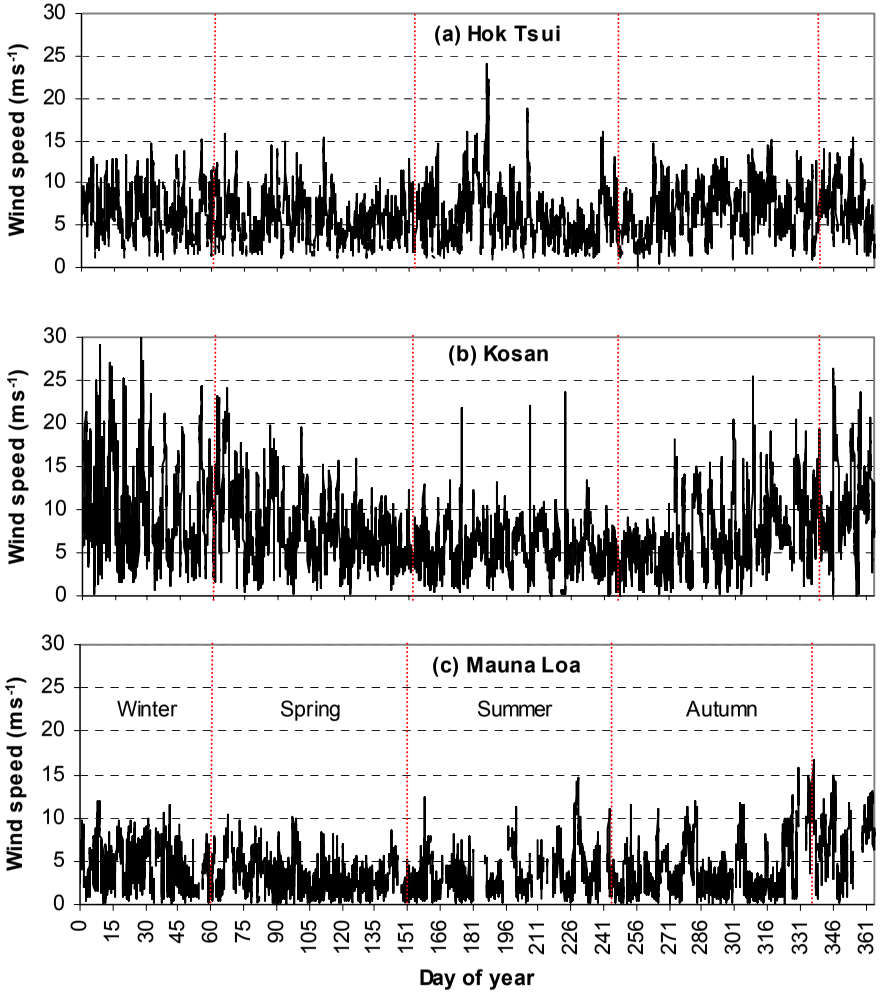

Figure 2.12: Hourly wind speed (ms^{-1}) at selected ACE-Asia sites for 2001.

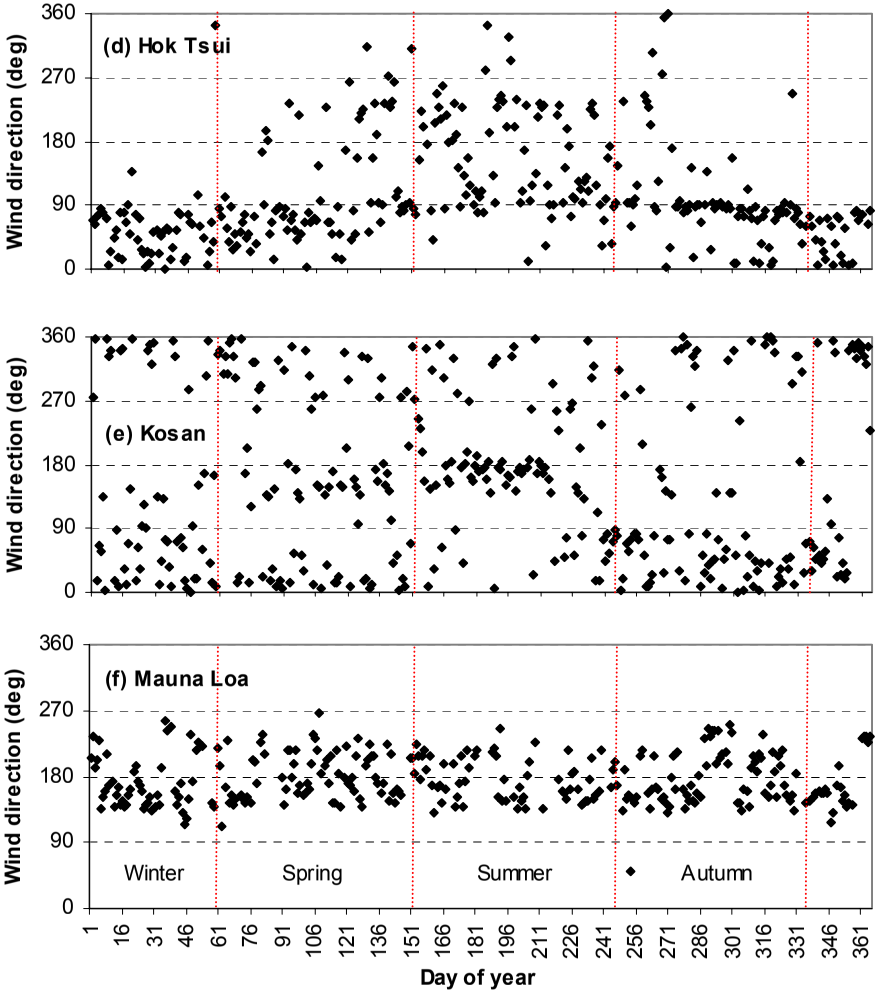

Figure 2.13: Daily wind direction (degrees) at the time of minimum radon concentration at selected ACE-Asia sites for 2001.

T2.5.2 Regional meteorology

Meteorological conditions at each of the radon measurement sites are considerably different (Figure 2.12; Figure 2.13). No meteorological data from Sado Island for the observation period has yet been released. Kosan has the highest mean annual wind speed, and the lowest is at MLO. The most pronounced seasonality in wind speed is observed at Kosan, with the highest mean monthly wind speed in Autumn/Winter and lowest in Spring/Summer (Table 2.3). The same seasonal trend in wind speed is evident at Hok Tsui and MLO, though to a lesser degree.

Although there is a slight preference to southerly wind directions at Kosan in Spring and Summer (Figure 2.13), and northeasterly directions in Autumn and Winter, there is generally a high degree of variability in wind direction at this site regardless of season. In contrast, at Hok Tsui there is a more consistent and gradual change in wind direction from northeast in Winter to southerly in Summer. Wind direction at MLO is constrained primarily to a band between southeast and southwest without a pronounced seasonal trend.

Table 2.3: 2001 seasonal statistics for the ACE-Asia radon detector sites.

Season	Hok Tsui		Kosan		Sado Island		MLO	
	Rn (mBq m^{-3})	WS (ms^{-1})	Rn (mBq m^{-3})	WS (ms^{-1})	Rn (mBq m^{-3})	WS (ms^{-1})	Rn (mBq m^{-3})	WS (ms^{-1})
Winter	8734 ±390	7.0	3027 ±82	10.5	1711 ±53	-	245 ± 8	5.8
Spring	3534 ±203	6.0	2303 ±75	8.1	1284 ±29	-	272 ± 7	3.3
Summer	1284 ±99	6.2	1385 ±91	5.6	1234 ±34	-	178 ± 2	3.5
Autumn	5696 ±271	6.9	2717 ±124	7.1	1392 ±38	-	201 ± 4	3.8

T2.5.3 Hok Tsui radon data

Seasonal variability

There is a pronounced seasonality in observed radon concentration at Hok Tsui (Figure 2.14). The highest values are observed in winter when the near surface winds are strongest (Table 2.3) and predominantly from the continent, driven by the land-sea temperature gradient (winter monsoon). The land-sea temperature gradient reverses in the summer and near surface winds at the Hok Tsui station are predominantly from the ocean (summer monsoon), resulting in lower radon concentrations. Similar seasonal cycles of radon concentration have been reported in Japan/China (Iida *et al*., 2000) and India (Debaje *et al*., 1996). Another factor contributing to lower radon concentrations in the summer months are the monsoonal rains. Increased soil moisture has been shown to reduce the terrestrial radon flux (Jacob and Prather, 1990).

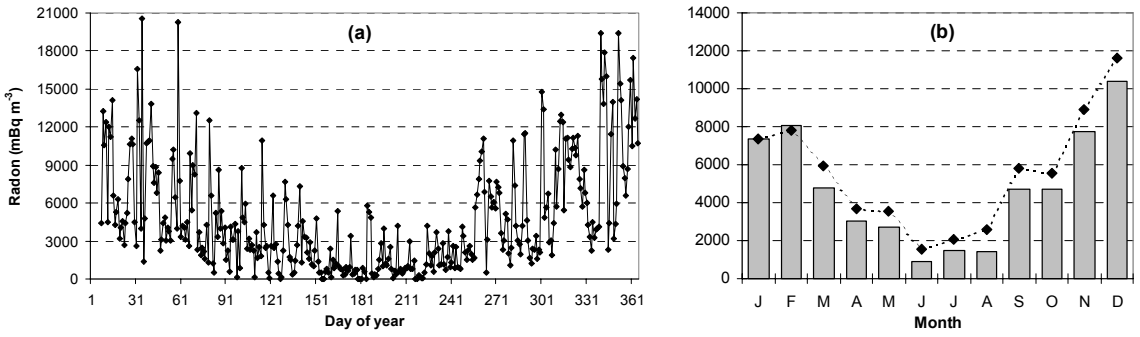

Figure 2.14: (a) Daily minimum radon concentration, and (b) mean monthly radon based on daily minimums (bars) and complete days (diamonds) at Hok Tsui, China, 2001.

Diurnal variability

On shorter timescales, there is also a diurnal trend in atmospheric radon concentrations at Hok Tsui (Figure 2.15a). The diurnal course of radon concentration is characterised by a mid-

morning maximum and a late afternoon minimum. In this case, the dominant influence on the amplitude of the diurnal radon concentration signal is concentration of radon in the nocturnal boundary layer. Assuming a relatively consistent terrestrial source of radon, as the shallow nocturnal inversion layer develops, radon concentrations increase. The converse is true as the convective boundary layer develops in the afternoon. The amplitude of the 2001 composite diurnal signal at this coastal site (1113 mBq m^{-3}) is less than half that observed inland at a site near Tokyo (2560 mBqm^{-3}; Hattori and Ichiji, 1998).

In contrast to the diurnal course of radon concentration near Tokyo, the morning radon maximum at Hok Tsui (Figure 2.15a) is both more prominent, and broader than the afternoon minimum. To investigate this feature further the annual diurnal composite plot was broken down by season (Figure 2.15b). A large difference in mean composite day radon concentration is immediately apparent that reflects the seasonal cycle previously discussed. Although a distinct diurnal trend was observed in each season, the amplitude is maximised in winter (almost 2000 mBq m^{-3}) and minimised in summer (<1000 mBq m^{-3}). This is opposite to the behaviour that would be expected at a continental site given that the depth of the ABL is driven by surface heating. The reason for this is that in Spring and Summer as the Asian continent warms relative to the ocean, winds swing onshore. Consequently, the mixing depth at Hok Tsui during these times is closely linked to that of the surrounding ocean, which is relatively constant. In Winter and Autumn when winds are predominantly offshore, the mixing depth at Hok Tsui is similar to that of the mainland. However, since Autumn and Winter temperatures in mainland China are relatively low, daytime mixing is not intense so dilution within the ABL is not very pronounced compared to the concentration of radon within the shallow nocturnal boundary layer.

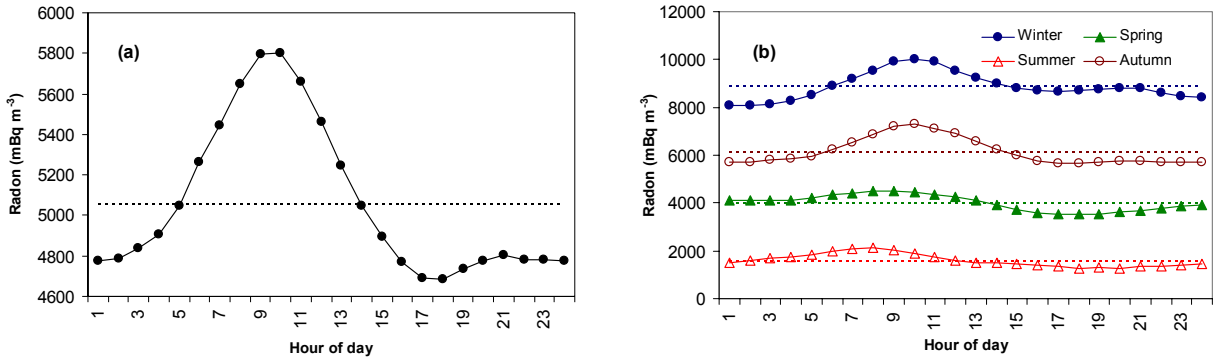

Figure 2.15: Diurnal course of observed hourly radon concentration at Hok Tsui by (a) year and (b) season. Dotted lines represent mean of composite day.

Data selection criteria

Since the vertical resolution of most atmospheric models is insufficient to capture the shallow nocturnal boundary layer, radon concentrations observed in the afternoon, when the boundary layer depth is maximised, are most useful for comparisons (Zahorowski *et al*., submitted). As indicated in Figure 2.15b, the minimum afternoon radon concentration can be quite different to the daily mean. To account for this potential discrepancy between modelled and observed radon concentrations, results presented in Figure 2.14a are averages of observations at 17:00 and 18:00 in the afternoon. The average radon concentration from this two hour period will henceforth be referred to as the "afternoon minimum". As indicated in Figure 2.14b differences of almost 500 mBq m^{-3} can occur between monthly average radon concentrations determined from daily minima and whole days.

Air mass characterisation

The analysis of aerosol and trace gas samples collected at all ACE-Asia sites will rely heavily upon reliable air mass sourcing. The suitability of wind direction for the determination of air mass origin was assessed by investigating the angular distribution of atmospheric radon concentrations. The angular distribution of afternoon minimum radon concentrations at Hok Tsui

for 2001 is presented in Figure 2.16a. Care should be taken with the interpretation of this figure since not all directions are equally represented in this short, 1-year, dataset (Figure 2.16b). In particular the north-west region is poorly represented within this initial year's data. Radon concentration statistics from this quadrant will improve as the length of the dataset is extended.

The angular distribution of radon at Hok Tsui has features that correspond well to the distribution of continental and oceanic fetch for approaching air masses. Excluding the poorly represented NW sector, the maximum radon concentrations are observed from mainland China, secondary peaks to the NE and SW correspond to Taiwan/Japan and Hainan Island/Indochina Peninsula, respectively, and the minimum radon concentrations are observed between 80-220°, the oceanic sector. This indicates that wind direction is a relatively reliable indicator of air mass origin at this site. The contrast in radon concentration between typical oceanic and continental sector air masses is not as stark as at baseline stations such as Cape Grim - radon concentrations from the Hok Tsui oceanic fetch are frequently an order of magnitude greater than from the oceanic sector of Cape Grim.

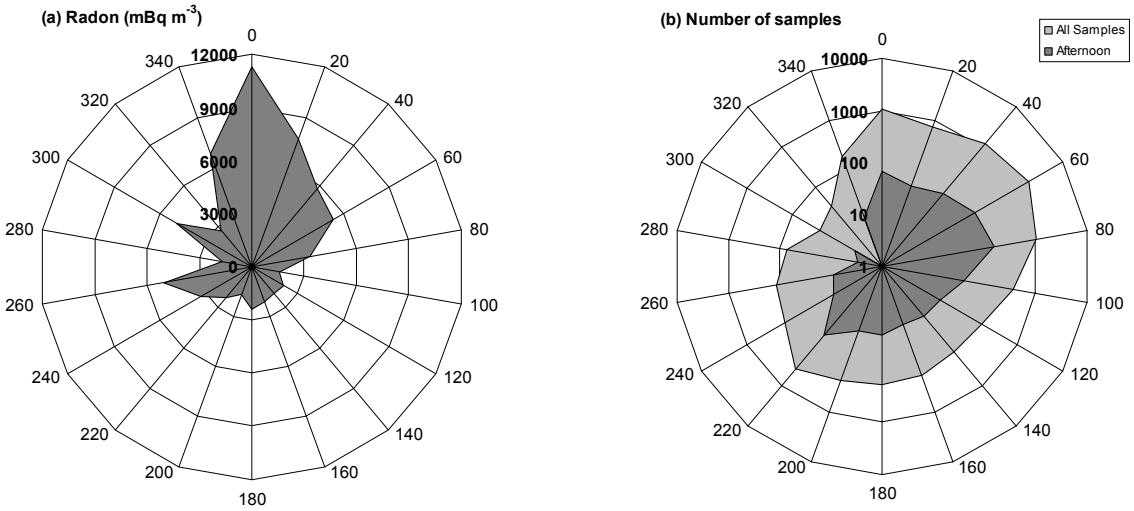

Figure 2.16: (a) Angular distribution (at 20° resolution) of daily minimum radon concentration observations at Hok Tsui, and (b) number of samples as a function of wind direction for complete dataset and afternoon (17:00 and 18:00 samples only). Note the logarithmic scale for the second plot.

Although it has been demonstrated that wind direction is a relatively good indicator of air mass origin at Hok Tsui, the ability of radon observations to unequivocally identify baseline conditions makes it a superior tool for this purpose, particularly if wind directions are close to sector boundaries.

Figure 2.17a demonstrates the ability of the Hok Tsui radon measurements to identify key continental pollution events such as those that occurred in early and mid March.

The radon data was investigated for a suitable baseline indication threshold. Examination of the time series revealed a strong seasonality in the ambient background level. For instance, the monthly 10th percentile radon concentration for February and March, equal to about 3000 mBq m^{-3}, seems to indicate the "cleanest air mass" in that period. However, throughout the year the monthly 10th percentile radon varies a lot as shown in Figure 2.17b (red solid line). This large seasonal variability in radon concentration precludes establishment of a radon baseline threshold as can be determined for remote baseline stations.

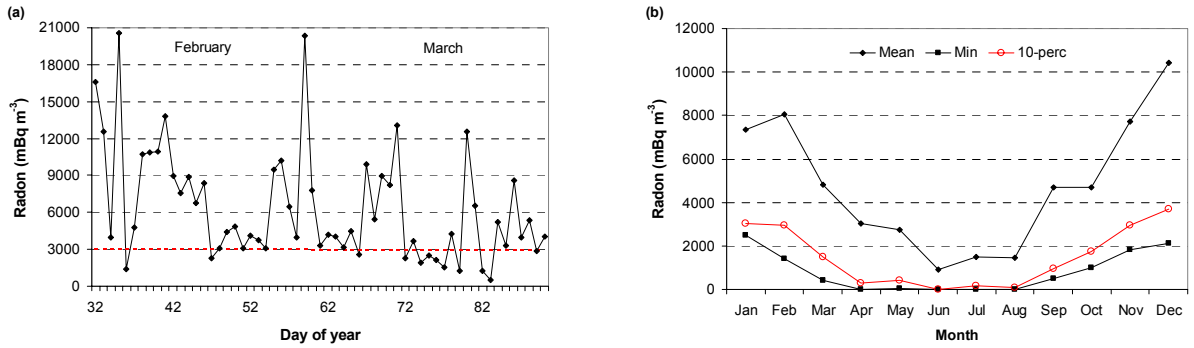

Figure 2.17: (a) Daily minimum radon concentration for Feb/Mar 2001 (solid line) and monthly 10th percentile radon concentration (red dotted line), and (b) monthly median (diamonds), 10th percentile (open circles) and minimum (squares) radon concentration at Hok Tsui.

Model intercomparisons

As well as providing long term, high resolution radon time series that are suitable for atmospheric model validation, further analysis of the ACE-Asia radon dataset can provide a wide range of benchmarks against which model performance may be evaluated. For example, if it can be assumed that the maximum and minimum radon concentrations equate to the longest land and oceanic fetches, respectively, one benchmark would be the distribution of radon concentration within these two 20° sectors as presented in Table 2.4. Such an assumption may not be valid in winter however, if the continental fetch is snow or ice bound. Under such conditions an air mass potentially carrying anthropogenic pollution could have a comparatively low radon concentration.

Table 2.4: The distribution of radon concentrations (mBq m^{-3}) over maximum ocean and land fetches (for number of hourly samples N).

	Ocean	**Land**
# samples	39	68
minimum	<40[f]	2578
10th percentile	368	5792
25th percentile	615	8569
Median	855	10862
75th percentile	2777	13376
90th percentile	3375	19241
maximum	5041	21012

[f] 40mBq m-3 is the lower limit of detection for radon with these detectors.

T2.5.4 Kosan radon data

Seasonal variability

As for the Hok Tsui site, there is also a pronounced seasonality in radon concentrations observed at Kosan. Although the Kosan seasonal pattern is also characterised by a winter maximum and summer minimum, the amplitude of the Kosan seasonal variability is less than at Hok Tsui. This is particularly obvious in the case of the mean monthly concentrations (Figure 2.18b).

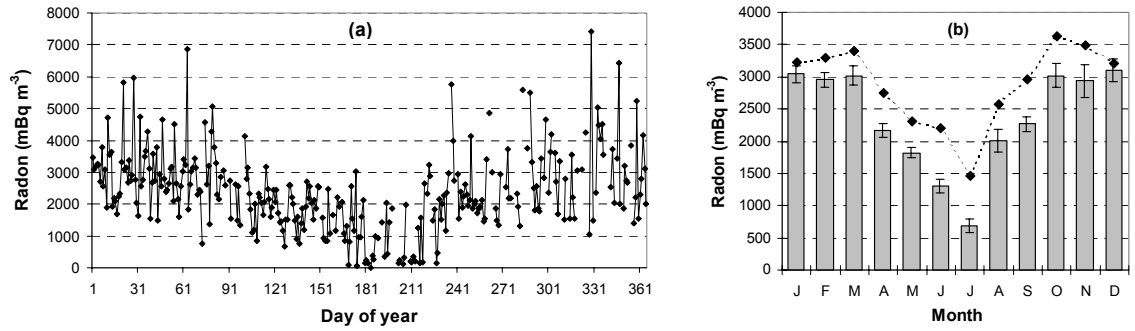

Figure 2.18: (a) Daily minimum radon concentration, and (b) mean monthly radon based on daily minimums at Kosan, South Korea, 2001. Error bars denote standard error.

One reason for this is that Hok Tsui is a coastal site (ie. with an adjacent terrestrial radon source), and Kosan a perturbed marine site (ie. radon can be diluted or decay in transit to the site across the Yellow or East China Seas). Other differences are that the period of low radon concentrations is shorter (one month not three), and the difference in mean monthly radon concentration from October through March is barely significant compared to the standard error of the observations.

Diurnal variability

The diurnal cycle of observed hourly radon concentrations at Kosan based on the annual composite day is characterised by a mid morning maximum and afternoon minimum (Figure 2.19). The amplitude of the Kosan 2001 composite diurnal cycle of radon concentration (1040mBq m^{-3}) is smaller than that of Hok Tsui as would be expected of a perturbed marine site. However, the emphasis in the diurnal trend is shifted from the morning maximum to the afternoon minimum, in closer agreement to the continental diurnal signal reported by Hattori and Ichiji, (1998). This implies that the ABL over this island site is behaving more like that of a continental site than is the case for the Hok Tsui site, which is surprising given its location. Looking at the seasonal breakdown of the diurnal radon signature (Figure 2.19b) the maximum and minimum amplitudes of the diurnal radon cycle occur in summer and winter, respectively, as would be expected of a continental site, opposite to that observed at Hok Tsui. Also evident is the reduced spread in composite daily mean radon concentration in spite of large seasonal changes in wind direction. As indicated in Figure 2.19b, the enhanced radon dilution within the ABL at this site means that differences in excess of 700 mBq m^{-3} occur between daily average radon values and minimum afternoon values. This will be important to take into account for model validation studies.

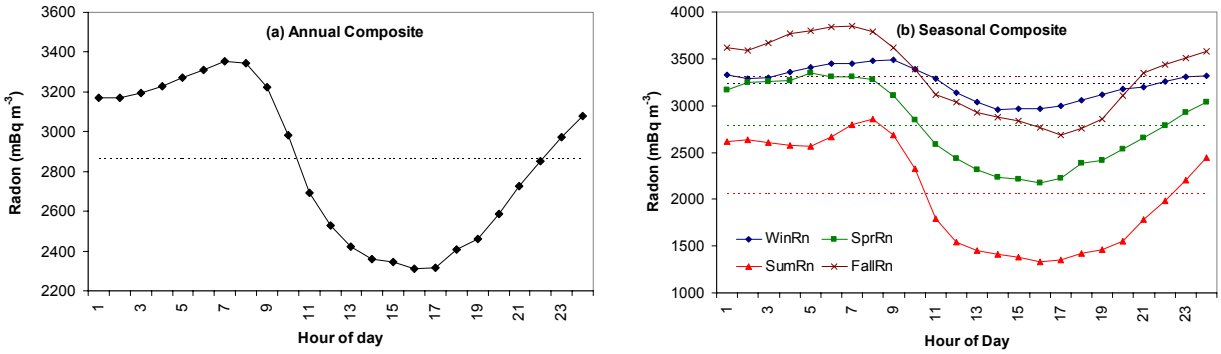

Figure 2.19: Diurnal course of observed hourly radon concentration at Kosan by (a) year and (b) season. Dotted lines represent mean of composite day.

Observations by Iida *et al*., (2000) indicate that the Beijing area, roughly 1000km northwest of Kosan across the Yellow Sea, has a mean annual radon concentration of 7000 mBq m^{-3}. Since it would usually take an air mass about one day to traverse this distance there must be considerable vertical or horizontal mixing of the air masses that maintain their trajectory over this distance given that the 90th percentile radon concentrations at Kosan from the northwest are only 4300 mBq m^{-3}.

Air mass characterisation

In spite of substantial oceanic fetch between the southeast and southwest at Kosan, the angular distribution of afternoon minimum radon concentrations shows little structure (Figure 2.20a). Apart from peaks at 100° and 220°, which correspond to the two least represented sectors (Figure 2.20b), the only significant deviation from a rather homogeneous distribution occurs for the southern sector, 180°. Excluding the 100° sector that is only represented by 4 hourly samples for the entire year (which would likely be strongly influenced by the local Cheju Island radon signal), air masses with the highest radon concentrations originate from the Sea of Japan (40°). The implication of this observation and the homogeneous angular distribution of radon at

this site is that wind direction is a poor indication of air mass origin. That is, that the long term trajectories of air masses are not consistent with the direction of travel upon reaching the site. Under these circumstances, it will be essential to use radon concentration data to identify reference conditions for aerosol and trace gas sampling.

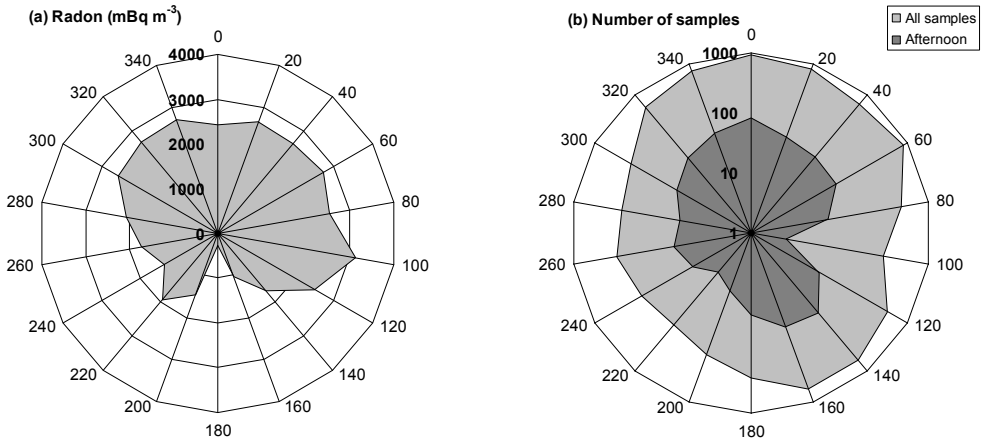

Figure 2.20: (a) Angular distribution (at 20° resolution) of daily minimum radon concentration observations at Kosan, and (b) number of samples as a function of wind direction for complete dataset (light grey) and afternoon (16:00-17:00) values only (dark grey). Note the logarithmic scale for the second plot.

Based on the monthly 10th percentile radon concentration values for Kosan (Figure 2.21), there were three days per month throughout the IOP that would be suitable as reference sampling days for aerosols and trace gases. Although these periods are not representative of true baseline conditions it is most likely that the represent the least perturbed oceanic fetch for the respective periods.

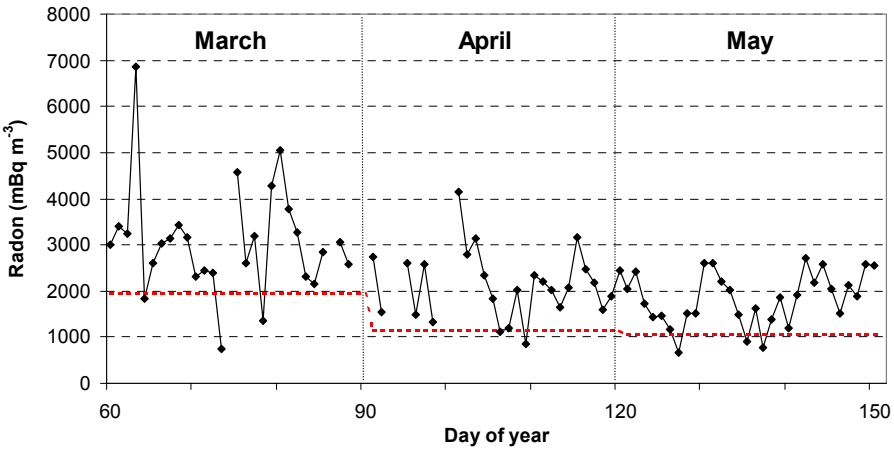

Figure 2.21: Daily minimum and 10th percentile monthly radon concentration at Kosan during the 2001 ACE-Asia intensive operation period.

T2.5.5 Sado Island radon data

Seasonal variability

Based on the first year of radon observations at Sado Island, there appears to be no well defined seasonal cycle to the radon concentrations. The only notable feature of the annual time series is a winter maximum as was the case at the other sites (Figure 2.22).

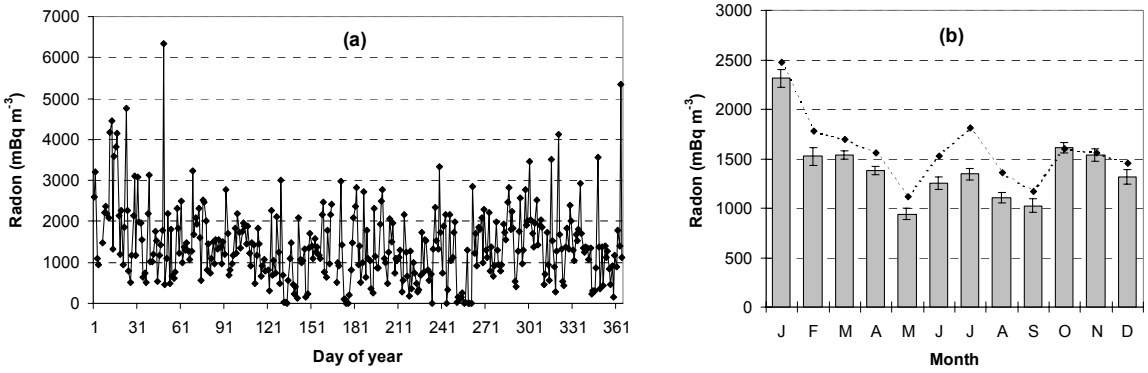

Figure 2.22: (a) Daily minimum radon concentration, and (b) mean monthly radon based on daily minimums at Sado Island, Japan, 2001. Error bars denote standard error.

Diurnal variability

The diurnal cycle of radon concentration at the site is characterised by an early afternoon minimum (Figure 2.23). The amplitude of the composite diurnal radon concentration at this site (360 mBq m^{-3}) is markedly less than that of the inland site near Tokyo (2560 mBqm^{-3}; Hattori and Ichiji, 1998), and less than half that of Hok Tsui or Kosan. Small amplitude diurnal fluctuations of radon at island sites near Japan have also been reported by Yoshioka, (1998) and Yamada *et al*., (1998), and were attributed to the large maritime influence on mixed layer depths, and minimal oceanic radon flux. Only in Spring is the afternoon minimum accompanied by a mid-morning maximum as for the other sites. Autumn has the least typical diurnal variation of radon concentrations.

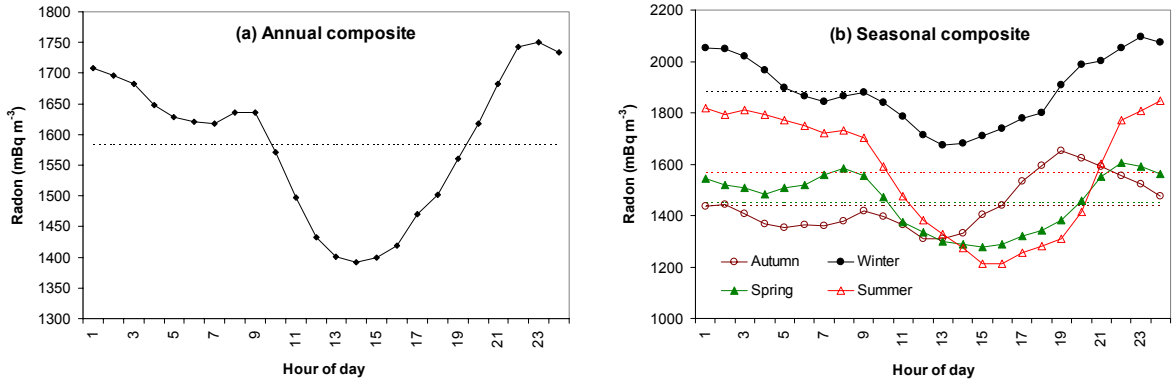

Figure 2.23: Diurnal course of observed hourly radon concentration at Sado Island by (a) year and (b) season. Dotted lines represent mean of composite day.

Air mass characterisation

Iida *et al*., (1997) report radon concentrations observed from aircraft between 300-600m ASL at coastal and oceanic sites around Japan (Table 2.5). The oceanic observations are in good agreement with ground based observations at Sado Island for the same months of the year.

Based on the monthly 10th percentile radon concentration threshold (Figure 2.24), 3-4 days per month across the ACE-Asia IOP could be selected that would be most suitable for reference monitoring at Sado Island. Without overlapping meteorological data available for this site a more detailed analysis of data from this site is not yet possible.

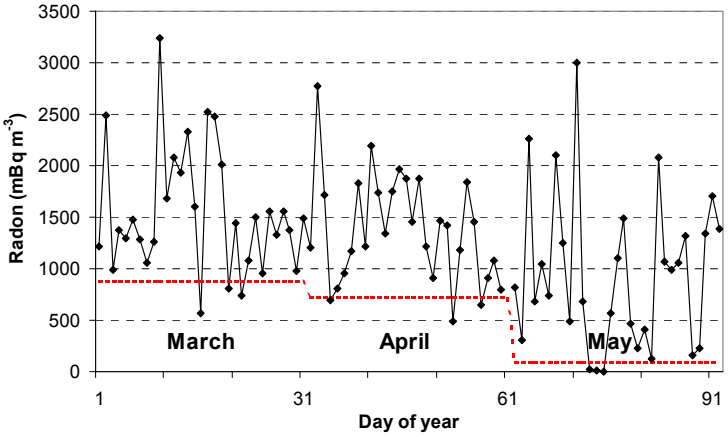

Figure 2.24: Daily minimum and monthly 10th percentile radon concentration at Sado Island during the 2001 ACE-Asia IOP.

Table 2.5: Comparison of average radon concentrations observed from an aircraft at coastal and oceanic sites around Japan between 1994-1997 to ground based radon observations at Sado Island.

	Aircraft (1994-1997)	**Sado Island (2001)**
March	2730±240 mBq m^{-3} (coast)	1540±615 mBq m^{-3}
September	1080±440 mBq m^{-3} (ocean)	1030±900 mBq m^{-3}
December	1550±240 mBq m^{-3} (ocean)	1320±1050 mBq m^{-3}

T2.5.6 Mauna Loa radon data

Bearing in mind the >3000m difference in altitude between the east Asia sites and the Mauna Loa Observatory, it is expected that the diurnal and seasonal characteristics of radon concentration at MLO will not be directly comparable. However, there is clear evidence in the radon record of tropospheric transport to MLO of air masses originating from the Asian continent.

Seasonal variability

There is a more prominent seasonal cycle in the radon concentrations at the Mauna Loa Observatory than for the Sado Island site (Figure 2.25), but less than for the other two sites. The time of peak concentrations is shifted slightly toward Spring compared to either the Hok Tsui or Kosan observations. There is a close correlation between the highest peaks in radon concentration and periods when the wind direction at MLO shifts west of south (Figure 2.26).

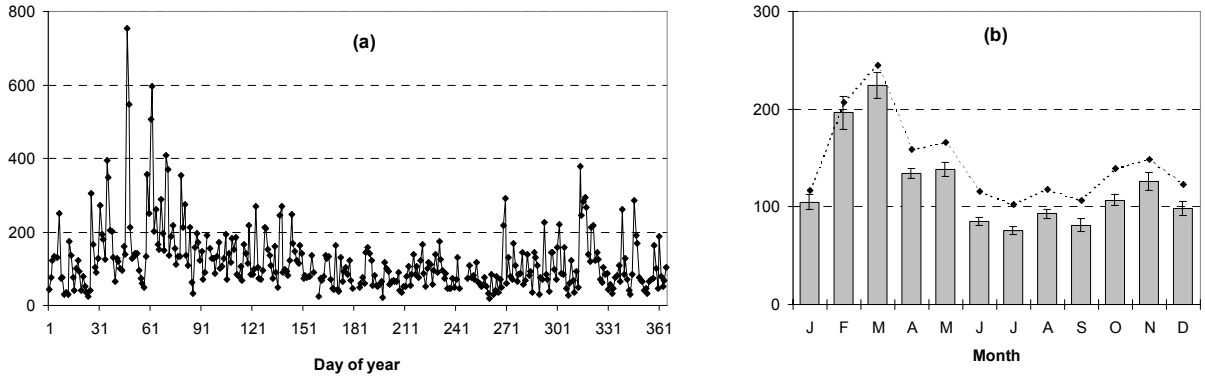

Figure 2.25: (a) Daily minimum radon concentration, and (b) mean monthly radon based on daily minimums at the Mauna Loa Observatory, Hawaii, 2001. Error bars denote standard error.

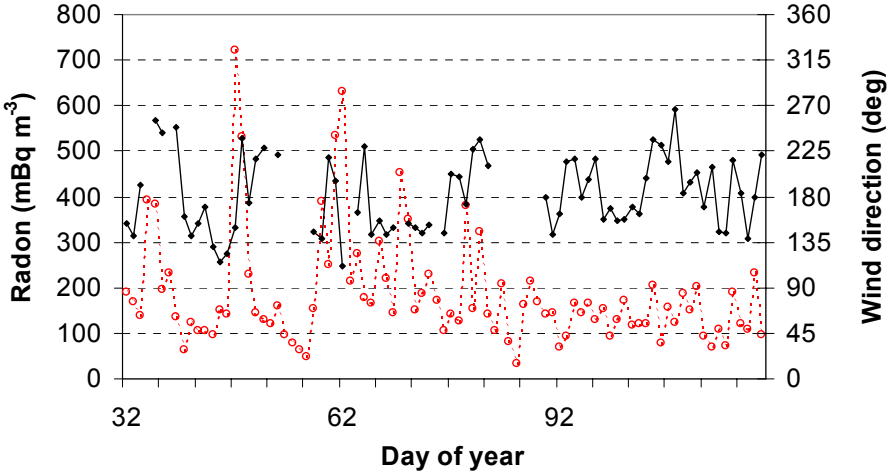

Figure 2.26: Comparison of daily minimum radon concentration (open circles) and wind direction (diamonds) at MLO between Feb-Apr 2001.

Diurnal variability

The diurnal cycle of radon concentration at this site (Figure 2.27a) is unique amongst the ACE-Asia sites in that it is characterised by a morning minimum, and an afternoon maximum. This behaviour is a result of the geographic location of the site (Dentener *et al*., 1999), since the Mauna Loa Observatory is located on a mountain side ~3,400m ASL. During the day, anabatic winds rise up along the mountain slopes and bring radon-rich air to the site. Consequently, only at night time are observations likely to be representative of the regional troposphere. Final selection criteria for a data sampling window considered to be representative of tropospheric radon concentrations were determined based on the diurnal composite information as well as wind direction.

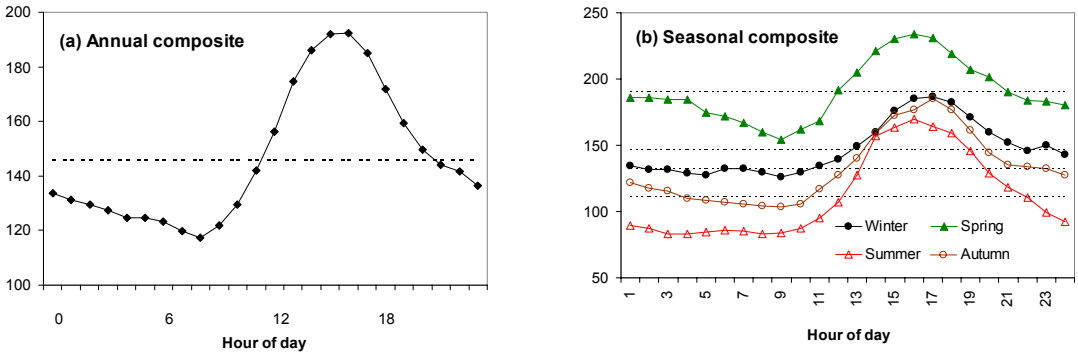

Figure 2.27: Diurnal course of observed hourly radon concentration at Mauna Loa Observatory by (a) year and (b) season. Dotted lines represent mean of composite day.

Data selection criteria

The composite plot of Figure 2.27a indicates decreasing radon concentrations from sunset, through the night until sunrise with the exception of a brief plateau from 05:00. A 3-hour daily sampling window was chosen (05:00, 06:00 and 07:00), the start of which coincided with the plateau in nocturnal radon concentrations. The reason for limiting the extent of the sampling window to three hours was based on an analysis of the corresponding wind direction data. Observed wind directions at 07:00 and 08:00 were compared on a daily basis (Figure 2.28a). Whilst the wind direction estimates were similar in the winter months, they diverged in the summer months. A comparison of the absolute difference between wind directions observed at 06:00-07:00 and 07:00-08:00 (Figure 2.28b) confirmed that the discrepancy must be due to the onset of anabatic winds by 08:00 in the summer months. Diurnal composite wind speed at the site also shows a dramatic change at this time (Figure 2.29).

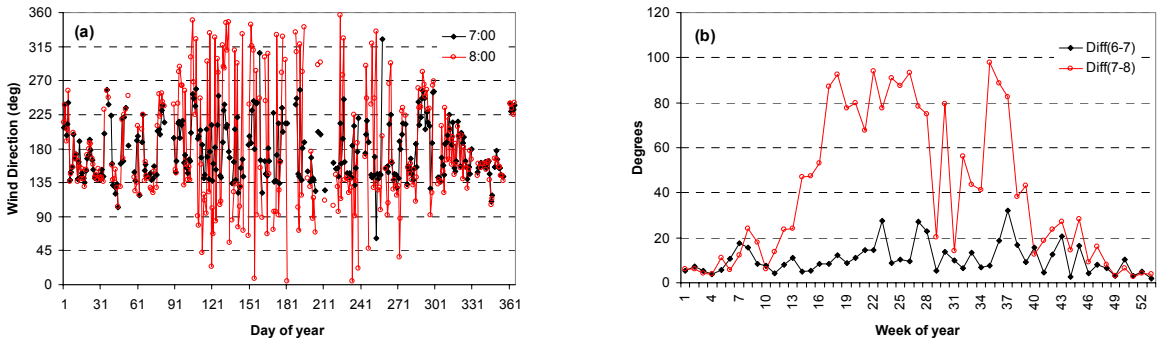

Figure 2.28: (a) Comparison of hourly wind direction data at 07:00 and 08:00 at MLO, and (b) absolute differences in hourly wind directions observed at 06:00-07:00 and 07:00-08:00.

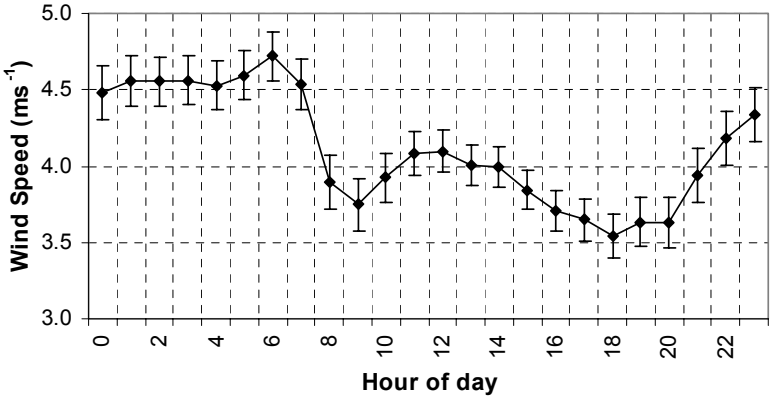

Figure 2.29: Diurnal composite hourly wind speed at Mauna Loa Observatory for 2001. Error bars denote the standard error.

Air mass characterisation

A directional analysis of hourly radon concentrations within the 3-hour morning sampling window (Figure 2.30a) indicated that air masses originating from the WSW and ESE were the primary source of elevated radon concentrations. As indicated by Figure 2.30b, imposing the 3-hour sampling window on the year of observations at Mauna Loa limits the representativeness of results to an arc of 160°.

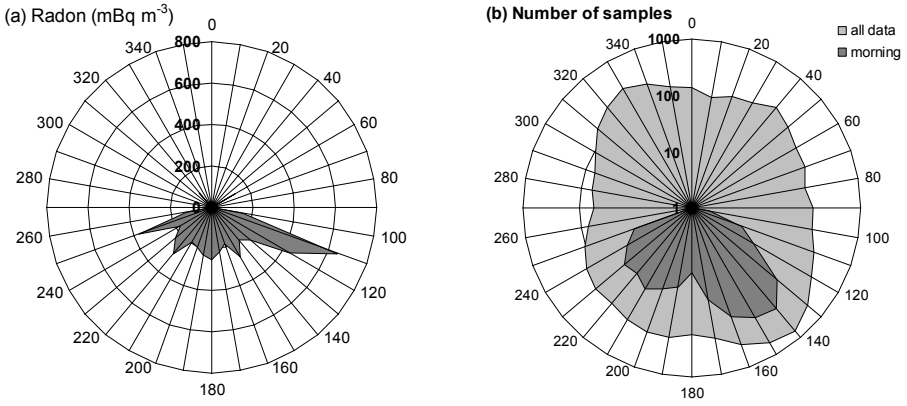

Figure 2.30: (a) Angular distribution of 90 percentile radon concentration observations at Mauna Loa Observatory, and (b) number of samples as a function of wind direction for complete dataset (light grey) and morning values only (dark grey). Note the logarithmic scale for the second plot.

The highest radon concentration observed at Mauna Loa from the west in 2001 (within the 3-hour sampling window) was ~740 mBq m^{-3} in February. The distance to Mauna Loa from Hok Tsui and Kosan is approximately 9200km and 7700km, respectively. Assuming that the air parcels travelled the distance at the mean February wind speed (5.1 ms^{-1}), the journey would

have taken 21 and 18 days, respectively. Given the 3.8day half life of radon, if it is further assumed that the air mass originated from one of these two sites, and arrived at Mauna Loa relatively undiluted the initial concentrations of radon in the air parcels would need to have been at least 30,700 mBq m^{-3} or 17,100 mBq m^{-3}, from Hok Tsui or Kosan respectively. Considering that the 90th percentile February 2001 radon concentrations at Hok Tsui and Kosan were 14,300 and 4,840 mBq m^{-3}, respectively, the air masses must have travelled to MLO considerably faster. It would be necessary to reduce the transit time by 5 days (from Hok Tsui) or 7 days (from Kosan) to yield the observed concentration. Furthermore, it is unlikely that the air mass would travel that distance undiluted, which would further decrease the required transit time.

Aerosol data collected at the Hok Tsui site during the 2001 ACE-Asia IOP (Figure 2.1b), indicated a severe pollution event on or about 10 March that spanned several days. Ten days later a 3-day radon event (20-22 March) is observed at MLO (Figure 2.31) during a period of south westerly winds. This would require an average wind speed of ~11ms^{-1}.

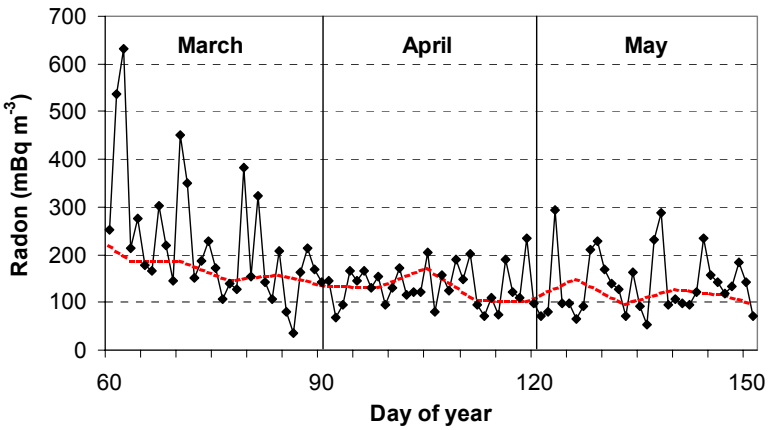

Figure 2.31: Daily minimum and weekly median (red dotted line) radon concentration at MLO for the 2001 ACE-Asia IOP.

As evident in the trajectory analysis of 22 March 2001 (Figure 2.32), tropospheric transport can carry an air mass from the Asian continent to near Hawaii in as little as two days. High speed tropospheric transport of Asian continental air masses to MLO and across the Pacific have been reported by several authors (Jacob *et al*., 1997; Kritz *et al*., 1998; Dentener *et al*., 1999; Jaffe *et al*., 2001). This analysis confirms that the air mass responsible for the 3-day radon event at MLO indeed originated from the Asian continent.

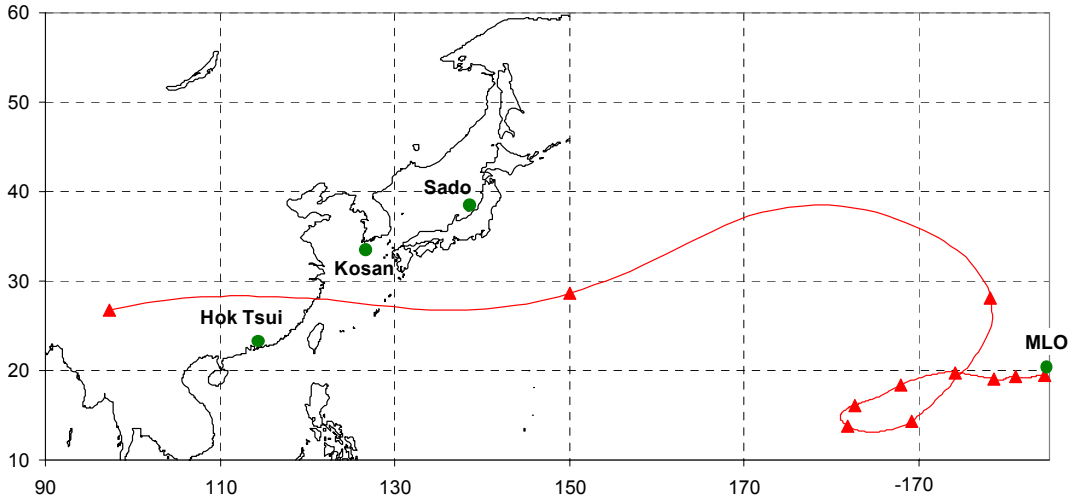

Figure 2.32: A 10-day back trajectory for an air mass originating at MLO (3,400m ASL) on 22 March 2001. Filled triangles represent 24-hour periods.

T2.5.7 Discussion

Radon source distribution in east Asia

As indicated by the weekly averages of diurnal minimum radon concentration at each of the ACE-Asia sites (Figure 2.33), the amplitude of the seasonal cycle of radon concentration decreases with latitude (north) in east Asia, and with distance (east) from the Asian continent. As expected, the sites that exhibit the maximum and minimum amplitude seasonal cycle are the coastal site (Hok Tsui), and marine site (Mauna Loa), respectively. The perturbed marine sites (Kosan and Sado Island) have intermediate amplitude seasonal cycles of radon concentration. All three east Asian sites show similar radon concentrations in the summer months when large scale flow is onshore.

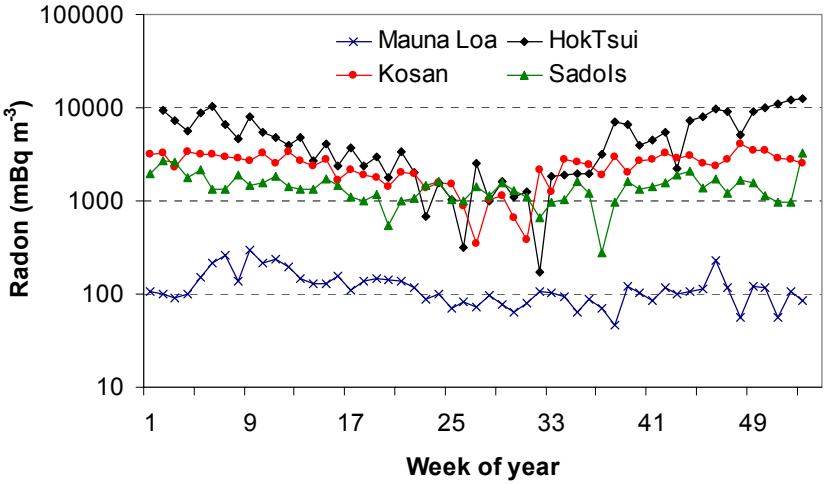

Figure 2.33: Weekly averages of minimum diurnal radon concentration at the ACE-Asia radon detector sites (note the logarithmic scale).

Although a significant difference in amplitude of the seasonal radon cycle would be expected between a coastal and perturbed marine site (as a result of different mixing and transit time over water), the magnitude of the difference indicated in Figure 2.33 suggests that other factors are contributing to this difference. Assuming that the 90th percentile radon concentration in Winter is representative of a prolonged continental fetch at each of the east Asian sites, values are similar between Kosan (4450 mBq m^{-3}) and Sado Island (3350 mBq m^{-3}), whereas the value for Hok Tsui is 15,850 mBq m^{-3}.

The 90th percentile radon concentration from the Australian continent observed at Cape Grim between 1993-2001 was 4054 mBq m^{-3}, a similar value to that observed at Kosan and Sado Island. It is possible that compared to the other sites, a significant portion of the Sado Island land fetch is frozen in Winter (Yamada *et al*., 1998), which would reduce terrestrial radon emission.

Our findings indicate that there is at least one large localised radon source in the vicinity of Hok Tsui. The possibility of a particularly large radon source in south-east Asia has previously been suggested (Jacob *et al*., 1997), who also commented on a lack of observations in the region. Several studies have in fact been published (Iida *et al*., 2000; Jin *et al*., 1998; Yamanishi *et al*., 1991) that identify localised radon "hot spots" in mainland China from northwest to northeast of the Hok Tsui site (some just over 500 km away). The mean annual outdoor radon concentrations at some of these sites exceeds 12,000 mBq m^{-3}, which is attributed to regional geology. For much of the globe, terrestrial radon sources are regionally similar, however the range of mean annual outdoor radon concentrations in Japan and China are 2.4-9.7x10^3 mBq m^{-3} and 4.8-14.6x10^3 mBq m^{-3}, respectively (Ikebe *et al*., 1997; Jin *et al*., 1998). This regional heterogeneity in terrestrial radon flux will complicate inventory analyses in the region. Presumably, the particularly large amplitude of seasonal radon concentrations observed at Hok Tsui are due to the monsoonal continental outflow carrying air masses from these radon hot-spots across the Hok Tsui site.

Some of the identified radon hot-spots lie approximately 1000-1500 km to the southwest of Kosan. As indicated in Table 2.6 the maximum afternoon radon concentration observed in the sector 220-240° at Kosan is more than a factor of two greater than adjacent sectors. However, the small difference in median radon concentration between these sectors indicates that few such concentrated events reach Kosan (or that few air masses arriving at Kosan with a direction of ~230° have actually been travelling in that direction for more than 1000 km). Assuming that an air mass does travel from the nearest radon "hot-spot" to Kosan, at the typical Kosan winter wind speeds of 10 ms^{-1}, it would take the air mass about 1.5 days to reach Kosan. Given the 3.8 day half life of radon, there would only be a ~25% loss of the initial radon in transit (since the track is may not be over water, the reduction in radon may well be less). Since maximum radon concentrations at Hok Tsui exceed 20,000 mBq m^{-3}, there must be substantial dilution of boundary layer air masses en-route. Given the distribution of maximum radon concentrations indicated in Table 2.6 it is most likely, this involves loss to the troposphere rather than lateral dispersion.

Table 2.6: Daily minimum radon concentration (mBq m^{-3}) statistics for the southwestern quadrant of the Kosan site.

Direction (°)	Median	Maximum
200-220	1730	3260
220-240	1710	7150
240-260	1220	3360

Duration of observations

As indicated by Figure 2.34, the advection of Asian continental air masses from the west over the ACE-Asia ground station network is not commonly observed at the surface level (ie. the western sector is the least represented in all measurements). It is likely that most of the large scale transport east from the Asian continent occurs in the troposphere, not the boundary layer. Given that continuous upper atmospheric sampling is not feasible, to characterise continental outflow events using observations in the boundary layer, the surface observations will need to continue for several years to capture a statistically viable number of events.

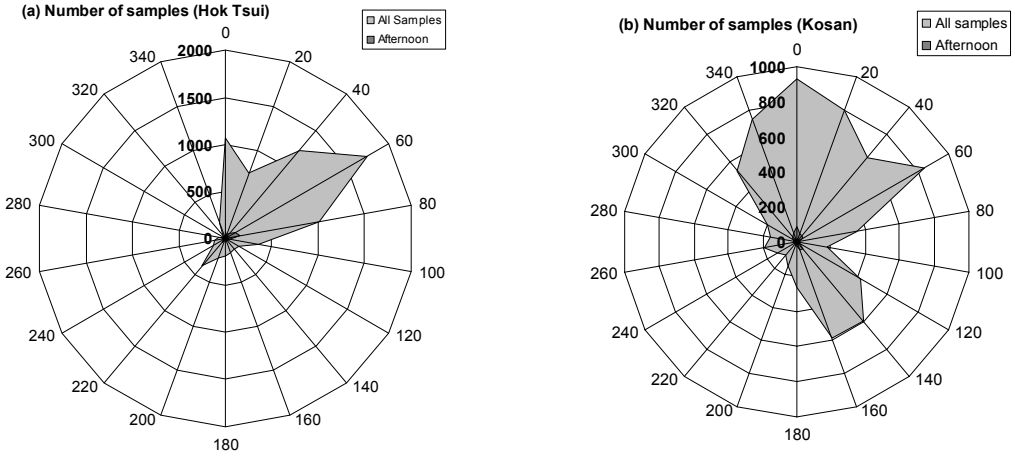

Figure 2.34: Number of hourly samples as a function of wind direction at (a) Hok Tsui and (b) Kosan. Reproductions of Figure 2.16b and Figure 2.20b with linear instead of logarithmic axes.

ACE-Asia baseline observations

The primary differences between using radon for the identification of reference (baseline) conditions at the east Asian sites as compared to remote baseline stations is the magnitude and seasonal variability of ambient background radon concentration. In Winter, when the primary air flow is off the Asian continent, the radon concentration of maritime air masses 2000-4000 km off the Asian coastline is considerably enhanced. This is depicted clearly by the radon transect of the RV Ron Brown (Figure T2.4; HACV, 2001). The large seasonal variability does not allow for establishment of one baseline radon threshold value even for "pure" oceanic events. However, accurate assessment of the baseline radon concentration and its seasonal variability is an

important part of air mass characterisation studies. Hence, an alternative approach needs to be developed and tested. For instance, instead of using one baseline value, one can use a series of 10th percentile radon concentrations calculated using observations from a three month moving window. The approach will need to be tested for consistency using a multiyear dataset. Using the data already available, this method yields values at Hok Tsui that range from 3020 mBq m^{-3} in Winter to 90 mBq m^{-3} in Summer. By comparison, the Winter/Summer ratio of median baseline radon concentrations determined for the Cape Grim oceanic fetch was 57/43 mBq m^{-3}. The corresponding Winter/Summer baseline radon concentrations at Kosan and Sado Island are 1840/240 mBq m^{-3} and 620/360 mBq m^{-3}, respectively. The outlined approach seems to be supported by an observation that the further north the ground station is located, the weaker the monsoonal signature, and the smaller the difference between winter and summer baseline conditions.

Interannual variability

At present, the complimentary set of meteorological data for the 2002 radon observations is not available. This prevents an extension of the complete directional analysis to present time. However, as an example of the magnitude of interannual variability, Figure 2.35 compares monthly radon concentration statistics at Hok Tsui for 2001-2002 between January to June. In particular, for Spring (the time of the 2001 ACE-Asia IOP), mean radon concentrations in 2002 are significantly lower than for 2001 (see also Figure 2.36), the converse is true for Winter. Whilst there is little difference in the 10th percentile radon concentrations for these periods, larger differences are observed for both the median and 90th percentile radon concentrations. It is likely that these differences are the result of changes in larger scale weather patterns, possibly associated with the El Nino/La Nina cycles, which will be further investigated when the 2002 site meteorological data is available.

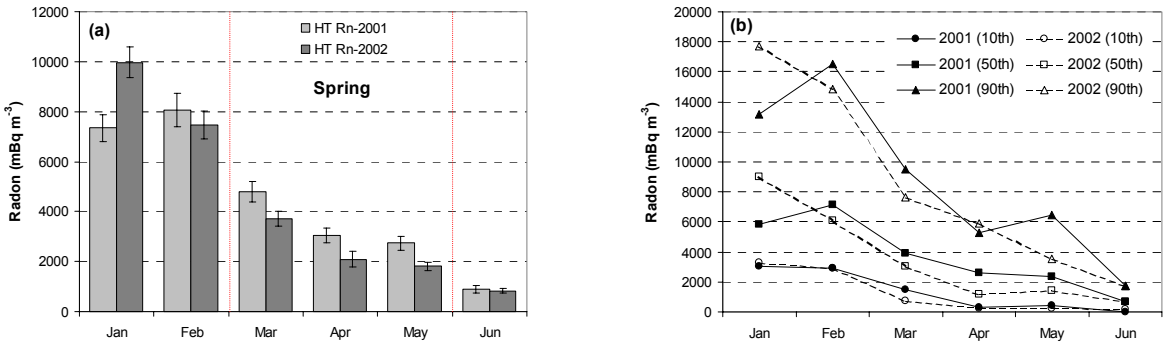

Figure 2.35: Comparison of daily minimum radon concentrations by month, (a)means and (b) distributions from January to June at the Hok Tsui site. Error bars denote standard error.

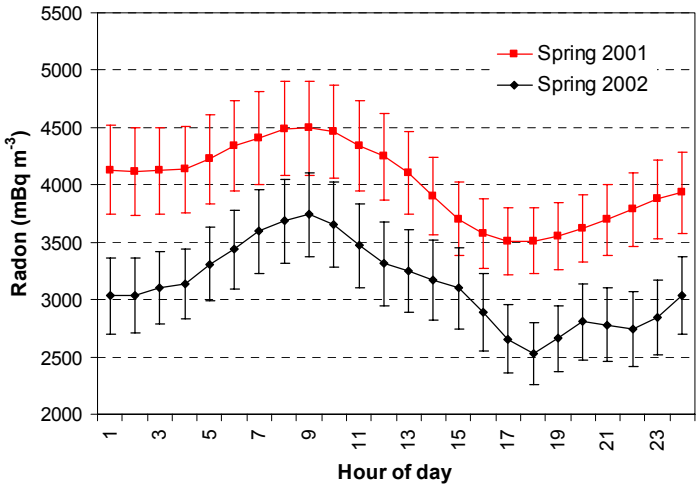

Figure 2.36: Comparison of diurnal composite radon concentration at Hok Tsui between Spring 2001 and Spring 2002. Error bars denote standard error.

T2.6 Longer term monitoring

The most significant progress in the long term radon monitoring programmes during the past reporting period has been made at the Cape Grim and Mauna Loa Observatory (MLO) sites. Since reporting on the findings from the MLO has already been made in conjunction with the ACE-Asia results, the following sections will focus on outcomes from the Cape Grim radon monitoring programme. This research has led to the submission of two manuscripts, one describing a new method to estimate oceanic radon fluxes, the other proposing a set of radon derived benchmarks for atmospheric model evaluation. This section summarises the first of these manuscripts.

T2.6.1 The oceanic radon flux

A method to estimate regional oceanic radon fluxes and their relation to environmental parameters was derived using the extended CGBAPS radon dataset and applied to the Southern Ocean. A preliminary assessment of the technique is presented here, that does not take into account venting of the marine boundary layer to the free troposphere. The large difference between terrestrial and oceanic radon fluxes sometimes leads to the oceanic flux being neglected in atmospheric models (Mahowald *et al*., 1997). However, including a realistic oceanic radon flux within models would improve comparisons between observed and simulated atmospheric radon concentration at remote sites with extended oceanic fetch (Mahowald *et al*., 1997; Heimann *et al*., 1990; Jacob *et al*., 1997).

Contemporary estimates of oceanic radon fluxes are poorly constrained, with values ranging between 0.0011 and 0.15 atoms $cm^{-2}s^{-1}$ (Wilkening and Clements, 1975; Hoang and Servant, 1972). The primary factors contributing to the poor characterisation of oceanic radon fluxes are the limited number of observations, and the representativeness of the published results. Historically, either the accumulation (Wilkening and Clements, 1975) or gradient methods (Hoang and Servant, 1972; Peng *et al*., 1979) have been employed, which are both spot measurements subject to local conditions. It is not obvious how to relate such results to environmental parameters such as wind speed and sea state, which have a significant effect on ocean-atmosphere exchange.

Data and selection criteria

A subset of the Cape Grim hourly atmospheric radon and meteorological observations (1993 to 2001) was used to derive a new method for estimating regional oceanic radon fluxes. The method was based on the assumption that, due to the short half-life of radon, after sufficient time over the ocean the radon remaining in the marine boundary layer would be in equilibrium with the oceanic radon flux.

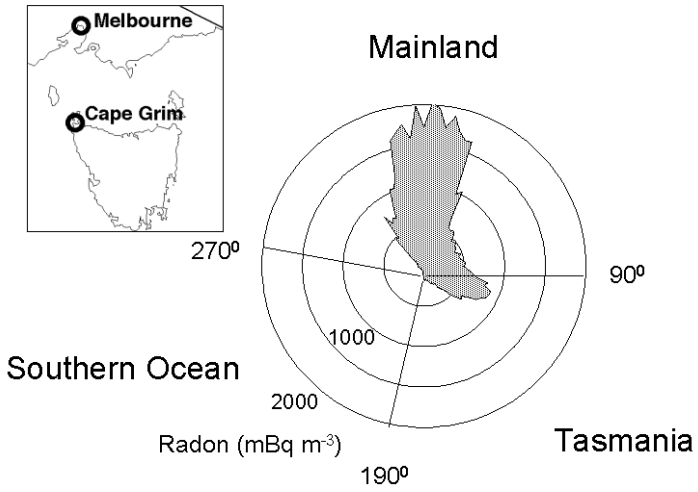

Figure 2.37: The angular distribution of median hourly Cape Grim radon concentrations at 3° resolution for the 9-year data subset.

To perform this analysis it was necessary to select from the 9-year data subset air parcels representative of a minimally perturbed oceanic fetch. Since the hourly radon concentrations at Cape Grim have a very distinctive angular distribution (Figure 2.37), the primary selection criteria was based on wind direction, $190^\circ \leq \theta < 280^\circ$ (eg. Zahorowski and Whittlestone, 1999).

A composite oceanic event was then formed from all observations within this oceanic wind sector. Based on this composite event, distributions of radon concentration were calculated for consecutive hours after wind direction change to the oceanic sector (Figure 2.38).

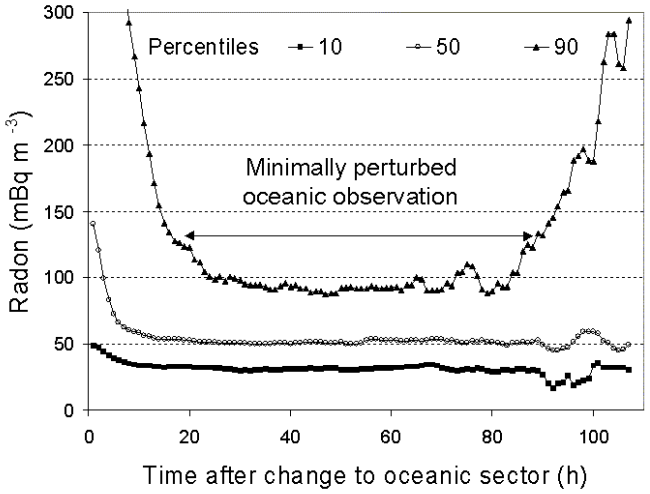

Figure 2.38: Median and 90 percentile radon concentration for consecutive hours after change to the oceanic sector.

The distribution of radon concentrations in the composite oceanic event was most consistent from 23-85 hours after change to the oceanic sector. For the present preliminary analysis it was concluded that air masses which had persisted in the oceanic sector for 23-85 hours offer the best approximation of air masses with a minimally perturbed oceanic fetch, and are most likely to be in equilibrium with the oceanic radon flux.

Model development

Assuming that the sole source of radon is the oceanic flux (F), and neglecting the exchange of radon between the marine boundary layer and the free troposphere, the mass balance of radon in a Lagrangian framework is:

$$\frac{dC}{dt} = \frac{F}{h} - \lambda C \qquad (1)$$

where C = N/V is the concentration of radon, N is the number of radon atoms, V=A h is the volume of the air parcel, A is the cross sectional area, h is the mixing depth and λ=0.182 day^{-1} is the radon decay constant. Assuming that the oceanic flux and mixing depth are relatively constant and can be represented by their average values $\overline{F}$ and $\overline{h}$, respectively, and that the average oceanic flux is spatially homogeneous, the solution to Equation 1 is:

$$C(t) = \left(\frac{\overline{F}}{\lambda \overline{h}}\right) + e^{-\lambda t}\left(C_o - \left(\frac{\overline{F}}{\lambda \overline{h}}\right)\right) \qquad (2)$$

Provided that C_o is not excessive, for an air parcel that has travelled over the ocean for several or more radon half-lives, the second term on the right hand side of Equation 2 will be negligible. This represents the ideal case of an air parcel that has come to equilibrium with the oceanic radon flux after a prolonged track over water, whereby the average concentration within the air parcel is dependant only upon the average mixing height and the average oceanic flux. Under these circumstances, the expression for the average oceanic flux is:

$$\overline{F} \approx \overline{C}\lambda\overline{h} \qquad (3)$$

Since the atmospheric radon concentration takes of the order 10 half-lives to equilibrate with the oceanic radon flux, this model should only be used to derive regional oceanic fluxes on monthly time scales, which is sufficient to identify seasonal changes in oceanic radon flux.

Results and discussion

Assuming a purely mechanically driven mixed layer over the Southern Ocean the 9-year median wind speed of 10 ms^{-1} equates to a mixing height of about 480 m. Based on the 9-year median radon concentration of minimally perturbed oceanic air masses (49 mBq m^{-3}), the model yields an oceanic radon flux of $5.0x10^{-5}$ Bq $m^{-2}s^{-1}$ (0.0024 atoms $cm^{-2}s^{-1}$). This supports the common assumption that oceanic radon fluxes are 2-3 orders of magnitude less than terrestrial fluxes.

Looking at the variability within the 9-year data sub set, there is a pronounced seasonality in the median radon concentration and the regional oceanic flux derived using the seasonal median wind speeds (Figure 2.39).

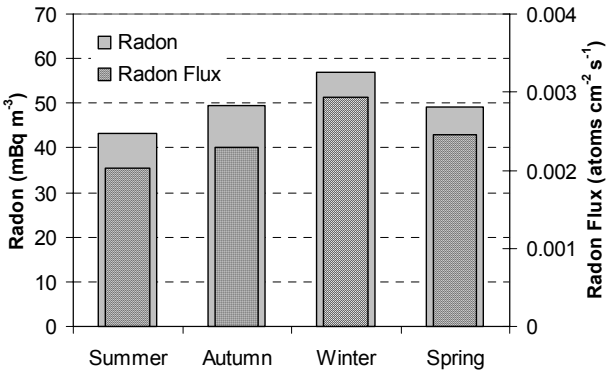

Figure 2.39: Seasonal variation of median radon concentration for oceanic air masses arriving at Cape Grim and estimated regional oceanic radon flux.

The median monthly wind speed for the 9-year data subset deviates less than 25% from the overall median wind speed. This suggests that the mixing height is relatively constant for prolonged periods. If a constant mixing height is assumed based on the 9-year median wind speed, the 10/90 percentile range of radon concentrations (30-73 mBq m^{-3}) corresponds to a variability of oceanic radon flux of $3.0x10^{-5}$ – $7.4x10^{-5}$ Bq $m^{-2}s^{-1}$ (0.0014 - 0.0035 atoms $cm^{-2}s^{-1}$). Alternatively, if it is assumed that the periods of lowest radon concentration coincide with highest mixing heights, and vice-versa, based on the 10/90 percentile wins speeds (5.4 - 15.9 ms^{-1}), then the variability in the oceanic radon flux would be considerably smaller ($4.1x10^{-5}$ – $4.8x10^{-5}$ Bq $m^{-2}s^{-1}$; 0.0020-0.0023 atoms $cm^{-2}s^{-1}$). These two ranges represent respectively upper and lower estimates of the variability in regional oceanic radon flux derived from the model.

Following the evaluation of simulations with the Model of Atmospheric Transport and Chemistry (MATCH), Mahowald *et al*., (1997) concluded that the oceanic radon flux rate from the Southern Ocean (around Kerguelen) had to be less than 0.003 atoms $cm^{-2}s^{-1}$. This conclusion compares well with the flux estimate of 0.0024 atoms $cm^{-2}s^{-1}$ from this study.

As a worst case scenario, if a 50% loss of marine boundary layer radon to the troposphere is assumed, as might be expected in summertime over a continental region, the oceanic radon flux predicted by this model would be 0.0048 atoms $cm^{-2}s^{-1}$. This is still less than the upper limit of 0.005 atoms $cm^{-2}s^{-1}$ for oceanic radon fluxes used by Jacob *et al*., (1997) in their World Climate Research Program sponsored intercomparison of 20 atmospheric models. However, this rather extreme flux estimate is still lower than most oceanic radon flux estimates by the accumulation or profile method, which vary from 0.0011 – 0.15 atoms $cm^{-2}s^{-1}$ (Wilkening and Clements, 1975; Hoang and Servant, 1972). The reasons for the magnitude and sign of

discrepancy between the regional radon flux estimates of this study and those of spot accumulation/profile methods are presently unclear.

An advantage of the model for regional radon fluxes presented here over the spot measurements is that the findings are more easily related to atmospheric conditions. The ocean-atmosphere exchange rate of trace gases is thought to be strongly affected by wind speed (and hence sea state). To briefly investigate the relationship between oceanic radon flux and wind speed, the radon flux was derived on a monthly basis taking into account monthly changes in mixing height. A regression of these fluxes against median monthly wind speeds yielded a significant positive correlation (R=0.76; Figure 2.40). Future studies, using a better constrained mixing height, would be able to investigate the relationship between wind speed and oceanic radon flux in more detail. In summary, the model presented offers a simple and inexpensive alternative to local/spot estimates of oceanic radon flux such as the accumulation method and gradient methods, as well as being representative of a larger region. Better constrained oceanic radon fluxes in regional and global atmospheric models will improve the evaluation of their transport schemes with radon data from remote sites.

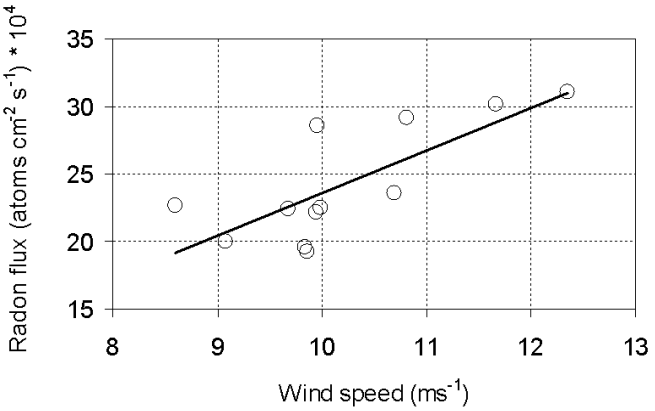

Figure 2.40: Regression of monthly regional oceanic radon flux against median monthly wind speed for minimally perturbed oceanic sector air masses at Cape Grim between 1993-2001.

T2.6.2 Radon derived benchmarks

The radon benchmarking manuscript reviews recent trends in the application of ground based radon observations to atmospheric research. The key operational requirements for baseline radon detectors are briefly discussed, including lower limit of detection and response time. Current radon-related benchmarks for the evaluation of regional and global models are reviewed, with particular consideration given to the implications of data availability, resolution, site location and model spatial/temporal resolution. An 9-year subset of radon observations from the Cape Grim Baseline Air Pollution Station is used to suggest new benchmarks that exploit long-term datasets. Particular emphasis is given to directional analysis, distribution analysis and directional analysis. Lastly an overview is presented of a technique that uses radon to estimate regional fluxes of climatically sensitive gases, with specific examples for CO_2, CH_4 and N_2O.

T2.7 Task 2 reports and papers (December 2001 – November 2002)

- Chambers, S.D., T. Wang, W. Zahorowski, S. Poon and A. Henderson-Sellers. 2001. Radon-222 measurements at the ACE-Asia Hok Tsui site: first eight months of observations. *ACE-Asia Workshop, California Institute of Technology, Pasadena, California, USA, Oct 29 - Nov 01 2001.*
- Chambers, S.D., Wang, T., Zahorowski, W., Poon, S. and Henderson-Sellers, A. 2002. Radon-222 measurements at a continental coastal site in Hong Kong. *Cape Grim Annual Science Meeting 2001, University of Tasmania, Hobart 6-7 February 2002.*
- E-report 749. HACV Annual Review. 2002. *ISBN 0-642-59996-3 ISSN 1030-7745.*

- Kim, J., Zahorowski, W., Chambers, S.D., Kang, C.-H., Oh, S.-N. and Henderson-Sellers, A. 2002. Seasonal trends in radon-222 observations at the Kosan ACE-Asia site. *The 7th Biennial SPERA Conference on Environmental Radioactivity: Migration, measuring and monitoring in the South Pacific. Lucas Heights Science and Technology Centre, Sydney, Australia, 13-17 May 2002.*
- Sisoutham, O., Werczynski, S., Chambers, S. and Zahorowski, W. 2002. Continuous radon detectors for industrial and environmental monitoring applications. *The 7th Biennial SPERA Conference on Environmental Radioactivity: Migration, measuring and monitoring in the South Pacific. Lucas Heights Science and Technology Centre, Sydney, Australia, 13-17 May 2002.*
- W. Zahorowski, Chambers, S.D., and Fukumura-Sawada, P. 2002. The ANSTO-CMDL Radon Program at MLO. *Climate Monitoring and Diagnostic Laboratory Summary Report 2000-2001. 26, 174-175.*
- W. Zahorowski, S. Chambers and A. Henderson-Sellers. 2002. A new method for the estimation of regional oceanic radon-222 fluxes. *To be submitted to Journal of Geophysical Research – Atmospheres.*
- Wang, T., Zahorowski, W., Chambers, S.D., Poon, S. and Henderson-Sellers, A. 2002. Comparison of radon-222 measurements between continental coastal and island sites. *The 7th Biennial SPERA Conference on Environmental Radioactivity: Migration, measuring and monitoring in the South Pacific. Lucas Heights Science and Technology Centre, Sydney, Australia, 13-17 May 2002.*
- Zahorowski, W., Chambers, S.D. and Henderson-Sellers, A. 2002. Characterisation of air mass origin using atmospheric radon concentration measurements. *The 7th Biennial SPERA Conference on Environmental Radioactivity: Migration, measuring and monitoring in the South Pacific. Lucas Heights Science and Technology Centre, Sydney, Australia, 13-17 May 2002.*
- Zahorowski, W., Chambers, S.D., Werczynski, S. and Henderson-Sellers, A. 2002. A brief review of key characteristics of radon measurements at Cape Grim 1987-2001. *Cape Grim Annual Science Meeting 2001, University of Tasmania, Hobart 6-7 February 2002.*
- Zahorowski, W., J. Kim, S.D. Chambers, C.-H. Kang, H.-J. Shin and A. Henderson-Sellers. 2001. Air mass characterisation using radon-222 at the ACE-Asia Kosan site. *ACE-Asia Workshop, California Institute of Technology, Pasadena, Calafornia, USA, Oct 29 - Nov 01 2001.*
- Zahorowski, W., Kim, J., Chambers, S.D., Kang, C.-H., Oh, S.-N. and Henderson-Sellers, A. 2002. First year of radon-222 observations at the ACE-Asia Kosan site. *Cape Grim Annual Science Meeting 2001, University of Tasmania, Hobart 6-7 February 2002.*
- Zahorowski, W., S.D. Chambers and A. Henderson-Sellers. 2002. Ground based radon-222 observations and their application to atmospheric studies. *Submitted to the Journal of Environmental Radioactivity.*

T2.8 External funding

As a result of collaboration established with the Hong Kong Research and Grants Council (RGC), Hong Kong Polytechnic University, University of California at Irvine and ANSTO funding of about HK$1.0M was received for three years of long term and intensive sampling within the ACE Asia Project starting in July 2001. ANSTO was allocated HK$40,000 of this grant for sampling in 2002.

A US$44,000 grant application for a new radon detector at the Mt Walliguan GAW station, and in support of radon research activities at two ground sites (Kosan and Hok Tsui), for one year starting in April 2003 has been prepared and submitted to the Asia-Pacific Network for Global Change Research (APN).

T2.9 Summary and future directions

T2.9.1 Summary of reported year

- The first 12 months of data for all ACE-Asia radon and fine particle sites is now available with preliminary analyses performed;
- The seasonal variability of background radon concentration at each of the radon monitoring sites has been characterised for the available data;
- Major components related to industrial pollution and soil sources in China have been identified and quantified;
- Regional and seasonal variations and trends in aerosol constituents have been measured and compared across more than 2.8Mk^2 of sampling area;
- The Hok Tsui and Kosan detectors were visited for general maintenance and recalibration;
- A grant application to the APN has been submitted in support of regional inventory analyses based on radon time series;
- Progress on the processing and interpretation of radon data was presented at the Cape Grim Science Meeting (6-7 February 2002) and the 7th Biennial SPERA Conference on Radioactivity (13-17 May 2002);
- One manuscripts has been submitted, and another soon to be submitted, that summarise findings from the recently extended Cape Grim Baseline Air Pollution Station radon concentration data base.

T2.9.2 Anticipated highlights for next year

By the next reporting period we expect to have:

- At least two years of radon data from all ACE-Asia sites that will improve directional analysis statistics, extend the time series for model validation, improve the suite of radon related benchmarks for model evaluation and enable a preliminary assessment of interannual variability;
- Visited the Sado Island site for general equipment maintenance and recalibration;
- Submitted two manuscripts pertaining to the ANSTO ACE-Asia site network, available data and initial findings;
- A minimal complete seasonal fine particle dataset for all ACE Asia sampling sites. This will enable preliminary source fingerprinting to be achieved statistically and Chemical Mass Balance (CMB) techniques to be used to quantitatively determine source contributions across a set of seasons;
- The ability to report on the first data from Positive Matrix Factorisation (PFM) of a complete dataset of aerosol analyses. This technique provides fingerprints and source contributions together and direct comparisons with established CMB techniques can be made. Success with these two techniques will provide, for the first time, confidence in the percentage source contributions to the PM2.5 size fraction pollution over the Asian sampling region;
- Established a collaboration with University of Newcastle and a PhD student that will be used to develop a new model based on Multi-linear Engines (ME), developed by Professor Pennti at University of Helsinki. This ME model will allow wind direction and speed as well as radon data to be included in our source fingerprint identification and apportionment. The historical Cape Grim data, which contains 25 different elemental species as well as hourly wind speed, direction and radon information, will be used to fully develop and test this ME model in the first instance. By the end of the year the Cape Grim version should be operational.

Task 3: Future - Climate modelling: evaluation and improvement

T3.1 Objectives, current research hypothesis and background

T3.1.1 Objectives

1. To investigate the use of naturally occurring isotopes in regional moisture studies.
2. To improve land surface parameterisation and investigate its potential to improve global climate models and thus improve our future climate change predictions.

T3.1.2 Current research hypotheses

1. Stable isotopes of water provide a novel data source for evaluation of Global Climate Model's (GCM's) simulations of regional hydrology.
2. Land-surface scheme (LSS) complexity improves the simulation of continental near-surface climates.

T3.1.3 Background

At the project review in November 2000 it was recommended that resources be primarily focused on AMIP II data analysis i.e. Objective 2. This direction has been taken, although some progress has also been made on Objective 1.

In year 2, Objective 1 focused on oxygen and hydrogen isotopes derived from the IAEA Global Network of Isotopes in Precipitation (GNIP). These data were investigated particularly in relation to the Amazon Basin. This year (year 3) attention has been transferred to another CEOP region – the Murray Darling Basin.

T3.2 Progress summary

<u>Within Objective 1</u>

1. GNIP and other data for the Murray Darling have been analysed and compared with available GCM simulations of the basin hydrology (proposal made to the Murray Darling CEOP project).
2. Radon sampling at Cape Grim has been pursued (refer to Task 2).

<u>Within Objective 2</u>

1. Surface energy and surface water budgets for 20 AMIP II AGCMs, three reanalysis products and one surface data based synthesis analysed for 17 years of simulation.
2. Continental surface energy and water budgets for the AMIP II period analysed in two discrete ways: by CEOP region and by de Martonne (1948) climate zone (papers presented and published).
3. Response of different land-surface schemes (LSSs) to atmospheric forcing.
4. Australia-specific analysis of AMIP II simulations initiated jointly with BMRC (internal BMRC report published).

T3.3 Details on objective 1

Research hypothesis: *Stable isotopes of water provide a novel data source for evaluation of global climate models' (GCMs') simulations of regional hydrology*

T3.3.1 Why study Isotopes?

The variation in the natural abundance of the isotopic species of both oxygen (^{16}O and ^{18}O) and hydrogen (^{1}H and ^{2}H or D which stands for deuterium) that results from the fractionations caused by the phase transitions (e.g. evaporation, condensation) are used to study the water cycle. Although the isotopic composition of precipitation at a particular location is approximately constant, it varies from season to season and from one rainstorm to another. The reasons for variations include different histories for individual air masses, different atmospheric temperature and different amounts of evaporation from raindrops as they fall through the atmosphere. These variations can be utilised to identify the seasons at which most recharge takes place and/or the source of runoff associated with individual storms: information which may be very difficult to obtain by physical measurements.

In this part of the project, Task 3 pursues the exploration of the use of isotopes as a novel and fully independent means of evaluating Global Climate Models (GCMs), which are the predominant tools with which we predict the future climate. In order that people can have confidence in such predictions, GCMs require validation. As almost every available item of meteorological data has been exploited in the construction and tuning of GCMs to date, Task 3 explores the independent means of evaluation of the GCMs using isotopic variations in the nature.

T3.3.2 What we did last year (2001)

During last year we focussed on Amazon. We examined:

- the monthly average values of temperature, humidity, precipitation, precipitation type, deuterium (D), oxygen-18 (^{18}O) and tritium obtained from the Global Network for Isotopes in Precipitation (GNIP) database (IAEA/WMO, 1999) for six stations (Belem, Manaus, Porto Velho, Sao Gabriel and Izobamba) of the Amazon Basin, and
- the isotopic evaluation of GCMs' simulation of the Amazon region.

From the analysis we found:

- the deuterium excess (δD) decreased in the wet season and increased in the dry season. Manaus' wet season δD decreased significantly in the 1980s compared to 1960s. The plausible explanations of the wet season decrease of δD involve either more non-fractionating (e.g. transpiration) or less fractionating (e.g. lake) recycling or both.
- at least one GCM simulates transpiration as the significant process in the Amazon forest's dry season budget of recycled water. The failure by the CCM1-Oz simulations to represent the relative seasonal importance of transpiration (non-fractionating) as compared to the fractionating evaporation seems likely to be traceable to the land-surface parameterisation scheme.
- there are grounds for suspecting that a more thorough examination of the components of the Amazonian water cycle using isotopic data could both reveal inadequacies in some current climate model simulations and, hopefully, indicate how simulations by GCMs could be improved to more completely and correctly capture important moisture exchanges.

T3.3.3 What we have done this year (2002)

This year, our focus is the Murray Darling Basin, which has a long history of isotope collection and analysis and also of climate modelling. Input has been made to the new proposal to GEWEX for a CEOP activity in the Murray Darling. This proposal was accepted in September this year. The following sections will briefly describe our proposal for the application of isotopes to the Murray Darling Basin (MDB) water budget study and the importance of the study in relation to global climate model predictions.

T3.3.4 Applications of Isotopes to the Murray Darling Basin Water Budget (MDBWB) Project

Objective of the MDBWB Project

Objectives of the MDBWB Project include (Draft Science and Implementation Plan Jan 02):

- To monitor key components of the water budget;
- To predict routinely key components of the daily water budget;
- To observe, understand and model processes controlling soil moisture in the MDB;
- To observe, understand and model surface fluxes of water, momentum, heat, radiation and carbon in MDB; and
- To improve representation of land surface processes in weather and climate models.

To achieve these objectives, ANSTO proposes to apply isotopes in the following three areas:

Mixing processes - origin of components:

- groundwater sub-surface mixing
- groundwater inflow to rivers and reservoirs
- salinity variations in surface and groundwaters

Dynamic processes:

- Infiltration through the unsaturated zone
- Evaporative processes

Evaluation of numerical models:

- Climate change models
- Groundwater models

In this report we briefly review why and how isotopic studies are likely to illuminate recently initiated investigations of the MDB water budget.

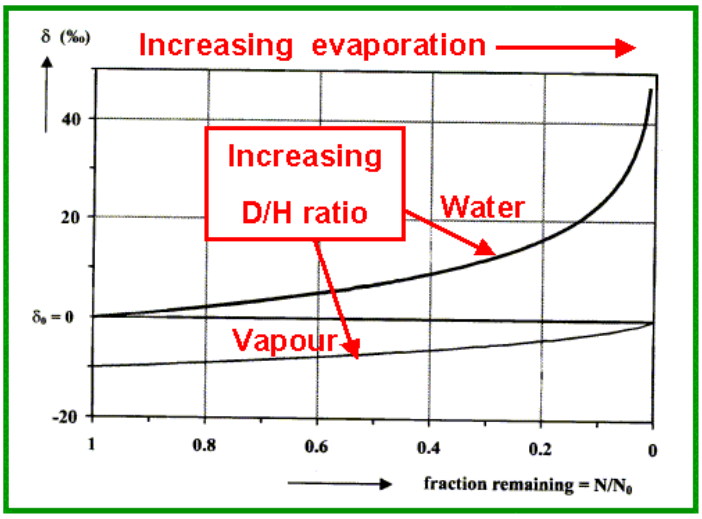

Figure 3.1: Plot of the increasing isotopic (D/H) ratio of the vapour and liquid phases as a finite amount of water is gradually evaporated at equilibrium, and constant pressure, without mixing with outside air.

Impact of evaporation on the isotopic composition of surface water

The evaporative process leads to the selective removal of vapour depleted in the levels of D (and ^{18}O). Consequently the residual water exhibits enhanced D/H (and $^{18}O/^{16}O$) ratios as shown in Figure 3.1. Thus extensive evaporation results in both increases in salinity and enrichment in the stable isotopes and also leads to a reduced slope in the D/H -$^{18}O/^{16}O$ correlation. Mixing processes resulting, for example, from a tributary or from groundwater ingress lead to predictable changes in the isotope levels. This information is invaluable in establishing a water balance. For example, the general enrichment in ^{18}O is observed in all rivers, except the MacKenzie, from the headwaters to the estuaries (Figure 3.2*a*). The Darling and the Rio Grande, which have the greatest potential evaporation, show the greatest effect. Discontinuities in the Darling River data are associated with tributary and groundwater inputs and changes to the flow regime. The general trends are consistent with the correlation graphs (Figure 3.2*b*), as data from the Darling and the Rio Grande show lower slopes and hence reflect higher evaporation than those of the Amazon. As noted below, these principles have been applied to studies in the Murray and the Darling Rivers.

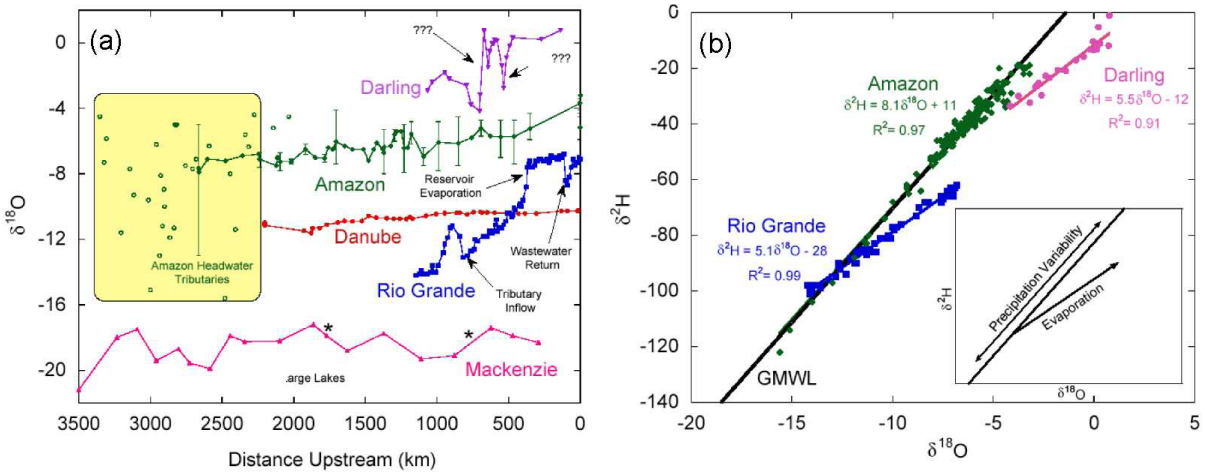

Figure 3.2: The progressive change of river water $\delta^{18}O$ as a result of increasingly fractionated rainfall and open water evaporation (a) progressing upstream, and (b) against $\delta^{2}H$

River isotopic evaporative enhancement

As illustrated in Figure 3.1 and Figure 3.2, it is likely that the rivers in the Murray darling Basin will exhibit an enrichment in the deuterium content as well as enhanced salinity as a direct result of the very large evaporative demand on their open water surfaces or mixing processes (eg.

from tributaries or ground water). A review of previous research (A Herzig, CSIRO, Land and Water) finds:

- Large enrichments in deuterium reflect cumulative evaporation;
- Large changes in chloride (without parallel deuterium increase) reflect groundwater inputs; and
- Total deuterium enrichment indicates that the integrated basin evaporative losses are similar to transpiration losses during the summer intensive irrigation period.

These findings are the basis of the new proposals made by ANSTO to the CEOP MDB project.

Analysis of Global Climate Model (GCM) simulations over the MDB

To highlight the use of isotopic data for evaluating evaporation rates, the simulations by 20 atmospheric global circulation models (AGCMs) (A-T), participating in phase 2 of the Atmospheric Model Intercomparison Project (AMIP II), three reanalyses (NCEP-DOE, NCEP-NCAR and ECMWF) and one global offline simulation of land-surface variables from the Variable Infiltration Capacity (VIC) model are analysed over the MDB for the period 1979-1995 (1979-1993 for ECMWF and 1979-1992 for VIC).

Partitioning of precipitation into evaporation and runoff

In this section, focus is on the partitioning of precipitation *Pr* into evaporation *Ev* and runoff *Ro*, water conservation and their ability to simulate observations (Figure 3.3) with the assumption that the change in soil-moisture (= *Pr*–*Ro*–*Ev*) over the 17-year period is negligible. Conservation of water in the model is seen when *Pr* = *Ro* + *Ev*, i.e. when the sum of the two ratios is 100 (e.g. VIC and AGCM B).

Based on Figure 3.3, nine AGCMs (B, G, I, J, M, O, P, Q and T) and VIC conserve water. Among these nine AGCMs, only AGCM B simulates the same range of observed runoff-evaporation ratio (i.e. runoff ratio: 8% and evaporation ratio: 92%); AGCMs G, M, P and Q simulate larger runoff (18-30%) and smaller evaporation (70-82%) ratio, while the other four AGCMs (I, J, O and T) simulate smaller runoff (2.5-4%) and larger evaporation (96-97.5%) ratio.

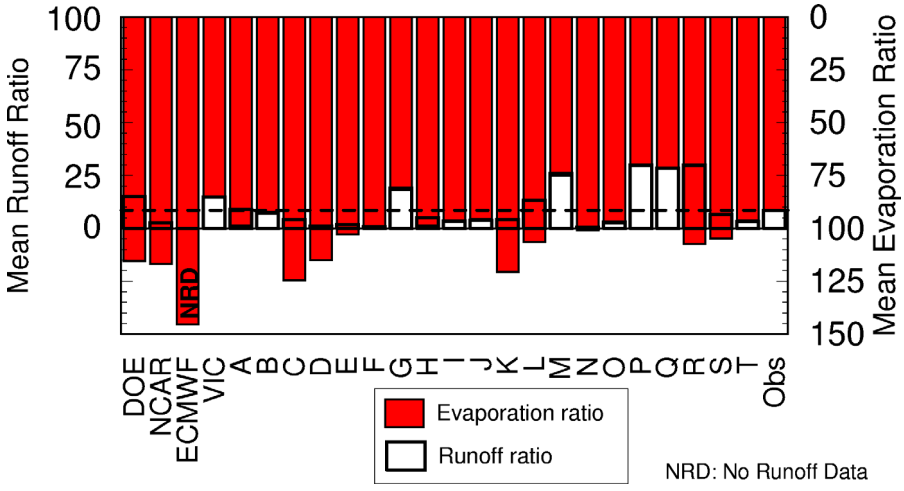

Figure 3.3: The 17-year (15-year for ECMWF and 14-year for VIC) mean total (=surface+drainage) runoff ratio (Ro/Pr, in %) and evaporation ratio (Ev/Pr, in %) over MDB. "Obs" is based on precipitation from Climate Prediction Center Merged Analysis of Precipitation (CMAP) and runoff from Global Runoff Data Centre (GRDC).

Compared to other GEWEX-CEOP basins (see section T3.4.5), the highest number of AGCMs (11 out of 20) lose water (i.e. *Pr*–*Ev*–*Ro*<0) in MDB and seven of which (AGCMs C, D, E, K, M, R and S) have evaporation alone greater than precipitation (i.e., *Pr*-*Ev*<0 or *Ev*/*Pr*>100%). None of the three reanalyses conserve water and in all of them evaporation is greater than precipitation.

Spatial distribution of the evaporation ratios

The spatial distribution of the evaporation ratio is also investigated for all AGCMs and reanalyses. The analysis shows that only eight AGCMs (A, G, I, J, M, P, Q and T) and VIC have evaporation less than precipitation over all grid points. Among these AGCMs, only A does not conserve water over the basin (Figure 3.3), which may be due to the error in its reported runoff values (negative runoff in some months of the year throughout the 17-year period).

The remaining 12 AGCMs and all reanalyses (NCEP-DOE, NCEP-NCAR and ECMWF) have *Ev* ratios greater than 100% (i.e. *Ev*>*Pr*) at least at some grid points of the basin (e.g. Figure 3.4). Though the basin mean *Ev* ratio for AGCM B is less than 100%, at a few grid points the ratio is greater than 100%. For all reanalyses, these *Ev* ratios become greater than 150% at some grid points of the basin (Figure 3.4*a*-*c*), while only four AGCMs (C, H, K, L) have this ratio greater than 150% at some grid points (Figure 3.4*d*-*g*).

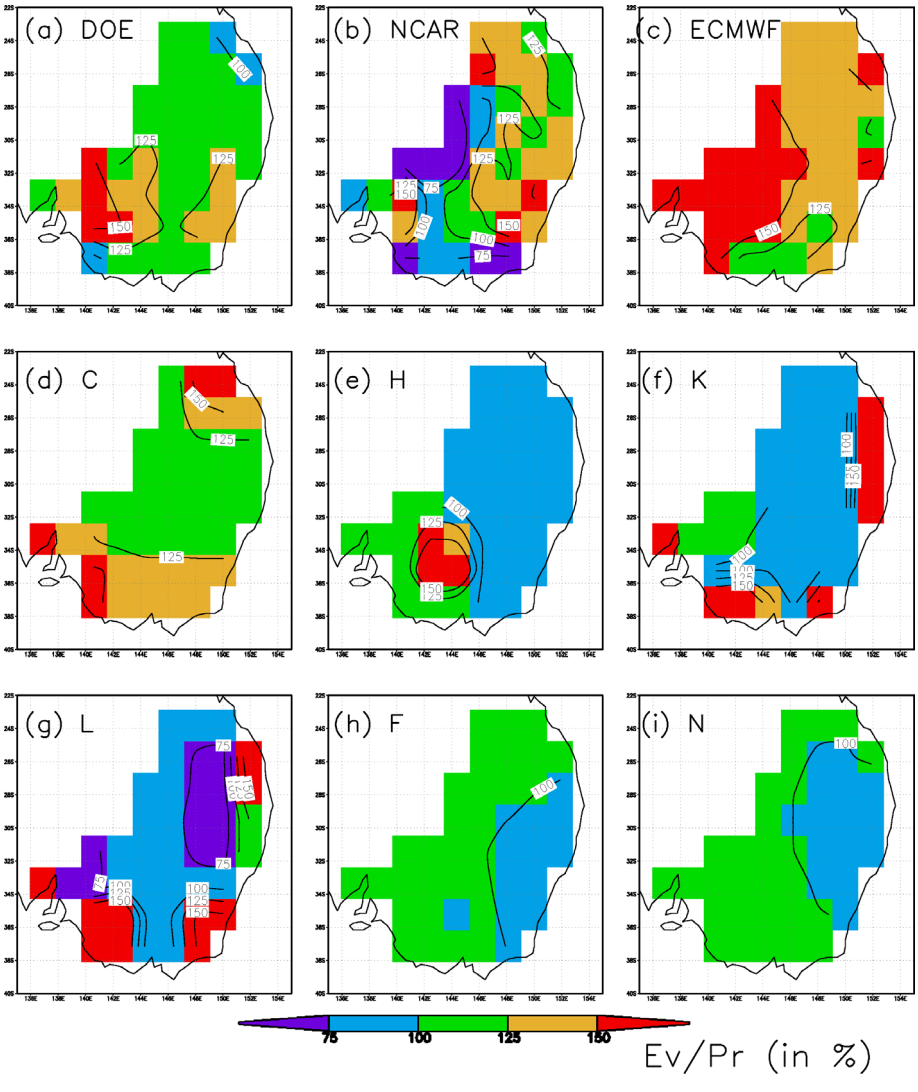

Figure 3.4: The spatial distribution of the 17-year (15-year for ECMWF) mean evaporation ratio (Ev/Pr, in %) for three reanalyses products (NCEP-DOE, NCEP-NCAR and ECMWF) and six selected AMIP II AGCMs over MDB (C, H, K, L, F and N).

Soil moisture anomalies

To assess the reason for surface water imbalances, we investigated the change in soil moisture with time. The analysis shows that soil moisture decreases with time at the grid points where *Ev*>*Pr* for both AGCMs and reanalyses. For some AGCMs and reanalyses, this decrease is sustained over the first few years (e.g. AGCM H, Figure 3.5*c*) and for some over the entire 17-year period (e.g. NCEP-DOE reanalysis, AGCM N, Figure 3.5*a*,*d*). Possible explanations for this anomalous trend could be (i) poor initialisation, (ii) long spin-up period for the soil moisture, (iii) problematic parameterisation or (iv) a combination of these. As the long spin-up period for some

AGCMs lasts over the entire 17-year period, it is not possible to solve the initialisation problem from the data by excluding the first few years of the analysis period. So far, there are no global or CEOP observations against which we can evaluate AGCMs' soil moisture trends. It is also difficult to compare them against each other and deduce any reasonable explanations for such behaviour, because of the very large (orders of magnitude) difference in their values. This is because many modelling groups have not submitted soil moisture outputs according to the definition and in the standard units required by the AMIP.

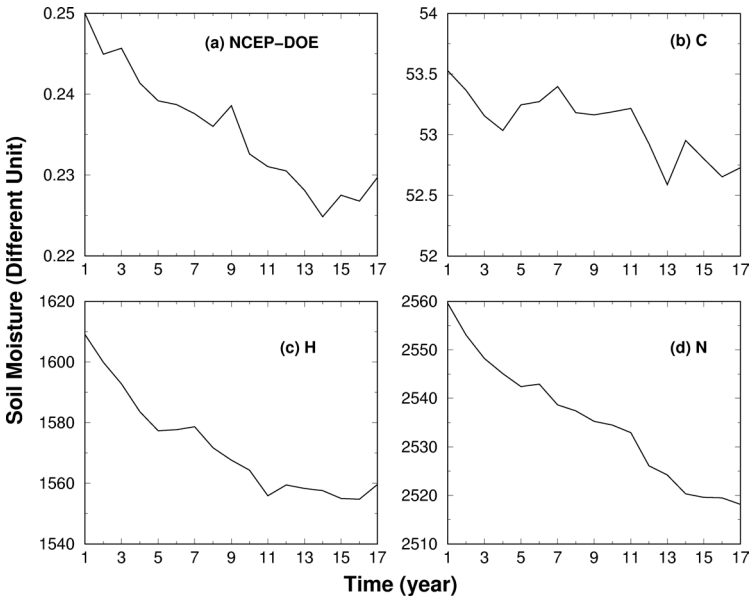

Figure 3.5: The reported soil moisture trend over the MDB for NCEP-DOE reanalysis and AMIP II AGCMs C, H and N. [N.B. Different models have different total soil column capacities and, in some cases, failed to report as requested by AMIP. Here we simply give values as reported.]

Scatter plot analysis

In this section, focus is on the partitioning of surface available energy (E_a = SH+LH) into latent (LH) and sensible (SH) heat fluxes by the 20 AGCMs and how they compare against the reanalyses (Figure 3.6). Based on Figure 3.6, six, five and eight AGCMs (out of 20) remain within the ranges of the reanalyses' E_a, SH and LH respectively. The ranges of the reanalyses are around 3 W m^{-2} for E_a, 10 W m^{-2} for SH and 15 W m^{-2} for LH. These values for the AGCMs are around 80, 90 and 60 W m^{-2} respectively. Compared to other GEWEX-CEOP basins, the AGCMs' ranges are larger in the MDB. For example, the range for SH is around 90 W m^{-2} over MDB, as compared to 50-60 W m^{-2} over other basins.

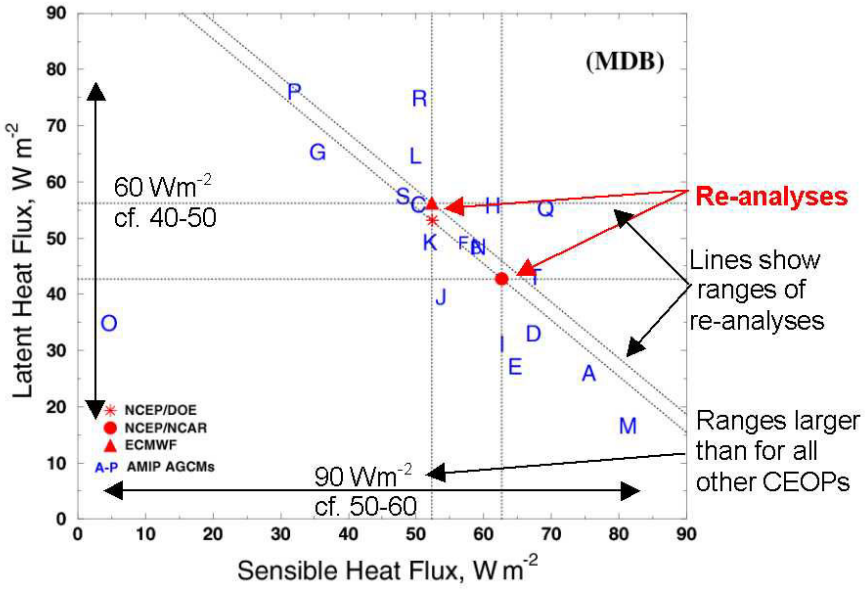

Figure 3.6: Scatter diagram showing the partitioning of surface available energy (LH+SH) between mean sensible (SH) and latent (LH) heat fluxes of 20 AMIP II models (A-T) as compared to three reanalysis products (NCEP-DOE, NCEP-NCAR and ECMWF) for MDB. The dotted lines are the range of the reanalyses (vertical: SH, horizontal: LH, and diagonal: SH+LH).

Summary

The above results show that very few AGCMs simulate well in the MDB and also their ranges are larger in this basin compared to other GEWEX-CEOP basins. For better predictions of the land-surface variables (like evaporation, soil moisture) by the AGCMs, we need observations. But many of these variables (e.g. evapotranspiration, infiltration) are not directly observable at scales appropriate to atmospheric model grid areas. However, if we could use the isotopic data to evaluate the evaporation rates from the MDB (as shown in the previous section), then attempts to improve land-surface scheme parameterisation can be evaluated using isotopic evaluation.

Proposed isotope sampling location and study

Figure 3.7 shows the proposed seven sampling locations over the Darling and Naomi rivers. The studies that will be conducted on the collected samples are as follows:

Infiltration Studies:

Aim: To measure the rate of infiltration of water through the unsaturated zone (a significant component of the MDB water budget).

Action: Use artificial tritium or deuterium tracer techniques to measure the infiltration and dispersion of water in the unsaturated zone over the duration of the project.

Water Vapour Studies[1]*:*

Aim: Using isotope methods, to improve the understanding of water vapour origin (marine, evaporation, transpiration).

Action: Sample water vapour under well controlled and monitored conditions to assess the dominant sources.

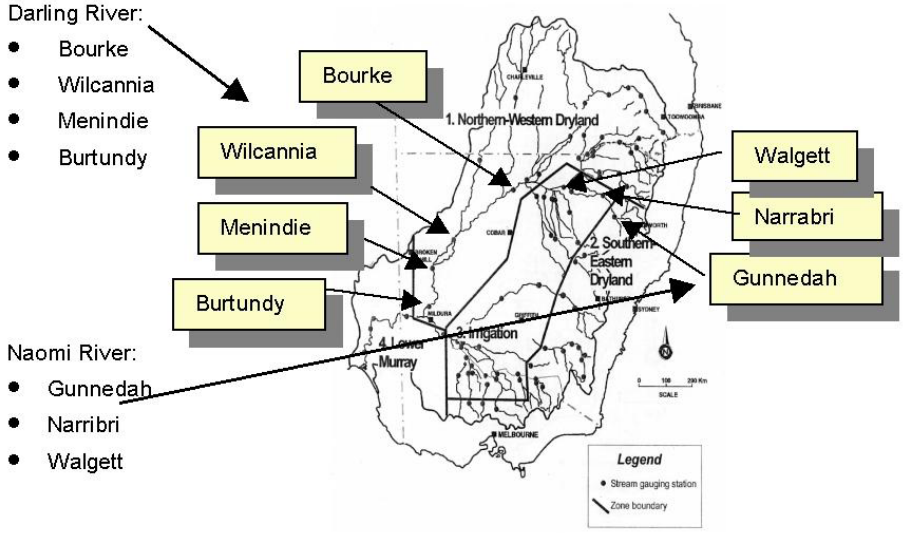

Figure 3.7: Proposed isotopic sampling locations on the Darling and Naomi river over the MDB

T3.3.5 Summary of objective 1

Future opportunities for Task 3 validation and model improvement include: (a) regional to basin-scale moisture convergence estimates; (b) evaluation of model partitioning among transpiration, free evaporation and canopy evaporation; and (c) detection and attribution of the impacts of

[1] The study would only be undertaken if water vapour transport were important to the water budget.

forest change and greenhouse gas increases. It is worth mentioning here that Dr. Manton of BMRC presented the full Murray Darling CEOP proposal to the GEWEX Hydrology panel in September 2002. The panel accepted the proposal and we are now part of the team participating in the CEOP observation, synthesis and analysis programme.

T3.4 Results from objective 2

Research hypothesis: *Land-surface scheme (LSS) complexity improves the simulation of continental near surface climates.*

T3.4.1 Why study land-surface simulations?

A land-surface scheme (LSS) is an algorithm for determining the exchanges of energy, mass and momentum between an atmospheric model and the simulated continental surface. These exchanges are complex functions of a number of processes that have a range of temporal and spatial scales and applicability. As it is impossible to incorporate all the details of all processes into a numerical scheme, LSSs have been developed based on various simplifications (e.g. Manabe, 1969; Avissar and Pielke, 1989; Avissar, 1992; Dickinson *et al*., 1993; Bonan, 1996; Cox *et al*., 1999; Henderson-Sellers *et al*., 2002b).

Conservation of energy and water, a fundamental requirement for all land surface modelling, is hard to demonstrate. Conservation of energy at the surface is achieved by balancing a change in the energy state of the surface with the net radiation (NR), sensible (SH) and latent (LH) heat fluxes, and the heat used to melt snow (SMH), i.e.,

$$\text{Energy Residual} = NR - SH - LH - SMH \quad (1)$$

while the conservation of water is achieved by balancing a change in the soil moisture with the precipitation (*Pr*), runoff (*Ro*) and evaporation (*Ev*), i.e.

$$\text{Soil Moisture change} = Pr - Ro - Ev \quad (2)$$

Irrespective of the differences in the level of complexity used in the LSSs in simulating land-surface variables, it is expected that, over a multi-annual time scale, total energy residuals (i.e. the ground heat flux) and the soil moisture change should be negligible. In addition to the conservation of energy and water, a good model should, we believe, exhibit only small differences from accepted observations.

T3.4.2 What we did last year (2001)

During last year (2001), we examined:

- the energy imbalances of 10 AGCMs over the four selected Global Energy and Water Cycle Experiment (GEWEX) Coordinated Enhanced Observing Period (CEOP) basins and over the global land surface (GLS);
- partitioning of energy over different climate regimes and also over the four selected GEWEX-CEOP basins;
- water budget over the GLS;
- spatio-temporal correlations between AGCMs and each of the three reanalyses and VIC's evaporation, and also between three reanalyses' and VIC's evaporation over different climate regimes, and
- a lag correlation analysis of the AMIP II simulations over Australia.

From the analyses we concluded that (HACV, 2001):

- the range and spatio-temporal correlations of the AMIP II simulations are similar to those of the reanalyses,
- globally, the AGCMs' simulated mean evaporation and runoff ratio compare better with the observations than the reanalyses, and
- the characteristics of climatic memory from land-surface processes (e.g. soil moisture), as shown by the lag-correlation analysis, have different features in the ten models: some models show rapid interactions between the land-surface and the overlying atmosphere, while others show some slowly varying processes in which the anomalous surface conditions have longer time-scale impacts.

T3.4.3 What we have done this year (2002)

This year (2002) we extended our analysis to 20 AGCMs. We analysed the AGCMs' energy and water budgets and evaluated their components over the different climate regimes (Figure 3.8) and seven GEWEX-CEOP basins (Figure 3.9). We also examined in detail the applicability of three reanalysis[2] data sets: ECMWF (Gibson *et al*., 1997), NCEP-NCAR (Kistler *et al*., 2001) and NCEP-DOE (Kanamitsu *et al*., 2000) and the global land-surface estimates (Nijssen *et al.,* 2001) by the Variable Infiltration Capacity (VIC) scheme (Liang *et al*., 1994) for evaluating the AMIP II land-surface simulations. As these evaluation data reflect the biases of the respective models (e.g. Betts *et al*., 1996), wherever possible, we used other global validation references (i.e, precipitation, runoff, near-surface air temperature) that are based primarily on gauge or satellite observing systems for applicable portions of the AMIP II period. In this study, we used observed precipitation derived from the Climate Prediction Center Merged Analysis of Precipitation (CMAP) (Xie and Arkin, 1997) and runoff from the Global Runoff Data Centre (GRDC) (Fekete *et al*., 2000).

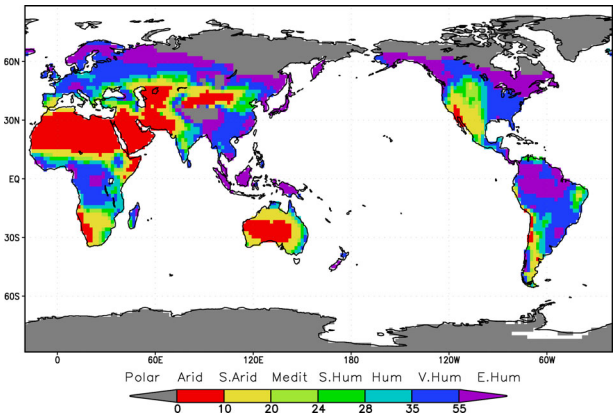

Figure 3.8: Global distribution of the de Martonne (1948) aridity index as calculated using mean annual precipitation (in mm yr^{-1}) from the Climate Prediction Center Merged Analysis of Precipitation CMAP and air temperature from ensemble reanalysis as Pr/(T+10).

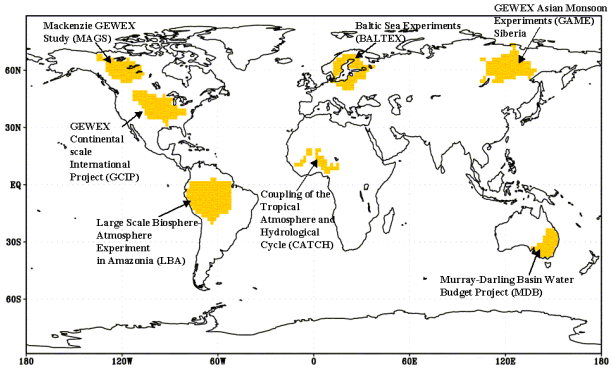

Figure 3.9: Location map of the Continental-Scale Experiments (CSEs) and Continental-Scale Affiliates (CSAs) of the Global Energy and Water Cycle Experiment (GEWEX) Coordinated Enhanced Observing Period (CEOP) regions

We have also summarised the processes used in the AMIP II LSSs (e.g. model soil discretisation for moisture and heat, presence/absence of vegetation) and examined the relation between the LSS complexity and AGCMs' surface flux simulations. Some of our findings are presented in the following sections. For details see Henderson-Sellers *et al.,* (2002*a*) and Irannejad *et al.,* (2002). Note the reanalyses (plus VIC) and the AGCMs have different

[2] Reanalyses use a frozen state-of-the-art analysis/forecast system and reanalyse the data from the recent past to develop a pseudo-climate record, even though the quality of the data inputs varies with time (Roads and Betts, 1999).

resolutions. In this study, all the reanalyses and model results are interpolated into T63 resolution for analysis.

T3.4.4 AMIP II AGCMs and their land-surface schemes (LSSs)

More than 30 AGCMs are participating in AMIP II. To date (November 2002), 20 AGCM simulations for the period 1979-1995 have completed the Program for Climate Model Diagnosis and Intercomparison (PCMDI) quality control processes and have been released under the protocol of AMIP II for analysis (Table 3.1). A brief summary of the LSSs used in these AGCMs to parameterise soil moisture and canopy resistance is given in Table 3.2 together with the model resolutions. Note that the AGCMs in Table 3.2 are not in the same order as in Table 3.1. It is emphasised here that the purpose of this analysis is not to identify good or poor models but rather to try to understand the strengths and weaknesses in the community's model prediction skill. However, the modelling groups are aware of their own model performances.

Table 3.1: AMIP II AGCMs use in the analysis

Model	***Name of Host Institution or Organisation***	***Country***
cccma	Canadian Centre for Climate Modelling and Analysis	Canada
ccsr	Centre for Climate System Research	Japan
cnrm	Centre National de Recherches Météorologiques.	France
cola	Centre for Ocean-Land-Atmosphere	USA
dnm	Department of Numerical Mathematics	Russia
ecmwf	European Centre for Medium-Range Weather Forecasts	UK
giss	Goddard Institute for Space Studies	USA
gla	Goddard Laboratory for Atmosphere	USA
jma	Japan Meteorological Agency	Japan
mgo	Main Geophysical Observatory	Russia
mpi	Max-Planck-Institut fur Meteorologie	Germany
mri	Meteorological Research Institute	Japan
ncar	National Centre for Atmospheric Research	USA
ncep	National Centers for Environmental Prediction	USA
pnnl	Pacific Northwest National Laboratory	USA
sunya	State University of New York at Albany	USA
Ugamp	The UK Universities' Global Atmospheric Modelling Programme	UK
uiuc	University of Illinois at Urbana-Champaign	USA
ukmo	United Kingdom Meteorological Office.	UK
yonu	Yonsei University	Korea

Table 3.2 shows that there is a wide range of land-surface complexity in the available AGCMs, ranging from simple Manabe bucket schemes representing soil hydrology with no canopy processes (e.g. AGCMs O, P); two-layer force restore models of soil hydrology with transpiration represented by apparently constant canopy (e.g. AGCMs G, S); bucket-type models with detailed interactive canopy (i.e. AGCM T); and multi-layer soil schemes where soil hydrology is represented by Richards' equation with fully parameterised 2-storey canopy processes including carbon-cycle, canopy interception and its re-evaporation (e.g. AGCMs I, J, F, N). Some LSSs also explicitly model frozen soil moisture and include the associated latent heat (e.g. AGCMs I, J, K, R). Among these AGCMs, the same LSSs (with or without modifications) occur coupled to the same atmospheric models (sometimes with different resolution or a different version). For example, E, L, M and Q use the variants of the Simple SiB schemes (Sellers *et al*., 1986) coupled to the same or different atmospheric models. Such a wide range of LSS complexity, plus the same LSSs coupled to the same or different host atmospheric models, provides an excellent opportunity to study the role of LSSs in land-surface simulations.

Table 3.2: AMIP II AGCM codes, and tentative soil and canopy features used in Land-surface Scheme (LSS) parameterisation. (AGCMs are not in the same order as in Table 3.1).

AGCM	Resolution	Soil Moisture (*w*)			Canopy		Intercep
		Hydrology	Layer #	Frozen *w*	Resistance	Layer #	Loss
A	T42L18	Bucket (W_{fc}= const)	1	N	Const	0	N
B	T63L45	Force-Restore	2 (1m)	N	f(PAR,*w,e,T*)	1	Y
C	4x5 L21	Richards' Eq.	24 (10m)	N	f(PAR,*w,q,T*)	1	Y
D	T63L50	Richards' Eq.	4 (2.9m)	N	f(PAR,*w*)	1	Y
E	T63L30	Richards' Eq.	3	N	f(PAR,*LT,LW,T*)	2	Y
F	T42L18	Richards' Eq.	6 (6.3m)	N	f(PAR,*w,e*,CO_2, *LT*)	2	Y
G	T42L18	Force-Restore	2 (1m)	N	Plant Factor	1	Y
H	T42L18	Richards' Eq.	3 (10m)	N	f(PAR,*w,e,T*)	1	Y
I	3.75x2.5 L58	Richards' Eq.	4 (3m)	Y	f(PAR,CO_2…)	1	Y
J	3.75x2.5 L19	Richards' Eq.	4 (3m)	Y	f(PAR,CO_2…)	1	Y
K	T47L32	Richards' Eq.	3 (4.1m)	Y	f(PAR,*w,e,T*)	1	Y
L	4x5 L20	Richards' Eq.	3	N	f(PAR,*w,e,LT,T*)	1	Y
M	T42L30	Richards' Eq.	3	Y	f(PAR,*LW, LT,T*)	2	Y
N	T42L18	Richards' Eq.	6 (6.3m)	N	f(PAR,*w,e*,CO_2, *LT*)	2	Y
O	4x5 L24	Bucket (W_{fc}=var)	1	N	None	0	N
P	4x5 L24	Bucket (W_{fc}=const)	1	N	None	0	N
Q	1.8x2.8 L18	Richards' Eq.	3	N	f(PAR,*w,e,LT,T*)	1	Y
R	4x5 L12	Richards' Eq.	6 (10m)	Y	?	1	Y
S	T42L14	Force-Restore	2 (1m)	N	?	0	?
T	T42L19	Bucket (W_{fc}=var)	1	N	f(PAR,*w,LW*)	1	Y

PAR: photosynthetic active solar radiation; *w*: soil moisture, *e*: specific humidity, *q*: vapour pressure, *LT*: leaf temperature, and *LW*: canopy water content.

T3.4.5 Surface energy and surface water budgets for 20 AMIP II AGCMs

Partitioning of surface available energy between sensible (SH) and latent (LH) heat fluxes over the de Martonne climate regimes

Partitioning of surface available energy (SH+LH) between SH and LH of the 20 AMIP II models in different de Martonne climates are compared to that of three reanalyses as scaled by the average value of the surface available energy of the ensemble reanalyses (Figure 3.10). The analysis shows that the values of the reanalyses' scaled mean LH and SH, relative to each other, vary across the de Martonne climates. For instance, ECMWF produces the highest LH flux in the arid to sub-humid climates and much lower values than the other two reanalyses in very humid and extremely humid climates. While NCEP-NCAR has higher LH than NCEP-DOE in the very humid climates (figure not shown, for details see Irannejad *et al*., 2002), its scaled LH is smaller than NCEP-DOE in all climate types. These differences suggest that the caution previously noted by various authors (Kalnay *et al.,* 1996; Betts *et al.*, 1996; Betts *et al.,* 1998; Irannejad *et al.,* 2000; Maurer *et al.,* 2000) regarding the use of reanalysis surface variables, especially on the small-scale, should be reiterated and underlined.

Compared to reanalyses, over GLS only three AMIP II AGCMs' (P, S, and T) scaled LH and SH are within the range of the reanalyses, while 14 have smaller scaled LH and greater scaled SH and two (AGCMs G and O) have greater scaled LH and smaller scaled SH. Mostly as a consequence of the AGCMs' smaller scaled LH in more humid climates, only a few models (two-three) have their adjusted surface fluxes within the reanalyses' range. Most of the AGCMs' scaled LH and scaled SH are within the range of the reanalyses in the drier climates but deviate from the reanalyses towards the more humid climates. The AGCMs that use the bucket hydrology scheme with a variable (AGCM O) or constant (AGCM P) water holding capacity (Table 3.2) predict LH greater than the range of reanalyses in all climates (AGCM O) or in drier (Arid to Sub-humid) climates (AGCM P). AGCMs E, L, M and Q, which use variants of the SiB scheme (Sellers *et al.,* 1986), are among the least evaporating models in almost all climates. The AMIP II AGCMs are scattered around the NCEP-DOE reanalysis in the arid and semi-arid

climates; around the NCEP-NCAR reanalysis in the Mediterranean to humid climates; and around the ECMWF reanalysis in the very humid and extremely humid climates.

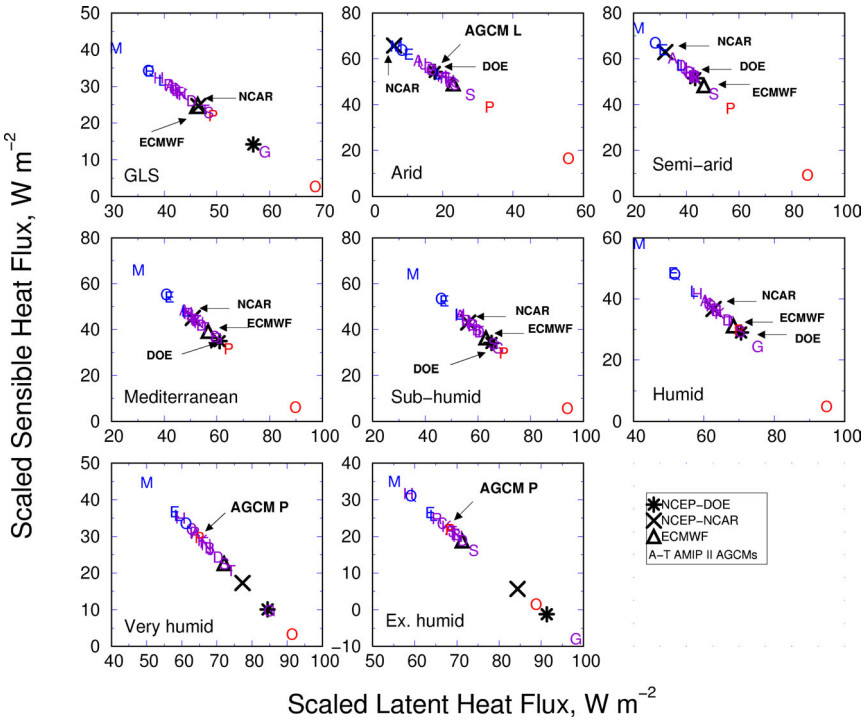

Figure 3.10: Partitioning of surface energy between sensible (SH) and latent (LH) heat fluxes by 20 AMIP II AGCMs (shown as the letters A-T) and three reanalyses (NCEP-DOE, NCEP-NCAR and ECMWF) after scaling the fluxes based on the surface available energy. The surface fluxes by all reanalyses and AGCMs have been scaled by the ratio of the sums of LH and SH of each to that of the ensemble reanalysis.

Spatio-temporal analysis of AGCMs' LH and SH over the de Martonne climate regimes

Latent heat (LH) flux

Compared to ensemble reanalyses, the AGCMs perform less well (smaller coefficient of correlation and larger deviation from unit of normalised standard deviation) in the arid climate (Figure 3.11a). The correlation coefficient between the simulated LH of AMIP II AGCMs and different reanalyses increases towards the more humid climates. The inter-model differences of the statistics are also greater in arid climates and become smaller (better inter-model agreement) in the wetter climates.

Sensible heat (SH) flux

Though the whiskers are extended over a large range due to some outlying models, the box plots for each climate show that 80% of the AGCMs have an amplitude ratio between 0.5 and 1.0 and correlation coefficients between 0.3 and 0.7 (Figure 3.11b). The whisker lines for the correlation coefficients suggest that the spatio-temporal correlations between the AGCMs' and the reanalyses' SH are smaller in the humid climates compared to that in the dry climates.

Ensemble AGCM versus ensemble reanalysis

Our analysis reveals that the spatio-temporal statistics among the reanalyses' LH or SH (not shown here, for details see Irannejad *et al.*, 2002) are not much better[3] than that between the AMIP II AGCMs and ensemble (Figure 3.11) or any one reanalysis. This implies that there are differences in spatial distribution and in temporal trends of mean monthly LH of the reanalyses that are of the same order of magnitude as differences between the models and the reanalyses.

[3] Here "better" means closer to one another.

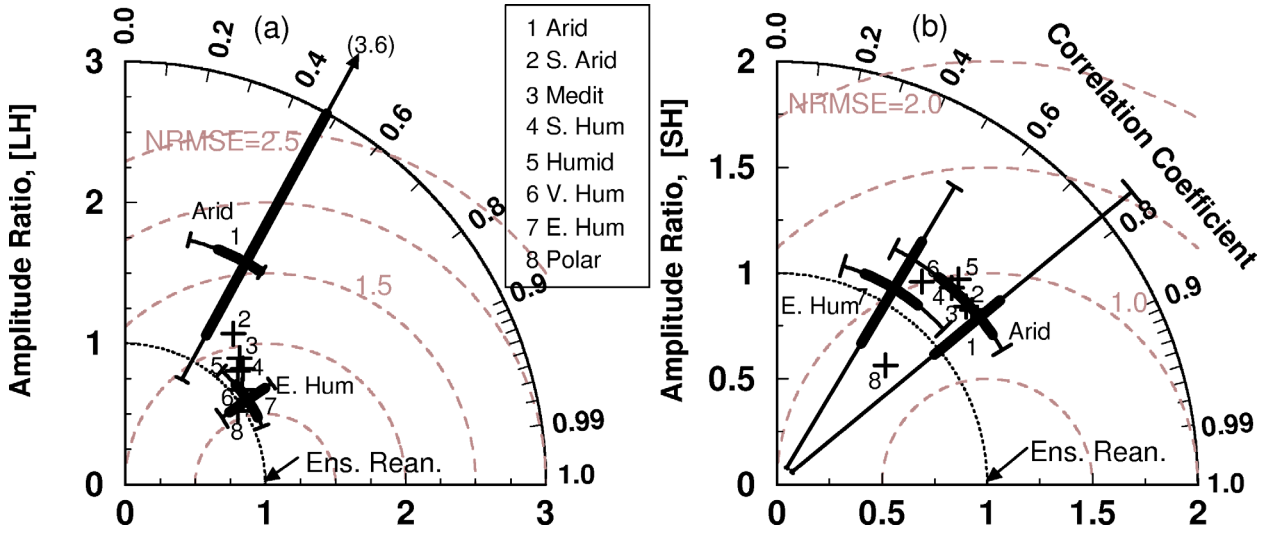

Figure 3.11: Modified Taylor diagrams demonstrating spatio-temporal statistics of 20 AMIP II AGCMs' (a) LH and (b) SH in different climate zones against ensemble reanalysis. In the figure, the radial distance is the spatio-temporal amplitude ratio; dotted quarter circle, passing through the amplitude ratio one, is the perfect match of standard deviations; angular dimension is cosine of spatio-temporal pattern correlation; the linear distance from the "Ens. Rean.", the point where AGCMs perfectly agree with the ensemble reanalysis, is the normalised root mean square error (NRMSE). Here the spatio-temporal statistics of 20 AGCMs in arid and extremely humid are shown as box plot, which produces two filled boxes and whiskers plots for each climate regimes. The filled boxes, along the radial line and also over the arc, show the range between the 10th and 90th percentile values (i.e. 80% of the AGCMs have values within this range) of the amplitude ratio and the correlation coefficient respectively. The point where two boxes meets show the median values of these two statistics. The whiskers are lines or arcs extending from each end of the box that pass through the median value to show the extent of the rest of the data. For other climates, semi-arid to very humid, only median values are shown using "+" symbol.

It has been found from the PILPS off-line experiments (Shao and Henderson-Sellers, 1996) that the ensemble of all models provides better estimates of land-surface processes than any single model. The large differences among the global reanalyses investigated here make it reasonable to try to extend such a hypothesis to these available reanalysis products. In Figure 3.12, we compared the spatio-temporal statistics of the ensemble LH and SH of all 20 AGCMs against the ensemble of all three reanalysis data sets. The results suggest that the conclusion regarding the climate-dependency of model performance holds when the ensemble values are compared. There is also a high degree of consistency between the spatio-temporal trends (higher correlation coefficients) and spatio-temporal variations (near to unit amplitude ratio) of the ensemble means. Assuming that the average of the three reanalysis data sets provides a better estimate of 'truth', we believe we can confirm the PILPS off-line finding about the superiority of the ensemble models' estimate to a single model simulation.

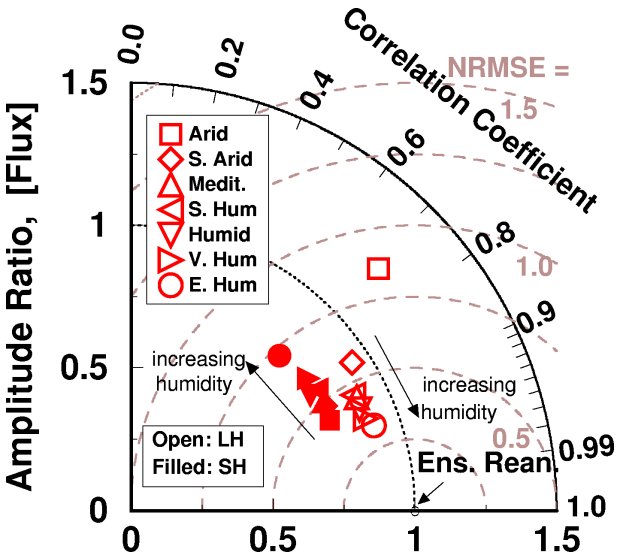

Figure 3.12: Taylor diagram demonstrating spatio-temporal statistics of the ensemble AMIP II AGCMs' LH (open symbol) and SH (filled symbol) against ensemble reanalysis in different climate regimes

Evaporation ratio and runoff ratio over the GEWEX-CEOP basins

The Following analysis (Figure 3.13) illustrates three features simultaneously: (i) land-surface water budget, (ii) partitioning of precipitation into evaporation and runoff through evaporation (*Ev*/*Pr*) and runoff (*Ro*/*Pr*) ratios, and (iii) comparison of AGCM simulations against observations. It is worth mentioning here that this analysis successfully identified an error in one model's code and has prompted the world's pioneer modelling groups to carefully investigate their code.

Based on this analysis over any GEWEX-CEOP regions, at least nine out of 20 AGCMs conserve surface water while only six conserve it over the GLS. Seven out of 20 AGCMs (I, J, N, O, P, Q, T) conserve water in all seven GEWEX-CEOP regions. Among these seven AGCMs, O and P use a one-layer classic "bucket" scheme with no canopy resistance, while T uses the same one-layer "bucket" scheme but with detailed physiological parameters for the canopy resistance calculation (Table 3.2). AGCM A also uses a "bucket" model with constant canopy resistance but fails to conserve water over five out of seven GEWEX regions because of its incorrect reporting of runoff. The remaining four AGCMs (I, J, N and Q) have SVAT schemes that use many hydrological and physiological parameters to simulate evapotranspiration.

At least one out of the 20 AGCMs simulates the same range of observed runoff-evaporation ratio over the GLS and five GEWEX-CEOP regions: GCIP, BALTEX, MAGS, GAME and MDB. BALTEX is the only basin where three AGCMs (C, D, J) simulate similar ranges. AGCM P, which uses the bucket scheme with no canopy resistance, fails to simulate any of the ratios as observed over any regions. The LBA is the only region where all AGCMs simulate smaller *Ro* ratios and larger *Ev* ratios compared to observations. The MDB has the highest number of AGCMs (11 out of 20) losing water (i.e., $Pr–Ev–Ro<0$); out of these 11 AGCMs, seven have evaporation alone greater than precipitation (i.e., $Pr–Ev<0$) as described in relation to Objective 1.

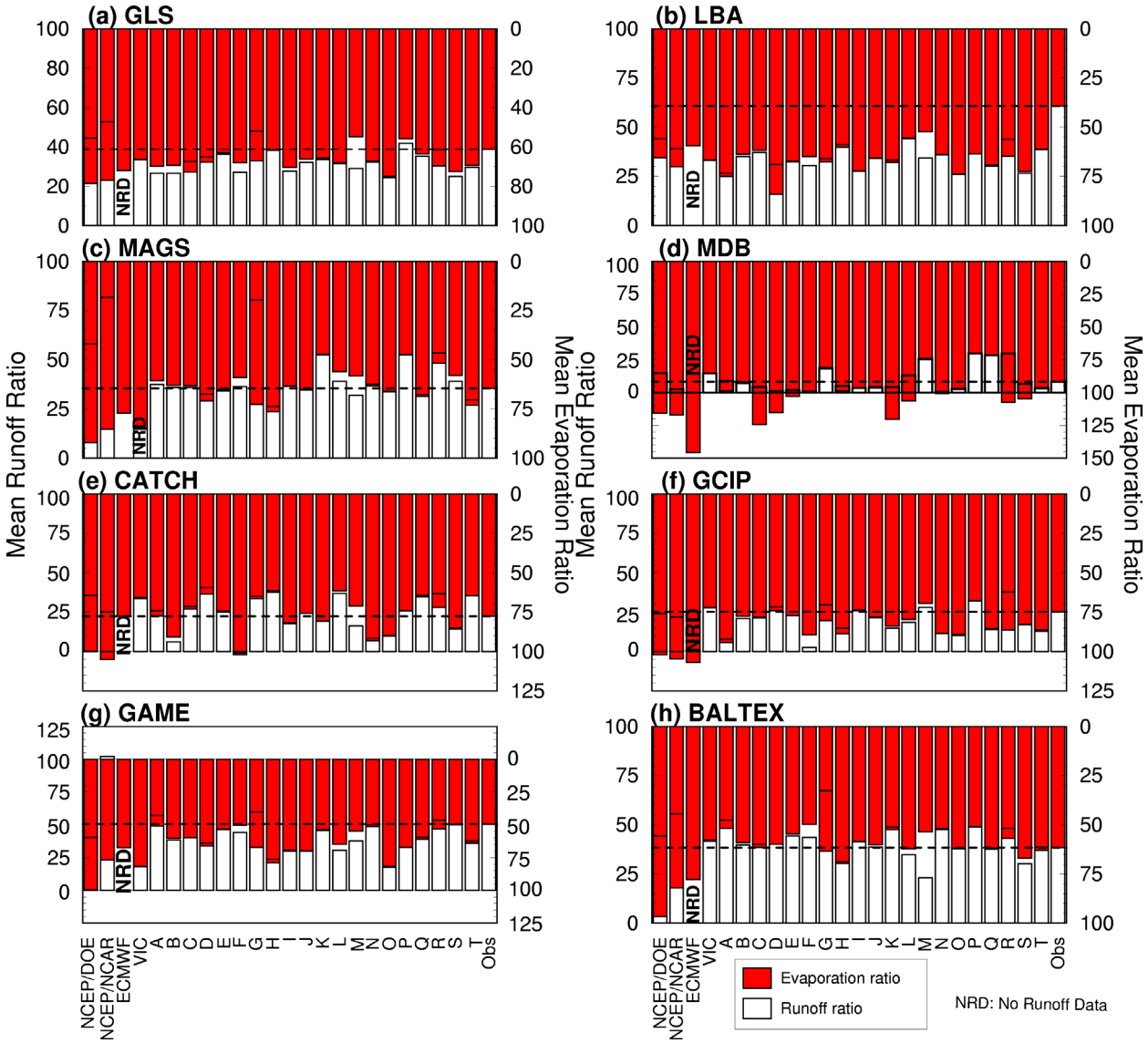

Figure 3.13: The 17-year (15-year for ECMWF and 14-year for VIC) mean runoff (total= surface +drainage) ratio (Ro/Pr, in %) and evaporation ratio (Ev/Pr, in %) over (a) GLS (global land-surface); (b) LBA; (c) MAGS; (d) MDB; (e) CATCH; (f) GCIP; (g) GAME; (h) BALTEX. "Obs" is based on precipitation from Climate Prediction Center Merged Analysis of Precipitation (CMAP) and runoff from Global Runoff Data Centre (GRDC). Observed Ev is the difference between Pr and Ro based on assumption that over the multi-year scale the change in soil moisture is negligible compared to other components (i.e. Pr, Ro, Ev). Conservation of water is seen when the sum of the two ratios is 100, i.e. when Pr = Ro + Ev (e.g. VIC and AGCM M).

Spatio-temporal correlation between observed and simulated precipitation, runoff and evaporation over the GEWEX-CEOP basins

The median correlation coefficients between observations and all AGCM simulations are relatively larger for precipitation (0.4-0.84; Figure 3.14) than those for runoff (0.34-0.58; Figure 3.15) and evaporation (0.03-0.7; Figure 3.16). The correlation coefficient is larger for precipitation over MAGS, CATCH and GAME (0.8-0.9), smaller over BALTEX and GCIP (0.45-0.55) and between 0.6 and 0.7 over LBA and MDB. Between evaporation and runoff, the correlation coefficient is very small for evaporation over LBA, BALTEX, GAME and MAGS (*Ev*: 0.03-0.15; *Ro*: 0.35-0.42), large over CATCH (*Ev*: 0.7; *Ro*: 0.45) but comparable over the remaining three basins (MDB, GCIP and CATCH) (between 0.4-0.5).

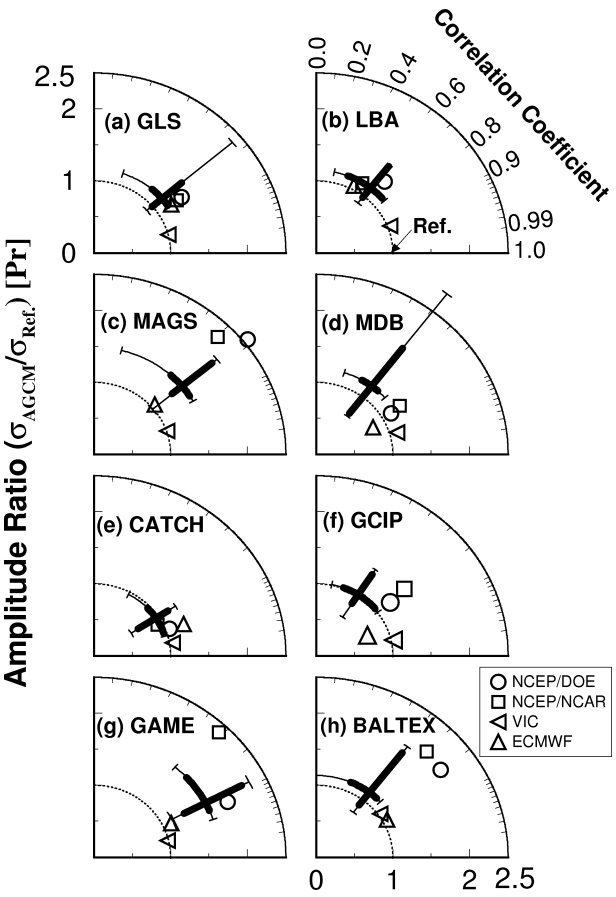

Figure 3.14: Taylor diagrams demonstrating spatio-temporal statistics of the ensemble AMIP II AGCMs' precipitation against ensemble reanalysis (a) GLS, (b) LBA, (c) MAGS, (d) MDB, (e) CATCH, (f) GCIP, (g) GAME, (h) BALTEX. [for description, see Figure 3.11]

The median amplitude ratios of the variables over the seven basins show that runoff has a smaller and precipitation has a larger deviation from the unit of normalised deviation. Amplitude ratios are greater than unity over almost all basins (except CATCH) for precipitation, over four basins (GAME, MDB, MAGS and GCIP) for evaporation and two basins (MAGS and MDB) for runoff.

Among the two reanalyses and one off-line simulations by VIC, VIC's precipitation agrees better with observed precipitation; for evaporation and runoff, the spatio-temporal statistics of these three model-derived evaluation data sets are similar. No apparent relationship can be seen between climate types and the spatio-temporal statistics of the basins. For example, LBA and GAME have similar spatio-temporal statistics despite very different climate type and climatologies (see Henderson-Sellers *et al.*, 2002*a*).

The inter-model differences of the statistics (shown by the ranges and boxes) vary in different basins. Among the seven GEWEX-CEOP basins, intermodel differences for precipitation and evaporation are largest over MDB and smallest over CATCH, both of which are classified as Mediterranean climate (see Henderson-Sellers *et al.*, 2002*b*). Similarly for runoff, intermodel differences are largest over MAGS and smallest over LBA. These two basins both have extremely humid climates, although they have very different climatologies.

From the above analysis, it can be concluded that the AGCMs' precipitation better matches with observations than do the AGCMs' evaporation and runoff. This result suggests that the spatio-temporal differences between AGCMs' evaporation and runoff are not purely due to the spatio-temporal differences between the AGCMs' atmospheric characteristics. It thus appears that land-surface parameterisation schemes are playing a role in the differences analysed here.

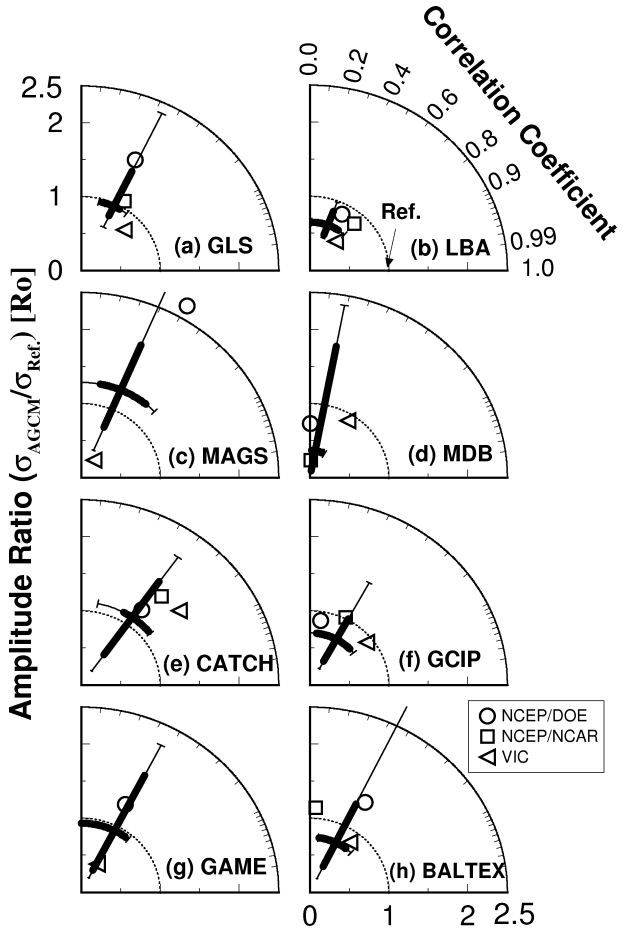

Figure 3.15: Taylor diagrams demonstrating spatio-temporal statistics of the ensemble AMIP II AGCMs' runoff against ensemble reanalysis (a) GLS, (b) LBA, (c) MAGS, (d) MDB, (e) CATCH, (f) GCIP, (g) GAME, (h) BALTEX. [for description, see Figure 3.11]

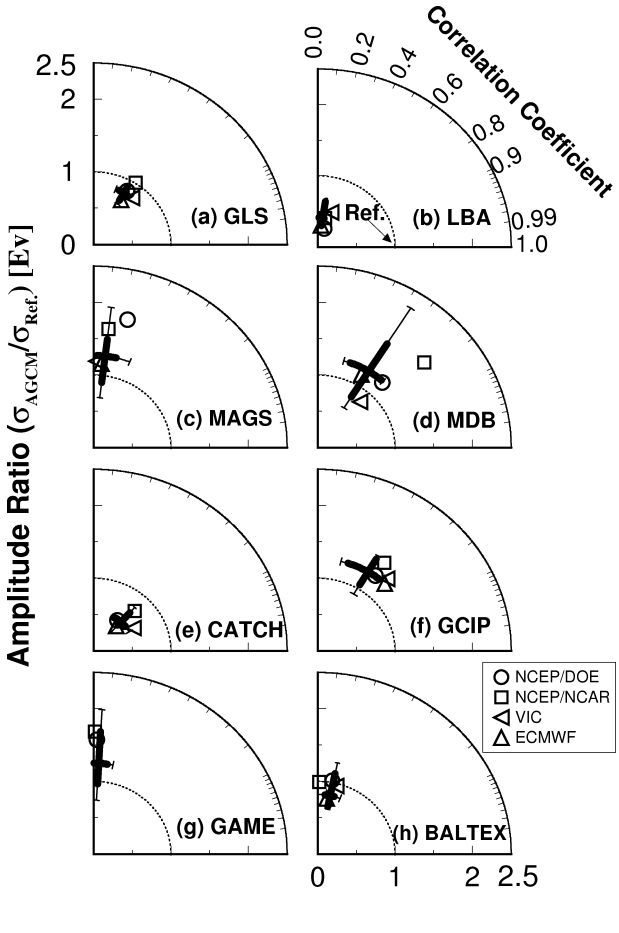

Figure 3.16: Taylor diagrams demonstrating spatio-temporal statistics of the ensemble AMIP II AGCMs' evaporation against ensemble reanalysis over (a) GLS, (b) LBA, (c) MAGS, (d) MDB, (e) CATCH, (f) GCIP, (g) GAME, (h) BALTEX. [for description, see Figure 3.11]

Evaporation and LSS complexity

In this study, an attempt has been made to relate AGCM simulations and land-surface scheme complexity. We naturally expect that the AGCMs' mean basin evaporation will increase with increasing precipitation and near-surface air temperature. Analysis shows that the basin-mean evaporation of AGCMs does indeed increase with increasing precipitation and near-surface air temperature but at different rates. To investigate whether the differences in rates across the AGCMs are due to the difference in the LSSs, a linear regression is fitted to the mean evaporation against both observed precipitation and observed air temperature data ($Ev=a_o+a_1$"*var*", where a_o is the regression intercept, a_1 is the slope, and "var" is either *Pr* or *T*). These slopes a_1 are sorted from minimum to maximum and plotted for corresponding AGCMs in Figure 3.17.

As shown in Figure 3.17*a*, in general the AGCMs that use classic "bucket" schemes (P, O) have a relatively smaller dependence on precipitation compared to complex SVAT schemes (e.g. I, F, N). The LSSs that use constant (AGCM A) or detailed (AGCM T) canopy resistance lie inbetween the buckets and the SVATs. The AGCMs F and N, which apparently use the same LSS and atmospheric model but with a different version, have a similar slope. AGCM I has a relatively larger slope than that for J, though they use the same LSS and atmospheric model. One possible reason could be that AGCM I has a finer vertical resolution (L58) than does J (L19) (Table 3.2). The larger slope for AGCM E compared to that for M may be also due to the finer horizontal resolution used in E. Similarly between L and Q, the slope is larger for Q (with its

higher horizontal and vertical resolution), though apparently they use a similar LSS but a different atmospheric model.

From these results, we may say that, within AGCMs that use the same LSS, evaporation is more dependent on precipitation in an AGCM with higher resolution. To compare across different schemes, we consider AGCMs L and M, where M is more complex than L (Table 3.2), though they are modified from the same LSS. Although M is more complex than L, they have very similar slopes with L just greater than M. At this stage, we cannot identify general rules that can be used to explain the relation across AGCMs that use different LSSs.

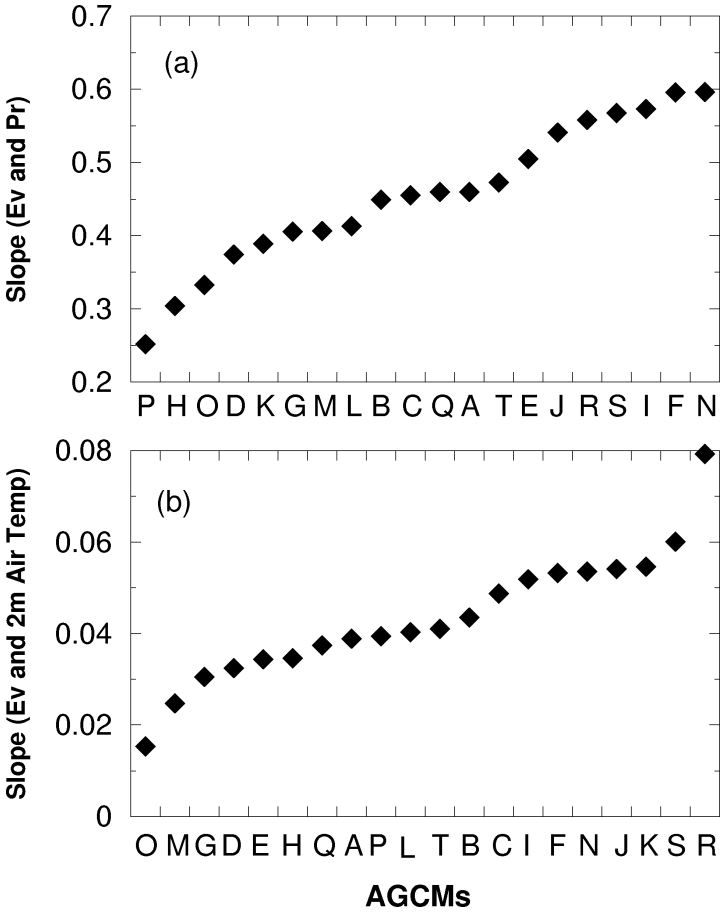

Figure 3.17: Slope of the regression line of 20 AMIP II AGCMs. Each linear regression is fitted to the AGCM simulated basin-mean evaporation against their (a) precipitation, and (b) near surface air temperature in ℃.

The ranking of the LSSs is changed for some AGCMs in Figure 3.17*b*. For instance, AGCM P moved from rank 1 in Figure 3.17*a* to 9 in Figure 3.17*b*. At this stage, we do not know the reasons for such shifting. Further analysis will be continued to identify the reasons/parameters, if any, that effects such ranking.

T3.4.6 Response of different land-surface schemes (LSSs) to atmospheric forcing

The main objective of Task 3 is to evaluate the dependence of AGCMs' simulated land surface (LS) variables, i.e. latent (LH) and sensible (SH) heat fluxes, on the land-surface scheme (LSS) complexity. The main problem, however, is that the comparison of land surface variables of different AMIP II models is difficult because of the differences in LSSs, atmospheric forcing and their corresponding feedback. The differences between the land surface variables across the AGCMs may not depend only on LSS complexity but also on atmospheric forcing and their corresponding feedback. Here we initiate (statistical) research to compare the land surface variables across the models by excluding their atmospheric forcing and feedback. For this we establish the determination equations, the pseudo land surface schemes (PLSSs), for the

regional latent heat flux of 19[4] AMIP II AGCMs as a function of a set of seven forcing variables and soil moisture as,

$$\mathrm{LH} = b_o + \sum b_i v_i \qquad (3)$$

where b_o is the regression intercept and b_i is the regression coefficient for forcing v_i. The forcing which we used for PLSSs are precipitation, near surface (2m) air temperature, near surface (2m) specific humidity, near surface (10m) wind velocity, surface pressure, and downward long wave and short wave radiation. These forcing variables are chosen based on the variables used in running land-surface schemes offline (e.g. Chen *et al*., 1997). We also used soil moisture as a variable because LH is a direct function of soil moisture.

To exclude the differences in the magnitudes of the variables (e.g. pressure: around 9000 N m^{-2}, precipitation: around10^{-5} kg m^{-2}, wind velocity: around 1 m s^{-1}), we used their normalised values, so that all the normalised variables had zero mean and unit standard deviation, and all the PLSSs' equations had zero intercept. Hence the regression coefficients of these PLSSs show the weight of each forcing variable on the simulated LH.

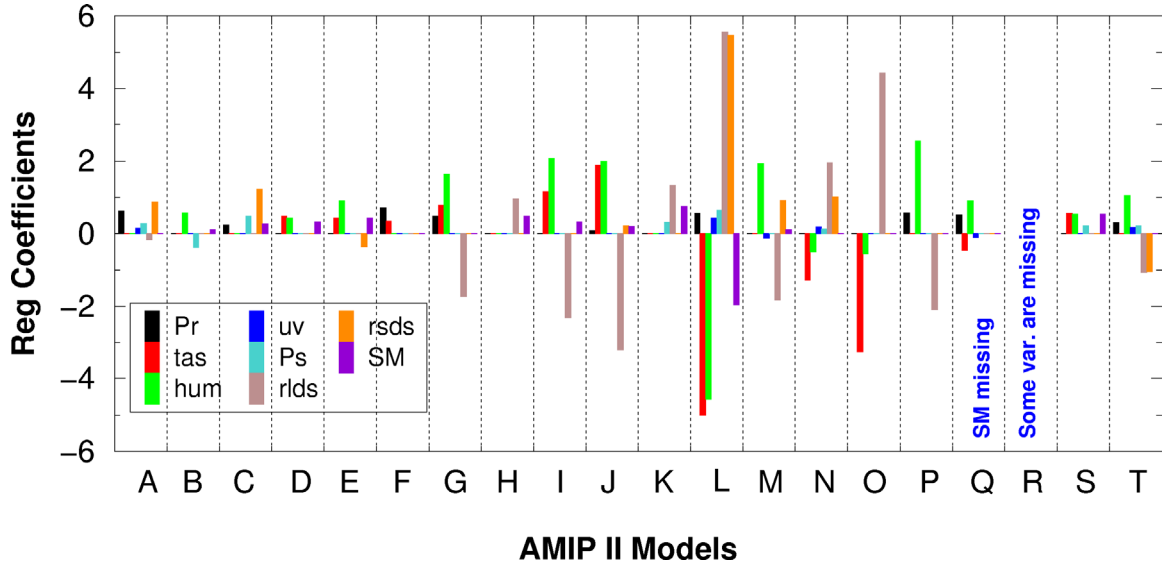

Figure 3.18: Regression coefficients calculated by fitting the normalised latent heat against normalised precipitation (Pr), air (2m) temperature (tas), specific humidity (hum), wind velocity (uv), pressure (Ps), soil moisture (SM) and long (rlds) and short (rsds) wave downward radiation over the GCIP basin.

The regression coefficient values thus calculated for GCIP are shown in Figure 3.18. Among the seven forcing variables, air temperature, humidity and longwave radiation are relatively more important in LH calculation, while wind velocity and pressure are less important. In most of the AGCMs, evaporation increases with increasing/decreasing air temperature and humidity (e.g. AGCM I, L, O). Evaporation should increase with increasing air temperature, but it should also theoretically increase when humidity is low in the air, which is not reflected in the regression coefficient values.

Figure 3.18 also shows that the AGCMs A, O, P and T that use bucket scheme with or without canopy resistance do not show any dependence on soil moisture in their LH calculation. This suggests that the long-term history of moisture is not important in the bucket-type schemes. Hence, monthly precipitation serves to define the moisture availability for evaporation in such

[4] AGCM R is excluded from this analysis because its five out of seven atmospheric forcing variables are not reported.

models. Although this conclusion is similar to that found from the lag-correlation analysis over Australia, we can not generalise this conclusion over LBA and BALTEX. Also, there are some SVAT schemes where soil moisture is not important for the simulated LH (e.g. AGCM F, G, N and Q in Figure 3.18). Due to lack of available information about the LSS parameterisations, at this stage we do not know whether this is a random effect or if it is the effect of LSS parameterisation. Further investigation will be carried out during 2003.

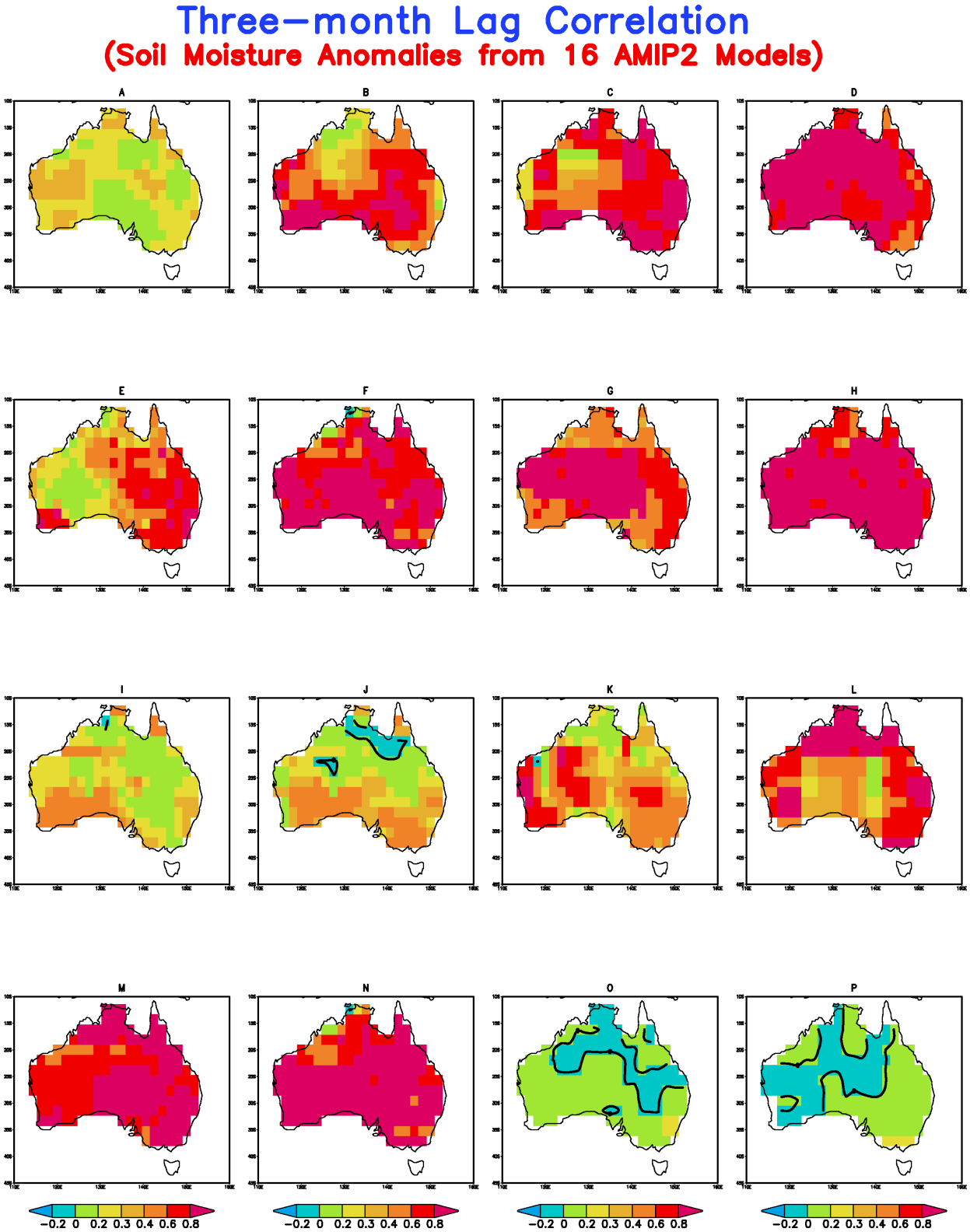

Figure 3.19: Three month lag-correlation, showing the soil moisture anomalies of the 16 AMIP II models

T3.4.7 Australian-specific correlation analysis of AMIP II simulations (jointly with BMRC)

The analysis of AMIP II model results over the Australian region has made progress in three important areas. We have expanded the analysis of AMIP II results from ten to sixteen models. A BMRC report (Zhang *et al*., 2002) has been produced to summarise the analysis. Results further consolidate the previous analysis. Numerous differences are found among the models and between models and observations. Specifically, models with simple bucket-type soil hydrology schemes tend to exhibit a rapid decay of soil water anomalies and exhibit too weak an influence on forecasts of surface climate anomalies resulting from changed soil moisture conditions. Figure 3.19 displays the auto-correlation of soil moisture anomalies across all the AMIP II AGCMs. Clearly, models O and P, both employing a simple bucket-type soil hydrology model (Table 3.2), have the lowest auto-correlation on a seasonal time scale.

AMIP II integrations from a version of the BMRC Atmospheric Model (BAM) have been analysed over the Australian region and results have been compared with the 16 AMIP II AGCM simulations (Zhang, 2002). Using a simple land-surface scheme with a bucket-type soil model, results from the BAM simulations have demonstrated similar features as seen from other bucket-type models. Further analysis of the model simulation using an improved land-surface model will be evaluated and the role of land-surface modelling will be further explored by contrasting the same host model simulations with two different surface schemes.

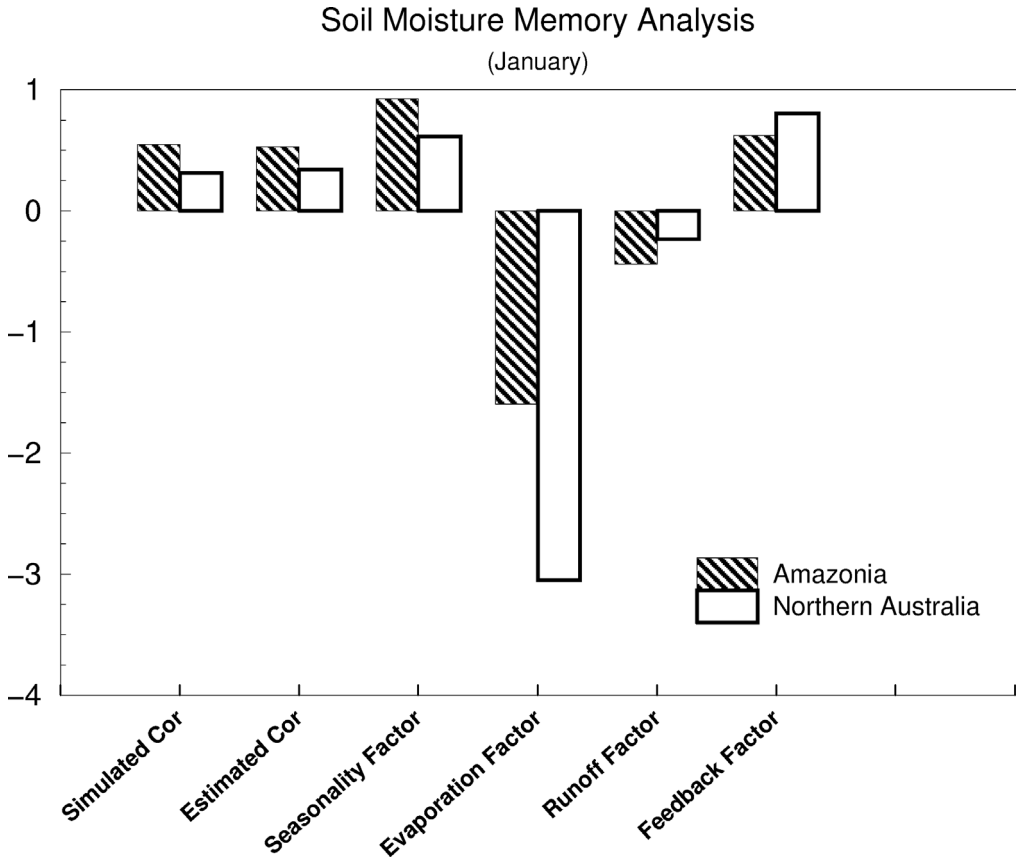

Figure 3.20: Soil moisture memory analysis over Northern Australia and Amazonia.

A detailed analysis of soil moisture memory has been conducted using the results from the BAM AMIP II simulations, following the approach of Koster and Suarez (2001). The aim was to investigate why soil moisture memory is short in the bucket schemes. Two competing processes can affect the soil moisture memory in the bucket model: one is that it lacks canopy constraints on the release of soil water, leading to a short soil water retention. The other is that in the bucket scheme, no runoff occurs until the whole volumetric soil is saturated and there is no rapid evapotranspiration due to canopy interception of precipitation, both leading to longer

memory associated with the soil. Figure 3.20 shows the preliminary results over the northern Australian and Amazonian regions. In both cases, rapid evaporation of soil moisture is the dominant reason why soil memory is short in the bucket scheme, even though it is relatively weaker in the Amazonian region.

T3.4.8 Summary and conclusions from objective 2

The results presented here have a number of facets:

- AMIP II Diagnostic Subproject 12 has been successful in the sense that we have already delivered useful information to the climate modelling community. Specifically, a number of AMIP modelling groups have revised their land-surface outputs as a result of interaction with us and a smaller number of modelling groups are reconsidering their land-surface schemes (LSSs).
- There is a high degree of consistency between the spatio-temporal trends (higher correlation coefficients) and spatio-temporal variations (near to unit amplitude ratio) of the ensemble mean AGCMs' fluxes and the ensemble of the evaluation products. If it can be assumed that the average of the three evaluation data sets provides a better estimate of 'truth' than any individual, then this study confirms the PILPS off-line finding about the superiority of the ensembles. Our analyses show that a combined model's estimate is superior to any single model simulation in almost every situation.
- Our analyses reveal for the first time two LSS "clusters": the buckets and the "SiBlings".
- Although there are very large variations between simulated surface climates, we do find coherence between AGCMs' land-surface states as a function of (pre-defined) climate type.
- Smaller spatio-temporal correlation coefficients between observed and AGCMs' simulated evaporation and runoff than those for precipitation suggest that the differences between the AGCMs' evaporation and runoff are not solely due to precipitation differences, i.e. different LSSs act differently in the partitioning of precipitation between evaporation and runoff.
- None of the AGCMs could predict observed ranges of the evaporation-runoff ratios over the LBA (which enjoys large precipitation and high air temperature).
- By contrast, some of the AGCMs simulated the observed ranges in the dry and warm basins (Mediterranean climate) such as MDB and CATCH, but their predictions differ most in these basins. This suggests that more attention should be paid by the modelling groups to aspects of their LSSs' parameterisations that affect surface water budgets in these basins. There may also be a need to enhance the CEOP observational effort in such basins (MDB and CATCH) but also in cold areas (GAME-Siberia and MAGS) so that attempts to improve LSS parameterisation can be evaluated using higher quality observations. It is worth mentioning here that such initiatives have already been taken in the MDB (see Objective 1, section T3.3).
- The analyses also show that land-surface scheme complexity has an effect on the simulation of surface water budgets in the major basins of the world. This is clear because the surface water variables from the AMIP II AGCMs depend on the LSS type to a greater extent than simulated precipitation and air temperature. Thus the selection of a land-surface parameterisation scheme by climate modelling groups is important for prediction of variables such as evaporation and runoff, which are themselves critical for many human activities including agriculture and water resource management.
- Long-term histories of soil moisture are not important for evaporative fluxes from AGCMs that use simple bucket-type schemes for representing soil hydrology.
- A detailed analysis of soil moisture memory over northern Australian and Amazonian regions, following the approach of Koster and Suarez (2001), suggests that rapid

evaporation of soil moisture is the dominant reason for having short soil memory in the bucket-type scheme.

T3.5 Reports and papers

T3.5.1 Objective 1

- Airey, P., Chambers, S.D., and Henderson-Sellers, A. 2001. Sustainable Groundwater Development: Climate Model Evaluation**.** Research proposal presented at the *Advisory Group Meeting on Isotope Applications in Integrated Climate System Studies*, 18-20 November 2001, IAEA Headquarters, Vienna, Austria.

- Henderson-Sellers, A., Chambers, S.D. and Airey, P. 2001. ANSTO Balance: Integrated Climate System Studies Using Isotopes. *Australian Nuclear Science and Technology Organisation promotional brochure*. pp 16, November 2001.

- Henderson-Sellers, A., Chambers, S. and Airey, P. 2001. Australia's Contribution to Isotopes in Integrated Climate System Study (ICSYS). Position paper for the *Advisory Group Meeting on Isotope Applications in Integrated Climate System Studies*, 18-20 November 2001, IAEA Headquarters, Vienna, Austria. pp 17.

- Henderson-Sellers, A. 2002. Isotopes, forests and global climate model predictions for the South Pacific, Oral presentation at *SPERA* conference, Lucas Height, NSW, 13-17 May 2002.

- Henderson-Sellers, A., McGuffie, K., Zhang, H. and Chambers, S. 2002. Testing global climate model predictions of the impact of land-use change in Amazonia using stable isotopes, Poster presentation at *SPERA Conference on Environmental Radioactivity: Migration, measuring and monitoring in the South Pacific*, Lucas Heights Science and Technology Centre, Sydney, Australia, 13-17 May 2002.

- Henderson-Sellers, A. 2002. South pacific in the global-warming hot seat, Article published in the *Canberra Times* on Thursday 20 June 2002.

- Henderson-Sellers, A., McGuffie, K., Zhang, H., Sharmeen, S. and Chambers, S. 2002. Investigating Water Recycling Processes in the Amazon using 20 AMIP II Models and Isotopes. Poster presentation at *AMIP International Workshop*, Toulouse, France, 12-15 November 2002.

T3.5.2 Objective 2

- Chambers, S.D. and Chapin, F.S. 2002. Fire effects on surface-atmosphere exchange in Alaskan black spruce ecosystems: implications for feedbacks to regional climate. *In press. Journal of Geophysical Research – Atmospheres*

- French, N.H.F., Kasischke, E.S., Colwell, J.E., Mudd, J.P. and Chambers, S. 2002. Preliminary assessment of the impact of fire on surface albedo. *In press for the Proceedings of The Role of Boreal Forests and Forestry in the Global Carbon Budjet*. 8-12 May 2000, Edmonton, Alberta, Canada, M.J. Apps and J. Marsden, eds.

- Henderson-Sellers, A. 2002. Land Surface Models and Isotopes. Presented at the Murray Darling Basin (MDB) Water Balance Project (WBP) meeting at Bureau of Meteorology Research Centre (BMRC) on 16th July 2002.

- Henderson-Sellers, A. and Pitman, A.J. 2002, Comments on "Suppressing impacts of the Amazonian deforestation by the global circulation change", *Bulletin of the American Meteorological Society*, 83, October, 2002.

- Henderson-Sellers, A. and Pitman, A.J., 2002, Evaluation of land-surface simulations - highest cited Australian research paper, *Bulletin of the Australian Meteorological and Oceanographic Soc.*, 15, 6-12.

- Henderson-Sellers, A., Irannejad, P., McGuffie, K., Sharmeen, S., Phillips, T.J. and Zhang, H. 2002. Evaluation of land-surface energy budget of AMIP II global climate models. Oral presentation at *AMIP International Workshop*, Toulouse, France, 12-15 November 2002.

- Henderson-Sellers, A., Irannejad, P., McGuffie, K., Sharmeen, S., Phillips, T.J. and Zhang, H. 2002. Evaluation of land-surface energy budget of AMIP II global climate models. *WCRP Workshop Proceedings*, WMO, Geneva, 2003.

- Henderson-Sellers, A., Irannejad, P., Pitman, A.J. and McGuffie, K. 2002. Is land-surface climate prediction capability Improving? *Geophysical Research Letters.* (submitted).

- Henderson-Sellers, A., Irannejad, P., Sharmeen, S., Phillips, T.J. and McGuffie, K. 2002. Evaluation of AMIP II global climate model simulations of the land-surface water budget and its components over the GEWEX-CEOP Regions. *Journal of Hydrometeorology*. (submitted) [also available at PCMDI web].

- Henderson-Sellers, A., Pitman, A.J., Irannejad, P. and McGuffie, K. 2002. Land surface simulations improve atmospheric modelling, *EOS*, 83(13), 26 March 2002, p. 145 and 152.

- Irannejad, P., Henderson-Sellers, A., Sharmeen, S., Phillips, T.J., McGuffie, K. and Zhang, H. 2002. Analysis of land-surface water budget in the AMIP II global climate models over the GEWEX-CEOP Regions. Oral presentation at *AMIP International Workshop*, Toulouse, France, 12-15 November 2002.

- Irannejad, P., Henderson-Sellers, A., Sharmeen, S., Phillips, T.J., McGuffie, K., Pitman, A.J. and Zhang, H. 2002. Evaluation of the Annually Averaged Land-surface Energy Budget Simulations of Twenty AMIP II Global Models. To be submitted to the *Journal of Climate*.

- Irannejad, P., Sharmeen, S., Henderson-Sellers, A., Phillips, T.J. and McGuffie, K. 2002. Energy and radionuclide evaluation of global climate model predictions of near-surface climates, Poster presented at *SPERA* conference, Lucas Height, NSW, 13-17 May 2002.

- Phillips T.J., Henderson-Sellers A., Irannejad P., McGuffie K., Zhang H., 2002, AMIP II diagnostic subproject 12: Landsurface processes and parameterizations (a joint AMIP/PILPS project). Accessible online at http://www-pcmdi.llnl.gov/pilps3/proposal/.

- Phillips, T. Henderson-Sellers, A., Irannejad, P., McGuffie, K., Sharmeen, S., Zhang, H. 2003. Validation and Diagnosis of AMIP II Land-surface Simulations, Abstract submitted in the *14th Symposium on Global Change and Climate Variations*, 83rd Annual AMS Meeting, Long Beach, California, 9-13 February, 2003 (in press).

- Phillips, T.J., Henderson-Sellers, A., Irannejad, P., McGuffie, K., Sharmeen, S. and Zhang, H. 2002. Large-scale validation of AMIP II land-surface simulations, Oral presentation at *AMIP International Workshop*, Toulouse, France, 12-15 November 2002.

- Zhang, H., Henderson-Sellers, A., Irannejad, P., Sharmeen, S., Phillips, T.J. and McGuffie, K. 2002, Land-surface modelling and climate simulations: results over the Australian region

from sixteen AMIP2 models, BMRC Research Report 89. BMRC, Australia. Also *published in the internal PCMDI web site* (www-pcmdi.llnl.gov/pilps3/bmrc2002/report.pdf).

- Zhang, H., Henderson-Sellers, A., Irannejad, P., Sharmeen, S., Phillips, T.J. and McGuffie, K. 2002. Analysing AMIP2 Model Data over Australian Region: Preliminary Results of Surface Climate and Surface Fluxes Simulations from Ten Models, *9th Australian Meteorological and Oceanographic Society Conference*, Melbourne, 18-21 February 2002.

- Zhang, H., Henderson-Sellers, A., Irannejad, P., Sharmeen, S., Phillips, T., McGuffie, K. 2002. Analysis of Sixteen AMIP2 Model Simulations over the Australian Regions. Oral presentation at *AMIP International Workshop*, Toulouse, France, 12-15 November 2002.

- E-report 749 HACV Annual Review 2002, ISBN 0-642-59996-3 ISSN 1030-7745.

Prof. A. Henderson-Sellers, participated in the Science Week Festival forum on "Complexity". The panel discussion in front of a 200 strong live audience in Canberra on 22 August debated the topic "Complex System Science". This discussion was broadcast by ABC Radio National on 26 and 27 August in "The Buzz" program entitled "It's not that Simple".

T3.6 Task 3 summary and future directions

The two objectives of Task 3 are:

1. To investigate the use of naturally occurring isotopes in regional moisture studies; and
2. To improve land-surface parameterisation and investigate its potential to improve global climate models and thus improve our future climate change predictions.

These have been turned into our two current research hypotheses:

1. Stable isotopes of water provide a novel data source for evaluation of GCM simulations of regional hydrology; and
2. Land-surface scheme (LSS) complexity improves the simulation of continental near-surface climates.

This year (i.e. since the previous external project review in November 2001) we have made significant scientific progress towards evaluating both these hypotheses. Specifically we have:

(i) confirmed and completed the GNIP Amazon isotopes study and published;

(ii) completed a preliminary investigation of the use of isotopic data for large basin hydrological evaluation of GCM simulations in the Murray Darling Basin;

(iii) contributed to the successful proposal to the GEWEX GHP that the MDBP become a new CEOP region;

(iv) evaluated the surface energy and water budgets of 20 AMIP II AGCMs and three re-analyses data sets and submitted three papers for publication;

(v) completed the lag correlation analysis of AMIP II simulations and published a BMRC report; and

(vi) four papers and one poster on these topics in the AMIP II Toulouse conference in November 2002.

References

Arimoto, R., Uematsu, M. *et al.* 1999. Science and Implementation Plan for ACE Asia Network Studies, August 1999.

Avissar, R. 1992. Conceptual aspects of a statistical-dynamical approach to represent landscape subgrid-scale heterogeneities in atmospheric models, *J. Geophys. Res., 97,* 2729-2742.

Avissar, R. and Pielke, R.A. 1989. A parameterization of heterogeneous land-surface for atmospheric numerical models and its impact on regional meteorology, *Mon. Wea. Rev., 117,* 2113-2136.

Betts A.K., Viterbo P. and Wood E. 1998. Surface energy and water balance for the Arkansas-Red River basin from the ECMWF reanalysis, *J. Climate*, 11, 2881—2897.

Betts, A.K., Hong, S.Y. and Pan, H.L. 1996. Comparing of NCEP-NCAR reanalysis with 1987 FIFE data, *Mon. Wea. Rev.*, 124, 1480-1498.

Bonan, G.B. 1996. A Land Surface Model (LSM Version 1.0) for Ecological, Hydrological, and Atmospheric Studies: Technical Description and User's Guide. NCAR Technical Note NCAR/TN-417+STR, National Centre for Atmospheric Research, Boulder, Colorado, 150 pp. Also accessible at Web site www.cgd.ucar.edu:80/cms/lsm/technote.html.

Chen TH. Henderson-Sellers A., Milly P.C.D., Pitman A.J., Beljaars A.C.M., Polcher J., Abramopoulos F., Boone A., Chang S. Chen F. Dai Y. Desborough CE. Dickinson R.E., Dumenil L., Ek M., Garratt J.R., Gedney N., Gusev Y.M., Kim J., Koster R., Kowalczyk E.A., Laval K., Lean J., Lettenmaier D., Liang X., Mahfoouf J.-F., Megelkamp H.-T., Mitchel K., Nasonova O.N., Noilhan J., Robock A., Rozensweig C., Schaake J., Schlosser A., Schulz J.P., Shao Y., Shmakin A.B., Verseghy D.L., Wetzel P., Wood E.F., Xue Y., Yang Z.-L. and Zeng Q. 1997. Cabauw experimental results from the Project for Intercomparison of Land-surface Parameterization Schemes, *J. Climate*, 10, 1194--1215.

Cheng Z.L., Lam K.S., Chan L.Y., Wang T. and Cheng K.K. 2000. Chemical characteristics of aerosols at coastal station in Hong Kong. I. Seasonal variation of major ions, halogens and mineral dusts between 1995 and 1996, *Atmos. Environ.,* 34, 2771-2783.

Cohen D. 1999. Seasonal and regional variations in ambient fine particle concentrations and sources in New South Wales, Australia: A seven year study. *Proceedings of International Congress of Biometeorology and International Conference on Urban Climatology,* Sydney, Australia. 8-12 November 1999, pp607-612.

Cohen D.D. 1998. Characterisation of Atmospheric Fine Particle Using IBA Techniques, *Nucl. Instr. and Methods*, 136B, 14-22.

Cohen D.D., Bailey G.M. and Kondepudi R. 1996. Elemental Analysis by PIXE and Other IBA Techniques and their Application to Source Fingerprinting of Atmospheric Fine Particle Pollution, *Nucl. Instr. and Methods*, 109, 218-226.

Cohen D.D., Ghassan, T., Ed, S., David, G. and Box, G. 2000. The Measurement and Sources of Fine Particle Elemental Carbon at Several Key Sites in NSW over the Past Eight Years, *Proceedings of 15th International Clean Air Conference*. Sydney, Australia, 27-30 November 2000, pp485-490.

Cohen D.D. and Gras, J.L. 1998. Characterisation and Source Fingerprinting of Fine Particle in the Jakarta Region by Ion Beam Methods. *Proceedings of 14th International Clean Air and Environment Conference,* Melbourne, Australia, 18-22 October 1998, p194-199.

Cox, P.M., Betts, R.A., Bunton, C.B., Essery, R.L.H., Rowntree, P.R. and Smith, J. 1999. The impact of new land surface physics on the GCM simulation of climate and climate sensitivity, *Climate Dyn.*, 15, 183-203.

de Martonne, E. 1948. Traité de Geographie Physique, 7th ed., Librairie Armand Colin, Paris.

Debaje,-S.B., Vernekar,-K.G. and Ramachandran,-T.V. 1996. Study of atmospheric radon-222 concentrations at Pune, *Indian Journal of Environmental Protection,* October 1996, 16(10), 755-760.

Dentener, F., Feichter, J. and Jeuken, A. 1999. Simulation of the transport of Rn^{222} using on-line and off-line global models at different horizontal resolutions: a detailed comparison with measurements, *Tellus,* 51B, 573-602.

References

Dickinson, R.E., Henderson-Sellers, A. and Kennedy, P.J. 1993. Biosphere-Atmosphere Transfer Scheme (BATS) Version 1e as coupled to the *NCAR Community Climate Model,* NCAR Technical Note: NCAR/TN-387+STR, National Centre for Atmospheric Research, Boulder, Colorado, 72pp.

Dockery, D.W., Pope C.A., Xu X., Spengler J.D., Ware J.H., Fay M.E., Ferris B.G. and Speizer F.E. 1993. An Association between air pollution and mortality in six US Cities, *New England Journal of Medicine,* 329 (1993), 1753-59.

Fekete, B.M., Vorosmarty, C.J. and Grabs, W. 2000. Global, Composite Runoff Fields Based on Observed River Discharge and Simulated water Balances, available on line www.grdc.sr.unh.edu/html/Data/runoff.zip.

Genthon, C. and Armengaud, A. 1995. Radon-222 as a comparative tracer of transport and mixing in two general circulation models of the atmosphere, *J. Geophys. Res.,* 100(D2), 2849-2866.

Gibson, J.K., Kallberg, P., Uppala, S., Hernandez, A., Normura, A. and Serrano, E. 1997. ERA description, ECMWF Re-Analysis Project Report Series, 1, 72pp. ECMWF Reading RG2 AX, UK.

HACV 1999. Human Activity and Climate Variability Project: Annual Report '99, *Environment Division, Australian Nuclear Science and Technology Division, Menai, NSW.*

HACV 2000. Human Activity and Climate Variability Project: Annual Report 2000, *Environment Division, Australian Nuclear Science and Technology Division, Menai, NSW.*

HACV 2001. E-report 749, HACV Annual Review 2001, *ISBN 0-642-59996-3 ISSN 1030-7745.*

Harris, G.P., 2001. Anthropogenic impacts on the ecosystems of coastal lagoons - fundamental processes and management, Unpublished manuscript.

Hattori, T. and Ichiji, T. 1998. Estimates of seasonal variations of ^{222}Rn from different origins by using the correlation between ^{222}Rn and ^{212}Pb concentrations in air. *7th Tohwa University international symposium.* Fukuoka (Japan) 23-25 Oct 1997. Katase,-A. and Shimo,-M. (eds.) Radon and thoron in the human environment Singapore (Singapore) World Scientific Publishing Co. Pte. Ltd. 594 p. p. 246-251. 1998.

Heimann, M., Monfray, P. and Polian, G. 1990. Modeling the long-range transport of ^{222}Rn to subantarctic and arctic areas, *Tellus,* 42B, 83-99.

Henderson-Sellers, A., Irannejad, P., Sharmeen, S., Phillips, T.J. and McGuffie, K. 2002*a*. Evaluation of AMIP II global climate model simulations of the land-surface water budget and its components over the GEWEX-CEOP regions, Prepared for submission in the *Journal of Hydrometeorology*.

Henderson-Sellers, A., Pitman, A. J., Irannejad, P., and McGuffie, K. 2002*b*. Land-surface Simulations Improve Atmospheric Modelling, *EOS*, 83(13), pp145-152

Hien P.D., Bac V.T., Tham H.C. and Vinh L.D. 2002. PM2.5 and PM2.5-10 in Southeast Asia monsoon conditions. A case study Hanoi, Vietnam, *accepted for publication Atmos. Environ.*

Hoang, C.T. and Servant, J. 1972. Radon flux from the sea. *C. R. Acad. Sci. Paris.* 274, 3157-3160.

Hopke P.K., Biegalski S., Landsberger S., Maenhaut W., Artaxo P. and Cohen D. 1997. Characterisation of the GENT PM10 Sampler, *Aerosol Science and Technology,* 27, 726-735.

IAEA/WMO. 1999. Global Network for Isotopes in Precipitation. The GNIP Database. Release 3, October 1999, URL: www.iaea.org/programs/ri/gnip/gnipmain.htm.

Iida, T., Yamada, K., Miyachi, H., Iwasaka, Y., Matsunaga, K. and Ishizaka, T. 1997. Vertical distribution of radon concentrations in the atmosphere. *7th Tohwa University international symposium.* Fukuoka (Japan) 23-25 Oct 1997. Katase,-A. and Shimo,-M. (eds.) Radon and thoron in the human environment Singapore (Singapore) World Scientific Publishing Co. Pte. Ltd. 594 p. p. 246-251. 1998.

Iida,-T., Yamada,-K., Hashiguchi,-Y., Moriizumi,-J., Nagao,-I., Komura,-K., Yoshioka,-K., Jin-Y. and Kim,-Y.-S. 2000. Measurements of atmospheric radon concentrations at various locations in east Asia. *Inaba,-J.; Hisamatsu,-S.; Ohtsuka,-Y. (eds.) Distribution and speciation of radionuclides in the environment Rokkasho, Aomori (Japan) Institute for Environmental Sciences.* 374 p. p. 123-132.

Ikebe, -Y., Iida, -T., Shimo, -M. and Sakashita, -T. 1997. On the properties and behavior of radon and its daughters in the atmosphere. *Memoirs of the School of engineering, Nagoya University.* October 1997. 49(1), p.1-47.

Intergovernmental Panel on Climate Change 1995. The Science of Climate Change, Report of Working Group I to the Intergovernmental Panel on Climate Change, IPCC-XI, Rome, 11-15 December 1995.

References

Irannejad, P., Henderson-Sellers, A., Phillips, T. and McGuffie, K. 2000. Analysis of AMIP II models' simulations of land surface climates, GEWEX News, 10, No.3.

Irannejad, P., Henderson-Sellers, A., Sharmeen, S., Phillips, T.J., McGuffie, K., Pitman, A.J. and Zhang, H. 2002. Evaluation of the Annually Averaged Land-surface Energy Budget Simulations of Twenty AMIP II Global Models, prepared for submission in the *Journal of Climate*.

Jacob, D.J., and Prather, M.J. 1990. Radon-222 as a test of convective transport in a general circulation model, *Tellus,* 42B, 118-134.

Jacob, J.J., Prather, M.J., Rasch, P.J., Shia, R.-L., Walkanski, Y.J., Beagley, S.R., Bergmann, D.J., Blackshear, W.T., Brown, M., Chiba, M., Chipperfield, M.P., de Grandpré, J., Dignon, J.E., Feichter, J., Genthon, C., Grose, W.L., Kasibhatla, P.S., Köhler, I., Kritz, M.A., Law, K., Penner, J.E., Ramonet, M., Reeves, C.E., Rotman, D.A., Stockwell, D.Z., van Velthoven, P.F.J., Verver, G., Wild, O., Yang, H., and Zimmermann, P. 1997. Evaluation and intercomparison of global atmospheric transport models using ^{222}Rn and other short lived tracers, *J. Geophys. Res.,* 102(D5), 5953-5970.

Jaffe, D., Anderson, T., Covert, D., Trost, B., Danielson, J., Simpson, W., Blake, D., Harris, J. and Streets, D. 2001. Observations of ozone and related species in the northeast Pacific during the PHOBEA campaigns 1. Ground-based observations at Cheeka Peak, *J. Geophys. Res.,* 106(D7). 7449- 7461.

Jin, -Y., Iida, -T., Ikebe, -Y., Wang, -Z. and Abe, -S. 1998. A sub-nationwide survey of outdoor and indoor ^{222}Rn concentrations in China by passive method. *7th Tohwa University international symposium.* Fukuoka (Japan) 23-25 Oct 1997. Katase,-A. and Shimo,-M. (eds.) Radon and thoron in the human environment Singapore (Singapore) World Scientific Publishing Co. Pte. Ltd. 594 p. p. 246-251. 1998.

Kalnay E., Kanamitsu M., Kistler R., Colins W., Deaven D., Gandin L., Iredell M., Saha S., White G., Woolen J., Zhu Y., Chelliah M., Ebisuzaki W., Higgins W., Janowiak J., Mo K.C., Ropelewski C., Wang J., Leetmaa A., Reynolds R., Jenne R. and Joseph D. 1996. The NMC/NCAR 40-year reanalysis project, *Bull. Amer. Meteor. Soc*., 77, 437—471.

Kanamitsu, M., Ebisuaki, W., Woolen, J., Potter, J. and Fiorino, M. 2000. An overview of NCEP/DOE Reanalysis-2. *Second WCRP International Conference on Reanalyses Proc,* WCRP 109.

Kistler, R., Kalnay, E., Collins, W., Saha, S., White, G., Woollen, J., Chelliah, M., Ebisuzaki, W., Kanamitsu, M., Kousky, V., van den Dool, H., Jenne, R. and Fiorino, M. 2001. The NCEP-NCAR 50-Year Reanalysis: Monthly Means CD-ROM and Documentation, *BAMS,* 82, 247-268.

Koster, R.D. and Suarez, M.J. 2001. Soil moisture memory in climate models, J. Hydrometeo, 2, 558-570.

Kritz, M.A., Rosner, S. and Stockwell, D.Z. 1998. Validation of an off-line three-dimensional chemical transport model using observed radon profiles: 1. Observations, *J. Geophys. Res.,* 103, 8425-8432.

Li, Y. and Chang, J.S. 1996. A three-dimensional global episodic tracer transport model: 1. Evaluation of its transport processes by radon-222 simulations, *J. Geophs. Res.,* 101(D20), 25,931-25,947.

Liang, X., D.P. Lettenmaier, E.F. Wood, and S.J. Burges, 1994, A Simple hydrologically Based Model of Land Surface Water and Energy Fluxes for GSMs, *J. Geophys. Res.*, 99(D7), 14, 415-14,428.

Maenhaut, W., Francois, F. and Cafmeyer, J. 1993. The GENT stacked filter unit sampler for collection of atmospheric aerosols in two size fractions, *IAEA NAHRES-19,* Vienna (1993), pp249-263.

Mahowald, N.M., Rasch, P.J. and Eaton, B.E. 1997. Transport of ^{222}Radon to the remote troposphere using the Model of Atmospheric Transport and Chemistry and assimilated winds from ECMWF and the National Center for Environmental Prediction/NCAR, *J. Geophys. Res.,* 102(D23), 28,139-28,151.

Malm, W.C., Sisler, J.F., Huffman, D., Eldred, R.A. and Cahill, T.A. 1994. Spatial and seasonal trends in particle concentrations and optical estimations in the US, *J. Geophys. Res*., 99, 1347.

Manabe, S. 1969. Climate and ocean circulation: 1. The atmospheric circulation and the hydrology of the earth's surface, Mon. Wea. Rev., 97, 739-774.

Maurer, E.P., Nijssen, B. and Lettenmaier, D.P. 2000. Use of Reanalysis Land Surface Water Budget Variables in Hydrologic Studies, *GEWEX News*, November 2000, pp6-8.

Nijssen, B., Schnur, R. and Lettenmaier, D.P. 2001. Global retrospective estimation of soil moisture using the VIC land surface model, 1980-1993, *J. Climate*, 14(8), 1790-1808.

Pamplin, R. 2001. Supplementary State of the Environment Report 200-2001. Great Lakes Council.

References

Peng, T.-H., Broecker, W.S., Mathieu, G.C. and Li, Y.-H. 1979. Radon evasion rates in the Atlantic and Pacific oceans as determined during the Geosecs program, *J. Geophys. Res.,* 84, 2471-2486.

Roads, J. and Betts, A. 1999, NCEP/NCAR and ECMWF Reanalysis Surface Water and Energy Budgets for the Mississippi River Basin, available on line http://ecpc.ucsd.edu/gcip/9906gcip.htm.

Sellers P.J., Mintz Y., Sud Y.C. and Dalcher A. 1986. A Simplified Biosphere Model (SiB) for Use within General Circulation Model, *J. Atmo. Sci.*, 43, 505—531.

Shao Y. and Henderson-Sellers, A. 1996. Validation of soil moisture simulation in landsurface parameterisation schemes with HAPEX data, *Global Planet. Change*, 13, 11-46, Special Issue.

Wallis Lake Catchment Management Plan, 2002. Volume 1: State of the Catchment Report.

Wilkening, M.H. and Clements, W.E. 1975. Radon-222 from the ocean surface, *J. Geophs. Res.,* 80(27), 3828-3830.

Xie, P.P. and Arkin, P.A. 1997. Global precipitation: A 17-year monthly analysis based on gauge observations, satellite estimates, and numerical model outputs, *Bull. Amer. Meteor. Soc*., 78, 2539-2558.

Yamada, K. Iida, T., Ikebe, Y., Miyachi, H., Nagao, I. and Komura, K. 1998. Time series analysis of atmospheric ^{222}Rn concentrations and meteorological factors in Japan. *7th Tohwa University international symposium.* Fukuoka (Japan) 23-25 Oct 1997. Katase,-A. and Shimo,-M. (eds.) Radon and thoron in the human environment Singapore (Singapore) World Scientific Publishing Co. Pte. Ltd. 594 p. p. 246-251. 1998.

Yamanishi, -H., Iida, -T., Ikebe, -Y., Abe, -S. and Hata, -T. 1991. Measurements of regional distribution of radon-222 concentration. *Journal of Nuclear Science and Technology Tokyo.* 28(4), 331-338.

Yoshioka, K. 1998. The vertical profile of ^{222}Rn concentration in the lower atmospheric boundary layer at Shimane Peninsula. *7th Tohwa University international symposium.* Fukuoka (Japan) 23-25 Oct 1997. Katase,-A. and Shimo,-M. (eds.) Radon and thoron in the human environment Singapore (Singapore) World Scientific Publishing Co. Pte. Ltd. 594 p. p. 246-251. 1998.

Zahorowski, W. and Whittlestone, S. 1999. Radon database 1987-1996: A review. *Baseline Atmospheric Program Australia 1996.* Gras, J.L., Derek, N., Tindale, N.W. and Dick, A.L. (eds.). Bureau of Meteorology and CSIRO Atmospheric Research. 71-80.

Zahorowski, W., Chambers, S.D. and Henderson-Sellers, A. 2002. Ground based radon-222 observations and their application to atmospheric studies. *7th South Pacific Environmental Radioactivity Association Conference.* Lucas Heights Science and Technology Centre, 13-17 May 2002, Sydney, Australia. Submitted to the Journal of Environmental Radioactivity.

Zhang, H. 2002. A version of the BAM's AMIP2 simulation over the Australian region: Contrasting its performance with other AMIP II models, BMRC report (in press).

Zhang, H., Henderson-Sellers, A., Irannejad, P., Sharmeen, S., Phillips, T. and McGuffie, K. 2002. Land-Surface Modelling and Climate Simulations: Results over the Australian Region from Sixteen AMIP2 models, BMRC Research Report 89, BMRC, Australia.